

DOT/FAA/TC-16/2

Federal Aviation Administration
William J. Hughes Technical Center
Aviation Research Division
Atlantic City International Airport
New Jersey 08405

Application of Rotorcraft Structural Usage and Loads Monitoring Methods for Determining Usage Credits

June 2016

Final Report

This document is available to the U.S. public through the National Technical Information Services (NTIS), Springfield, Virginia 22161.

This document is also available from the Federal Aviation Administration William J. Hughes Technical Center at actlibrary.tc.faa.gov.



U.S. Department of Transportation
Federal Aviation Administration

NOTICE

This document is disseminated under the sponsorship of the U.S. Department of Transportation in the interest of information exchange. The U.S. Government assumes no liability for the contents or use thereof. The U.S. Government does not endorse products or manufacturers. Trade or manufacturers' names appear herein solely because they are considered essential to the objective of this report. The findings and conclusions in this report are those of the author(s) and do not necessarily represent the views of the funding agency. This document does not constitute FAA policy. Consult the FAA sponsoring organization listed on the Technical Documentation page as to its use.

This report is available at the Federal Aviation Administration William J. Hughes Technical Center's Full-Text Technical Reports page: actlibrary.tc.faa.gov in Adobe Acrobat portable document format (PDF).

Technical Report Documentation Page

1. Report No. DOT/FAA/TC-16/2		2. Government Accession No.		3. Recipient's Catalog No.	
4. TITLE AND SUBTITLE APPLICATION OF ROTORCRAFT STRUCTURAL USAGE AND LOADS MONITORING METHODS FOR DETERMINING USAGE CREDITS				5. Report Date June 2016	
7. Author(s) Ray Beale and Mark Davis				6. Performing Organization Code	
9. Performing Organization Name and Address Sikorsky Aircraft Corporation 6900 Main Street Stratford, CT 06615-9129				8. Performing Organization Report No.	
12. Sponsoring Agency Name and Address U.S. Department of Transportation Federal Aviation Administration FAA Southwest Regional Office 10101 Hillwood Pkwy Fort Worth, TX 76177				10. Work Unit No. (TRAIS)	
				11. Contract or Grant No. DTFACT-11-D-00004 (DO-0002/3)	
				13. Type of Report and Period Covered Final Report September 26, 2012 – June 15, 2015	
				14. Sponsoring Agency Code ASW-112	
15. Supplementary Notes The Federal Aviation Administration William J. Hughes Technical Center Aviation Research Division CORs were Paul Swindell and Traci Stadtmueller (alternate).					
16. Abstract <p>The monitoring of an aircraft's actual structural usage has the potential to increase rotorcraft safety enhancements provided by Health and Usage Monitoring Systems (HUMS) and reduce operating costs via usage-based maintenance (UBM) credits. While flight regime recognition (RR) algorithms have been demonstrated, none has been fully validated, and obtaining UBM credit approval remains elusive due to both technical and certification challenges. The FAA has funded research and development (R&D) efforts to establish and demonstrate viable approaches for validating and certifying HUMS RR-enabled UBM credits. In a previous contract (i.e., DTFACT-06-C-00002), Sikorsky Aircraft Corporation defined an end-to-end UBM process that fulfills the objectives of Advisory Circular 29-2C and utilizes available HUMS data. This effort, as documented in FAA report DOT/FAA/AR-12/4 (September 2012), included the development of an RR-clustering approach for addressing the identified shortcomings of current RR algorithms that can be applied through post-processing of HUMS data without having to modify existing RR onboard software. The Delivery Order (DO) 0001 R&D effort under the subject contract (i.e., DTFACT-11-D-00004) further developed and validated usage and loads monitoring methods, which were documented previously in FAA report DOT/FAA/TC-15-10.</p> <p>The R&D effort under DO 0002 and 0003 for the subject contract (i.e., DTFACT-11-D-00004), which is documented herein, focused on the application of structural usage monitoring methods to achieve a "mock UBM credit." Building upon previous R&D efforts, selected usage monitoring methods and a viable end-to-end process for achieving UBM credits were applied to calculate a retirement time (RT) credit for a representative life-limited component based on individual aircraft RR usage statistics calculated from HUMS operational fleet data recorded on S-92[®] rotorcraft. The previously developed regime-clustering method was applied in automated fashion to operational HUMS data, resulting in individual aircraft usage statistics across the fleet for critical regimes driving the RT for the selected component. Usage statistics were compared to the composite worst case usage spectrum by individual tail number in order to identify the best candidates for UBM life credits. Finally, a UBM component retirement credit was calculated for a specific tail number using reliability factors and validated within a probabilistic framework to demonstrate that the goal of six-9s (0.999999) fatigue reliability was achieved. Further development of load monitoring technologies, such as landing gear load sensors, is also documented herein.</p>					
17. Key Words Structural usage and loads monitoring, Regime recognition, Structural usage credit, Usage-based maintenance, Retirement-time adjustment, Life extension, Health and usage monitoring systems			18. Distribution Statement This document is available to the U.S. public through the National Technical Information Service (NTIS), Springfield, Virginia 22161. This document is also available from the Federal Aviation Administration William J. Hughes Technical Center at actlibrary.tc.faa.gov.		
19. Security Classif. (of this report) Unclassified		20. Security Classif. (of this page) Unclassified		21. No. of Pages 121	22. Price

TABLE OF CONTENTS

	Page
EXECUTIVE SUMMARY	x
1. INTRODUCTION	1
2. UBM TECHNOLOGY SUMMARY	4
2.1 Regime Recognition	4
2.1.1 Regime Recognition Clustering	6
2.1.2 Parametric Prorating	8
2.2 Loads Monitoring	9
2.2.1 GW/CG Monitoring	10
2.2.2 Direct Monitoring of Loads	36
2.3 Reliability Framework	49
2.3.1 Background	49
2.3.2 Defining a Failure Model	50
2.3.3 Input Assumptions	51
2.3.4 Probabilistic Solver	53
3. MOCK REGIME-BASED UBM CREDIT CERTIFICATION	56
3.1 Credit Definition	56
3.1.1 Life Sensitivity Analysis	57
3.1.2 Component Selection	60
3.2 Definition of End-to-End Process	62
3.3 Credit Hazard and Criticality Analysis	63
3.3.1 Functional Description	65
3.3.2 Component FMECA	65
3.3.3 HUMS UBM FMECA	66
3.3.4 FHA Summary	69
3.4 Installation Qualification	70
3.4.1 Installed HUMS Equipment	70
3.4.2 OEM Analysis	72

3.5	Credit Validation	72
3.5.1	Description of Application and Associated Credit	73
3.5.2	Physics of the Application	73
3.5.3	Validation Methodology	97
4.	GENERAL APPLICABILITY TO OTHER CREDIT TYPES	105
5.	CONCLUSIONS AND RECOMMENDATIONS	106
6.	REFERENCES	108

LIST OF FIGURES

Figure		Page
1	Regime recognition algorithm data processing	5
2	Example of regime clustering	8
3	Regime clustering with parametric prorating	9
4	Optical LGLMS UH-60 MLG sensor	11
5	Optical LGLMS UH-60 TLG sensor	12
6	MLG sensor clamp screws	12
7	MLG shock strut reference sensor location	13
8	MLG calibration fixture	14
9	TLG calibration fixture	14
10	MLG axle calibration loads	15
11	TLG calibration loads	15
12	Optical LGLMS vertical sensitivity (right and left MLG)	17
13	Optical LGLMS drag sensitivity (right and left MLG)	17
14	Optical LGLMS vertical sensitivity (TLG)	18
15	Optical LGLMS Drag sensitivity (TLG)	19
16	Calibration fixture for strut sensors	20
17	Right and left main strut calibration sensitivity plot	20
18	Tail strut upper and lower calibration sensitivity plot	21
19	Aircraft calibration setup diagram	22
20	Optical LGLMS MLG A/C calibration sensitivity	23
21	Optical LGLMS TLG A/C calibration sensitivity	24
22	Optical LGLMS TLG A/C calibration sensitivity—corrected to yoke axis	24
23	MLG strut sensor A/C calibration sensitivity	25
24	TLG strut sensor A/C calibration sensitivity	26
25	IVHMS GW estimator performance	28
26	GW derived parameter plot for Flight #1	29
27	Flight #1 GW sensor output during ground ops	30
28	GW measurement performance	31
29	CG measurement performance	33
30	MLG strut in-flight output versus outside air temperature	34

31	Epsilon TLG in-flight output versus outside air temperature	35
32	Hard landing event from Flight #1	36
33	Sensitivity and bandwidth	38
34	Example of sample rate variation—down sampling signal	45
35	Example of sensitivity error—10% higher sensitivity	46
36	Example of sensor bandwidth variation— lowpass filtering with cutoff frequency of 36 Hz	46
37	Effect of sample rate variation of load data on the damage fraction	48
38	Effect of sensitivity error variation of load data on the damage fraction	48
39	Effect of sensor bandwidth variation of load data on the damage fraction	49
40	2D case limit state function	54
41	Component life sensitivity to load	60
42	End-to-end regime recognition credit process	62
43	S-92 HUMS system overview	71
44	S-92 main rotor swashplate	74
45	Sample S-N curve for stationary swashplate	76
46	Stationary swashplate damage regimes	79
47	Regime recognition of right turn, $45^\circ V_{NE}$	81
48	Regime recognition of moderate pullout, $0.8 V_{NE}$	82
49	Total 2013 HUMS flight hours by tail number	84
50	HUMS data integrity assessment results	85
51	Comparison of 30° and 45° turn E&R occurrence rate	87
52	HUMS monitored and unmonitored usage accrual	91
53	Left turn, $45^\circ V_{NE}$ usage Pareto	93
54	HUMS-based damage trend for A/C#3	95
55	A/C#3 HUMS credit calculation	97
56	Example of run log markers for transient maneuver	98
57	Detection and damage threshold for pullouts	101
58	Fleet average reliability for stationary swashplate	103
59	A/C#3 serial number reliability for stationary swashplate	104

LIST OF TABLES

Table	Page
1	5
2	6
3	27
4	32
5	39
6	44
7	57
8	61
9	63
10	69
11	75
12	77
13	80
14	83
15	86
16	89
17	89
18	90
19	92
20	94
21	96
22	100
23	102

LIST OF ACRONYMS

A/C	Aircraft
AC	Advisory Circular
AOB	Angle of bank
CERDEC	Communications-Electronics Research, Development and Engineering Center (U.S. Army)
CG	Center of gravity
CRT	Calculated retirement time
CWC	Composite worst case
DAL	Design Assurance Level
DO	Delivery Order
DTU	Data Transfer Unit
E&R	Entry and recovery
FBG	Fiber Bragg grating
FHA	Functional Hazard Assessment
FTP	File Transfer Protocol
FLS	Flight Loads Survey
FMECA	Failure Modes, Effects, and Criticality Analysis
FORM	First-order reliability method
GAG	Ground-air-ground
GBS	Ground-based system
GSS	Ground Support System
GW	Gross weight
HUMS	Health and Usage Monitoring System
IMD-HUMS	Integrated Mechanical Diagnostics - Health and Usage Monitoring System
ID	Inside diameter
IVHMS	Integrated Vehicle Health Management System
LF	Level flight
LLP	Life-limited parts
LGLMS	Landing Gear Load Measurement System
MLG	Main landing gear
MPU	Main processing unit
MR	Main rotor
OBS	Onboard system
OEM	Original equipment manufacturer
OD	Outside diameter
PCMCIA	Personal Computer Memory Card International Association
R&D	Research and development
RPM	Revolutions per minute
RR	Regime recognition
RT	Retirement time
S-N	Stress cycles fatigue curve
SAC	Sikorsky Aircraft Corporation
SME	Subject matter expert
TLG	Tail landing gear
UBM	Usage-based maintenance

UMRF	Usage Monitor Reliability Factor
VML	Virtual monitoring of loads
V_{NE}	Velocity, not to exceed
WOW	Weight-on-wheels

EXECUTIVE SUMMARY

The monitoring of an aircraft's actual structural usage has the potential to increase rotorcraft safety enhancements provided by Health and Usage Monitoring Systems (HUMS) and reduce operating costs via usage-based maintenance (UBM) credits. While regime recognition (RR) algorithms have been demonstrated, none has been fully validated, and UBM credit approval remains elusive due to both technical and certification challenges. The FAA has funded research and development (R&D) to establish and demonstrate viable approaches for validating and certifying HUMS RR-enabled UBM credits. In contract DTFACT-06-C-00002, Sikorsky Aircraft Corporation (SAC) defined an end-to-end UBM process that fulfills the objectives of Advisory Circular (AC) 29-2C, section MG-15, and utilizes available HUMS data. This effort, as documented in FAA report DOT/FAA/AR-12/4 [1], included the development of an RR-clustering approach for addressing shortcomings of current RR algorithms, which can be applied through post-processing of HUMS data without having to modify existing onboard software. Delivery Order (DO) 0001, under contract DTFACT-11-D-00004, further developed and validated usage and loads monitoring methods, which were documented previously in FAA report DOT/FAA/TC-15-10 [2].

DO-0002/0003, under contract DTFACT-11-D-00004, which is documented herein, continued to evaluate and demonstrate enabling structural usage monitoring technologies, including regime, gross weight (GW) and center of gravity (CG), and loads monitoring. In particular, regime clustering was further refined, validated, and applied. Data were also analyzed from a flight test of fiber-optic landing gear load sensors that can be used to calculate GW and CG as well as measure landing and ground handling loads. The flight test was conducted by the U.S. Army's Communications-Electronics Research, Development and Engineering Center. Finally, an investigation of load monitoring requirements was conducted to support future AC guidance on the integration of load sensor technologies into HUMS.

The primary focus of DO-0002/0003, and therefore this report, is on the application of structural usage monitoring methods to achieve a "mock UBM credit." Building upon previous R&D efforts, selected usage monitoring methods and a viable end-to-end process for achieving UBM credits were applied to calculate a retirement time (RT) credit for a representative life-limited component based on individual aircraft RR usage statistics calculated from HUMS operational fleet data recorded on S-92[®] rotorcraft. A comprehensive assessment of the life-limited components contained in an S-92 rotorcraft was conducted to identify candidate components for use in developing a mock credit. A total of 10 candidate components that had various advantages and disadvantages relative to the objectives of the FAA program were identified. The main rotor stationary swashplate was selected based on this assessment because it was a moderately complex, but tractable, application that could be completed within the allocated budget and schedule of the FAA program. The stationary swashplate required accurate recognition of six critical regimes in order to achieve a UBM credit.

The previously developed regime-clustering method was further improved using HUMS parametric data and applied in automated fashion to operational HUMS data, resulting in individual aircraft usage statistics across the fleet for critical regimes driving the RT for the stationary swashplate. Usage statistics for all S-92 aircraft were calculated for one year's worth of data and compared to the composite worst case usage spectrum, by individual tail number, to identify the best candidates for UBM life credits. The entire usage history of the selected serial

number was analyzed to calculate a usage credit and new RT, using regime-specific reliability factors to achieve six-9's (0.999999) fatigue reliability, as validated within a probabilistic framework.

This report and the mock certification example represent opinions and recommendations from SAC and are not FAA policy.

1. INTRODUCTION

One of the central goals of usage-based maintenance (UBM) is to change the maintenance paradigm from one that is currently flight-hour or schedule-based to one that is based on usage and loads. For example, life-limited parts (LLPs) are currently retired based on the number of flight hours flown regardless of whether the aircraft is only flown benignly (e.g., VIP transport) or flown much more aggressively (e.g., cargo transport with many ground-air-ground [GAG] cycles per hour). A certified UBM process that accurately monitors usage and loads would enable the attainment of retirement time (RT) credits (or debits) for LLPs based on measured aircraft configuration, usage, and loads rather than flight hours and underlying conservative design assumptions. Virtual sensing methods that utilize measured aircraft state parameters have been developed previously by Sikorsky Aircraft Corporation (SAC) to monitor key parameters, including: 1) regime recognition (RR) algorithms with associated clustering techniques, 2) virtual monitoring of loads (VML), and 3) gross weight (GW) and center of gravity (CG) estimation. Under previous FAA research and development (R&D) projects [1, 2], many of these usage and loads monitoring technologies were evaluated, validated, and demonstrated with respect to the potential UBM credit benefits and challenges remaining to be addressed before they could be considered mature enough to serve as the focus of a formal UBM credit application. The research documented herein focuses on the application of structural usage monitoring methods and algorithms to achieve UBM credits, such as extended RTs, allowing parts to remain on wing longer.

Dynamic component RTs are currently set by a rigorously defined fatigue damage calculation process [3] that computes a calculated retirement time (CRT) from three basic inputs: component strength with reliability-based safety factors, a composite worst case (CWC) usage spectrum, and a load spectrum derived from flight tests. Component strength is generally derived from full-scale component fatigue testing. The CWC spectrum combines conservative assumptions on aircraft usage with high envelope loads. The usage is typically given in the form of a list of flight regimes, each of which is assigned either a percentage of total flight time or rate of occurrence (maneuvers per 100 flight hours). Flight loads are developed in the flight loads survey (FLS), a comprehensive flight test program that exercises the extremes of aircraft performance to develop the highest expected loads for each regime. Each component is assigned a substantiating load parameter(s), which characterizes the load states for that component's critical failure mode(s). Common substantiating parameters for dynamic components are derived from calibrated bending and axial bridges such as a main rotor (MR) shaft bending bridge or push rod axial load bridge. They can also be based on more local stress/strain measurements when necessary. The three inputs (i.e., strength, usage, and loads) are then combined in a stress-life fatigue calculation which results in the CRT.

The Integrated Vehicle Health Management System (IVHMS) is the next generation system derived from the Integrated Mechanical Diagnostics—Health and Usage Monitoring System (IMD-HUMS). The IVHMS is standard equipment on the SAC UH-60M aircraft, while the IMD-HUMS is standard equipment on the S-92 aircraft. Aside from recording a plethora of aircraft state parameters, such as airspeed, engine power measurements, and pilot control inputs, both the IVHMS and IMD-HUMS execute similar RR algorithms from these state parameters. These algorithms translate aircraft state measurements into regime classifications (e.g., climbing

left turn or level flight [LF] at 0.8 VH) that can be used to better understand aircraft usage, which drives component RTs. The result is a recorded time sequence of regimes flown for each flight.

While the current onboard RR algorithms provide significant insight into the usage of operational aircraft, some shortcomings have been identified that must be overcome in order to develop a practical UBM process that can be certified for securing credits and benefits. One such issue is the frequent toggling of RR output data due to the precise second-by-second classification using state parameter data. In order to overcome some of the shortcomings of this system, additional offboard processing of these data is desired to enable existing onboard software capabilities to be exploited without the need to invest in costly onboard software changes. One such technique is called regime clustering, which was developed, refined, validated, and demonstrated in previous FAA R&D projects [1, 2, 4]. After being trained on a given data set, this additional processing gathers regime time sequences into contiguous maneuvers or target regimes that more accurately represent the aircraft usage—both in terms of pilot intent and CWC design assumptions—when compared with the fine, second-by-second granularity regime sequences produced by the IVHMS, IMD-HUMS, and similar systems. The regime clustering algorithms work by reprocessing the IVHMS RR sequence outputs into broader target regimes, which are based on statistical and physics/experience-based rules.

The state parameters collected by the IVHMS and IMD-HUMS can also be processed offboard to estimate additional aircraft configuration parameters such as the GW and CG locations [2]. The algorithms involved can be grouped into two classes: physics-based and mathematical models. Both classes of algorithms only operate upon a small subset of aircraft regimes, which are chosen to enhance algorithm accuracy. This typically is limited to hover and steady LF. In another offboard processing application of aircraft state parameter data, individual loads can be estimated in continuous time through VML algorithms [5, 6]. After being trained, these mathematical models recreate the readings of individual strain gages, bending bridges, or other load measurements that were included in the aircraft FLS as a substantiating parameter. If a given load is also a component substantiating parameter, it is possible to gain a better understanding of the remaining fatigue capacity of a component subjected to field usage. The use of physical sensors integrated into production aircraft are also being considered for monitoring of key loads and substantiating parameters [7].

Under previous FAA R&D projects [1, 2], many of these usage and loads monitoring technologies were evaluated, validated, and demonstrated with respect to the potential UBM credit benefits and challenges remaining to be addressed before they can be considered mature enough to serve as the focus of a formal UBM credit application. The current effort documented herein, under Delivery Order (DO) 0002/0003 (within contract DTFAC-11-D-00004), continued to evaluate and demonstrate certain enabling structural usage monitoring technologies, including regime, GW and CG, and loads monitoring. In particular, regime clustering was further refined, validated, and applied. Data were also analyzed from a flight test, conducted by the U.S. Army's Communications-Electronics Research, Development and Engineering Center (CERDEC), of fiber-optic landing gear load sensors that can be used to calculate GW and CG and measure landing and ground handling loads. Finally, an investigation of load monitoring requirements was conducted to support future AC guidance on the integration of load sensor technologies into HUMS. These efforts are documented in section 2.

The primary focus of DO-0002/0003 and, therefore, this report is on the application of structural usage monitoring methods to achieve a “mock UBM credit.” Previous R&D efforts, selected usage monitoring methods, and a viable end-to-end process for achieving UBM credits were utilized to calculate an RT credit for a representative life-limited component based on individual aircraft RR usage statistics calculated from HUMS operational fleet data recorded on S-92 rotorcraft. A comprehensive assessment of the life-limited components contained in an S-92 rotorcraft was conducted to identify candidate components for use in developing a mock credit. A total of 10 candidate components were identified that had various advantages and disadvantages relative to the objectives of the FAA program. The MR stationary swashplate was selected based on this assessment because it was a moderately complex, but tractable, application that could be completed within the allocated budget and schedule of the FAA program. The stationary swashplate required accurate recognition of six critical regimes in order to achieve a UBM credit.

The previously developed regime clustering method was applied in automated fashion to operational HUMS data—resulting in individual aircraft usage statistics across the fleet for critical regimes driving the RT for the stationary swashplate. Usage statistics for all S-92 aircraft were calculated for one year’s worth of data and compared to the CWC usage spectrum by individual tail number to identify the best candidates for UBM life credits. The entire usage history of the selected serial number was analyzed in order to calculate a usage credit and new RT using regime-specific reliability factors to achieve six-9’s (0.999999) fatigue reliability, as validated within a probabilistic framework. The mock certification is documented in section 3.

2. UBM TECHNOLOGY SUMMARY

2.1 REGIME RECOGNITION

HUMS RR algorithms are used to identify and categorize how the aircraft has been flown. They comprise a key element to short-term UBM approaches being pursued by various original equipment manufacturers (OEMs) to obtain approved UBM credits. Inputs required for RR are acquired by the HUMS system from various avionics systems across the S-92 aircraft via the digital bus. Many of these inputs are also essential for flight control and pilot decisions, and thus have the highest levels of hardware and software integrity. On older analog aircraft, HUMS may have dedicated sensors or acquired through physical connections to tie into the analog data stream. Consequently, this presents a number of challenges when it comes to the qualification and certification of a HUMS-based UBM credit for such a system. These challenges are beyond the scope of this report.

The RR data flow for the S-92 aircraft is illustrated in figure 1, wherein the standard input and output data types are shown. RR input data can be grouped into the following four categories.

1. Basic aircraft and system data
2. Air data parameters
3. Aircraft rates and attitudes
4. Aircraft “rigid-body” accelerations

While the details of RR algorithms vary, the above types of required input data are typical for most OEM rotorcraft platforms. The HUMS system output includes the regime sequence, start time and duration for each recognized regime, and all raw parametric data and derived parameters that were used in detecting the regimes.

As is typical for many HUMS, the RR algorithms deployed on the S-92 aircraft are based on hierarchal Boolean logic, which compares input parameters against a set of predefined ranges to determine the general aircraft flight condition/maneuver, such as steady level, turn, climb, or pullout. An example of a regime definition for a right turn during climb is shown in table 1. Some parameters, such as weight-on-wheels (WOW), landing flag, and takeoff flag, are considered in all regime definitions to ensure the aircraft is in a flight condition. The hysteresis parameters define the soft boundaries between regimes that are designed to reduce rapid toggling when the aircraft state jumps in and out of a regime. The hysteresis parameters come into play when exiting the regime by requiring that the specified parameter exceeds the defined threshold by the hysteresis amount. Finer regime classification is possible with knowledge of aircraft configuration such as GW, CG, external load, and external stores. This enables the prorating of regimes within usage categories to better understand the nature of the loads during a specific regime. Regime prorating is frequently used in fatigue substantiation for military rotorcraft and, to a lesser extent, commercial rotorcraft, which typically use only maneuver severity to form prorated regimes.

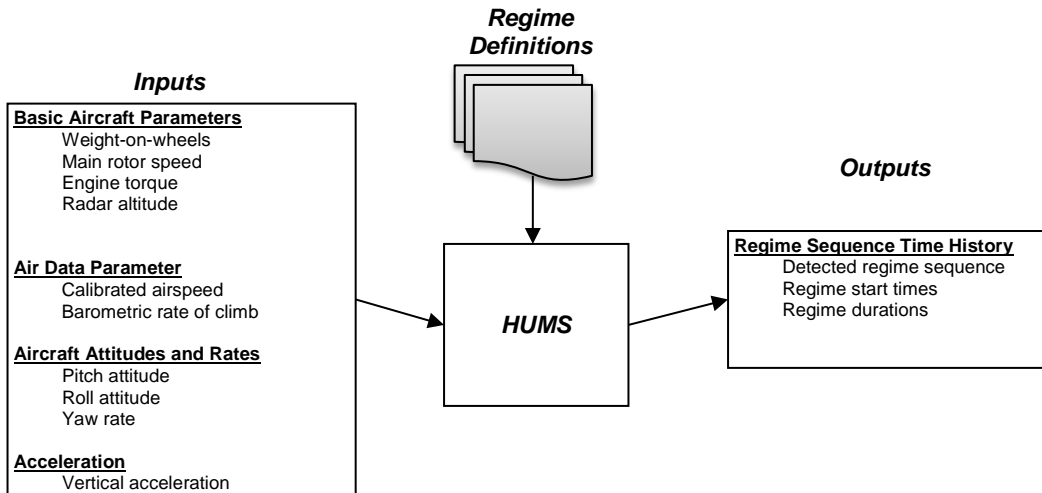


Figure 1. Regime recognition algorithm data processing

Table 1. Example regime definition for climb right turn

Description:	Right turn during climb		
Name:	Climb right turn		
Parameter	Operator	Threshold	Hysteresis
WOW	=	False	None
Landing flag	=	False	None
Takeoff flag	=	False	None
Calibrated airspeed	>	40	5
Corrected NZ	<=	1.3	None
Corrected NZ	>=	0.7	None
Rate of climb	>	400	200
Roll attitude	>	10	3

NZ = vertical acceleration

2.1.1 Regime Recognition Clustering

A fundamental requirement that must be satisfied before component RTs can be influenced by RR data is to demonstrate, with direct evidence from the flight test, that the algorithms correctly classify the flight regimes relevant to a particular credit application. Several previous efforts have focused on RR validation [1, 2]. Through these efforts, it has been shown that onboard RR classifications for many critical maneuvers do not correlate directly to independent pilot-declared maneuvers, which traditionally serve as the “truth” regime that RR is intended to capture. Two common issues that lead to these errors are: 1) RR makes independent second-by-second classifications based on current state parametric data without regard to the previous state (with the exception of the use of hysteresis for some parameters), whereas flight test regimes are defined holistically by the whole maneuver, and 2) generic HUMS regimes are defined with a different classification system than the flight test and usage spectrum regimes, which often do not map directly to the aircraft usage spectrum. For example, consider table 2, which shows a real example from an S-92 aircraft flight test of the RR output sequence during a 45° right turn. During this flight test maneuver, RR detected five distinct turn regimes. The maneuver starts with a few seconds of climb. Then, RR initially detects a generic right turn but does not capture the maximum angle of bank [AOB] until a few seconds later. As the aircraft descends, the regime changes from a level turn to a diving turn, before returning again to a level turn and then exiting the maneuver to an LF condition. The number of predicted turn regimes is due to independent second-by-second classifications and the fact that 45° turns normally have a large variation in altitude rate—which triggers the “toggling” from level to diving turn. For this reason, neither the flight test maneuver classification system nor the S-92 aircraft usage spectrum explicitly defines level and diving turns. Rather, turns are defined more broadly in the usage spectrum, such that it contains both level and diving turns. This is an example of how generic HUMS regimes may not map directly into the usage spectrum on a one-for-one basis for any particular aircraft model.

Table 2. Regime recognition output during 45° right turn

Pilot Declared Truth Regime	Regime Recognition Prediction
45° right turn	Steady climb
	Generic level right turn
	Generic level right turn, 45°, 0.8 V _{NE}
	Right turn in dive
	Right turn in dive, 45°
	Level right turn, 45°, 0.8 V _{NE}
	Forward flight 0.8 V _{NE}

While these issues are often perceived as errors in the output of RR, the output during these maneuvers is not random. RR is properly classifying the regimes based on the definitions that were used to design the software and the dynamic nature of certain key state parameters such as roll attitude, rate of climb, and load factor during transient maneuvers. While it is possible to define these regimes to be more consistent with flight test definitions, a simpler post-processing approach called clustering was developed under the FAA Structural Usage Monitoring

Technology program [1] to take advantage of hundreds of thousands of hours of existing RR data from the S-92 aircraft fleet. Clustering works by identifying the patterns in RR output that occur during targeted regimes and defining the logic for broadening or clustering the RR output into larger groups that correctly capture both the occurrence and duration of the intended regime. The objective of clustering is to find occurrences and duration of a particular usage spectrum regime within existing HUMS RR output data.

Cluster definitions consist of a set of target regimes and a set of cluster regimes. Due to the difference in regimes between HUMS and the S-92 aircraft usage spectrum, several different HUMS regimes can be associated with a usage spectrum regime. These regimes that map directly to the desired usage spectrum regime are called target regimes. However, examination of actual RR output shows that many other cluster regimes are in close proximity to or cluster within and around the usage spectrum regime. In processing the clustering algorithm, any contiguous set of target regimes are combined together into one regime, and any adjacent cluster regimes are added only after the target regimes are initially detected. Cluster regimes can be defined with persistence parameters such that only very short duration cluster regimes are included, but sufficiently long duration cluster regimes are treated as separate regimes. The process of designing a regime cluster involves a combination of determining the desired target regime set (e.g., “generic level right turn, 45° AOB, 0.8 velocity, not to exceed [V_{NE}]”) that aligns with the intended usage spectrum regime (e.g., “right turn, 45° 0.8 V_{NE} ”), along with the observation of RR test data to determine the cluster regime set (e.g., “generic level right turn”) that occurs within the usage spectrum regime.

Figure 2 shows the regime sequence from table 2 in a time series plot, along with the result of the regime clustering algorithm, and key parametric input data plotted for roll angle, altitude rate, and load factor. In this example, the clustering algorithm initially looks for the target regime, defined here as “generic level right turn, 45° AOB, 0.8 V_{NE} ” and highlighted in green. Based on the physics of the maneuver and the predictable behavior of the regime algorithm, there are several other regimes that will be classified along with the target regime, such as “right turn in dive.” These regimes are classified as cluster regimes and are highlighted in yellow. Once the target regimes are identified, the clustering regimes are then used to consolidate the regime sequence into a single regime cluster identified as “right turn, 45°, 0.8 V_{NE} .” The result is a single clustered regime that can be reliably counted on to provide both the proper number of occurrences and duration of the intended usage spectrum regime.

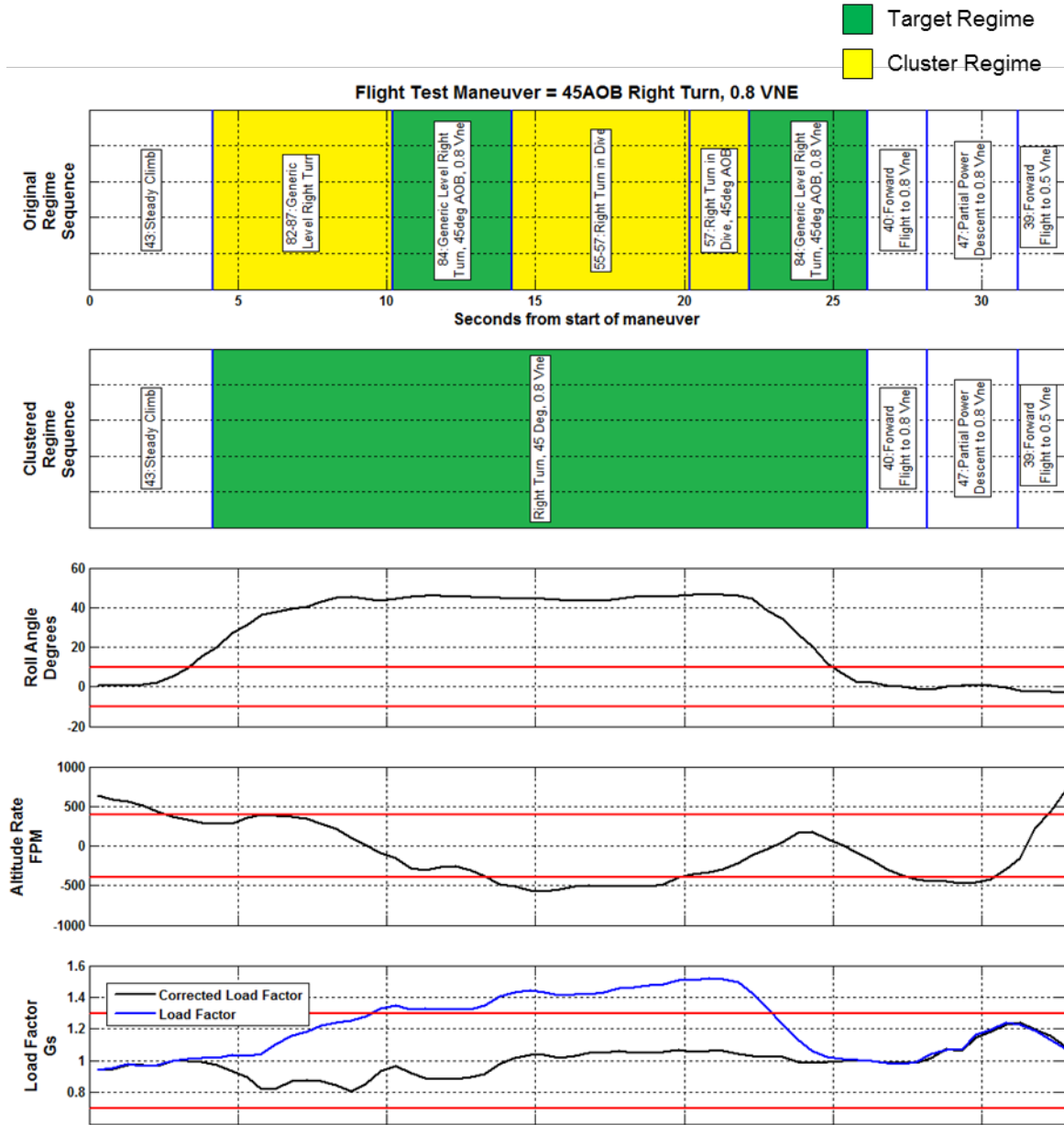


Figure 2. Example of regime clustering

2.1.2 Parametric Prorating

The clustering approach described above was initially developed under the effort of Bates, et al. [1] and refined under this project in support of the mock regime-based UBM credit application, as detailed in section 3. During the course of applying the clustering algorithm to the S-92 flight test data, there were cases found where clustering alone could not correctly map the HUMS regime sequence to the intended usage spectrum regime. This result is primarily caused by the multitude of target regime classifications in the same flight test maneuver, often obscuring what the true maneuver prorated value was (such as AOB or airspeed). The solution to this problem is to leverage parametric data (such as roll angle or airspeed) in the clustering process as a way to

ensure that each occurrence of a maneuver is prorated correctly, with consideration given to the variation of the relevant parameter across the entire duration of the maneuver. The basic strategy is to use RR clustering to capture broad maneuver categories such as turn or pullout, and then use the parametric data across the entire broadened regime to prorated the broad regime to a specific usage spectrum regime. This process is illustrated in figure 3.

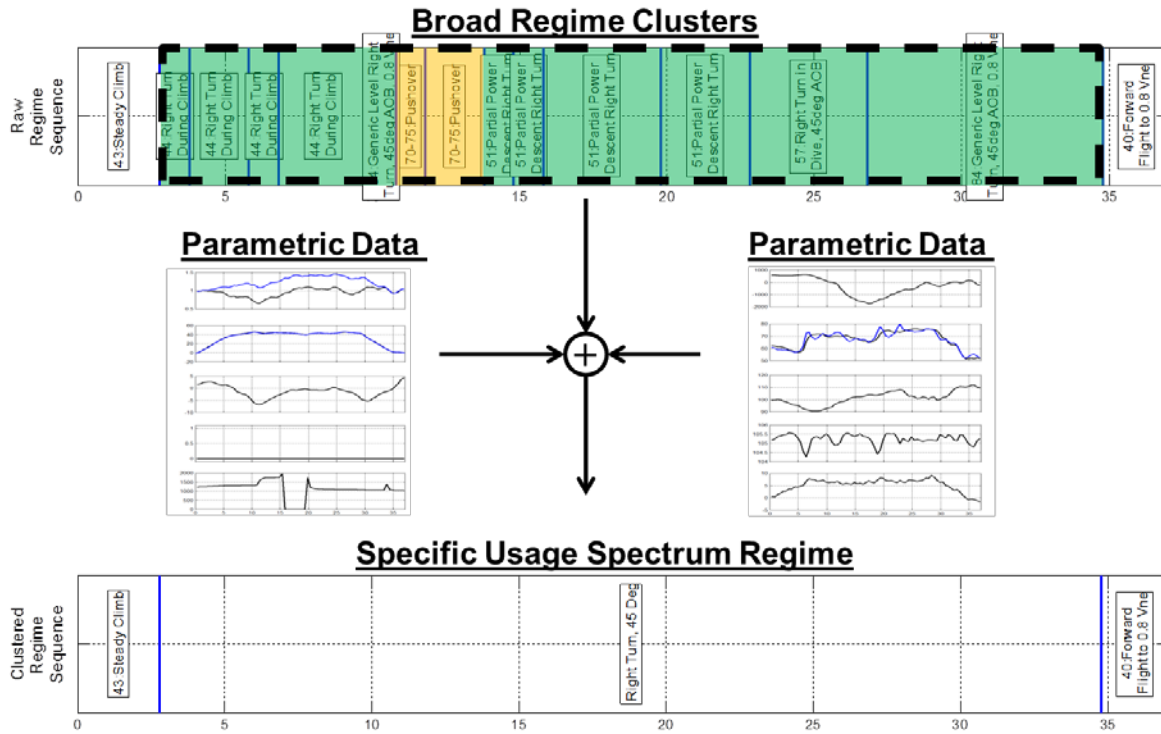


Figure 3. Regime clustering with parametric prorating

Using this approach, broad regime clusters were developed for turn, pushover, and pullout, as these broad regimes covered all of the critical damaging regimes that are relevant to the mock certification task detailed in section 3. As part of the mock UBM credit application effort, validation of the clustering/prorating approach to RR was carried out against flight test data. The results of the validation exercise are contained in section 3.5.3.1.

2.2 LOADS MONITORING

The ability to measure key loads on operational rotorcraft could radically change the way these products are designed, qualified, and managed throughout their life cycle. The lack of such measurements is indicative of the perceived difficulties, increased weight, and reliability issues associated with deploying the many physical sensors that would be required to monitor all such local loads, especially in rotor systems. This section presents the research for two load monitoring technology areas that can have significant impact to the way rotorcraft are maintained. First, flight test results for a Landing Gear Load Measurement System (LGLMS) used for estimating rotorcraft GW and CG are presented. Second, design considerations for a direct loads monitoring approach to fatigue management is studied by simulating the effect of digital signal processing on fatigue life estimation.

2.2.1 GW/CG Monitoring

2.2.1.1 Background

The ability to monitor vehicle GW and CG in service can enable more advanced UBM methods, provide safety enhancements, and potentially support the flight control system. While all rotorcraft are qualified to a maximum GW, they can spend much of their service life at GWs well below maximum. Estimating GW and CG usage across a fleet is important in the initial design and analysis of a rotorcraft structure, but conservative assumptions are usually relied on for design purposes. GW/CG monitoring can enable HUMS UBM approaches for tailoring maintenance requirements for specific rotorcraft that consistently operate below design assumptions. Knowledge of GW/CG in real time on the ground can also enhance safety by ensuring the vehicle is within safe limits prior to takeoff. Current pre-flight estimates of GW and CG are based on accurate measurements of an empty baseline aircraft, good estimates of fuel weight, and less accurate estimates of passenger and payload weight as well as location. Attempted takeoffs with unsafe aircraft weight and balance have historically been a key contributor to a number of aircraft accidents.

A system that measures landing gear loads would provide many benefits in addition to GW and CG monitoring. Landing loads can be monitored to automatically trigger inspections upon hard landings and direct the inspections to specific landing gear or portion of the aircraft. Strut health assessments can be made by monitoring load versus displacement and detect when servicing is required. WOW measurements can be used in flight controls to detect when an aircraft is in very light ground contact. While there are numerous benefits to a landing gear LGLMS, the technology has not sufficiently matured to the point where these sensors are being designed into the rotorcraft. Landing gear struts displace under landing loads and variations in GW. This displacement results in longitudinal and vertical translation, which affects the wheel position relative to the CG. To precisely monitor GW and CG in a sensor system, measurements of the weight on each wheel and the position of each strut must be taken.

To assess the viability of a landing gear LGLMS, the FAA contracted with Epsilon Optics to design a prototype fiber-optic-based LGLMS for the UH-60. The CERDEC flight test organization conducted the flight test of the LGLMS. SAC provided design support to Epsilon and test and analysis support to CERDEC. Prior to flight testing, SAC also assisted in the instrumentation and calibration of the landing gears fitted with prototype optical load sensors. Epsilon Optics specializes in fiber-optics measurement systems and has applications in the aerospace, civil engineering, marine, and energy sectors. Epsilon specifically has experience in prototyping an LGLMS for the SAC S-92 aircraft.

The initial effort between SAC and Epsilon involved providing UH-60 design data and stress analysis to allow Epsilon to configure a viable prototype sensor system for the UH-60 landing gears, including the two main gears and the tail gears. In August 2014, Epsilon built a prototype sensor system that was installed in the UH-60 landing gear at SAC and subsequently bench tested the system in order to assess sensitivity and calibrate the LGLMS. The UH-60 landing gears were then transported directly to the CERDEC test facility in Lakehurst, New Jersey for installation on a U.S. Army UH-60M test aircraft. CERDEC conducted an aircraft ground calibration procedure followed by a series of scripted flight tests from November–December

2014. In order to have an independent assessment of the performance of the LGLMS, SAC installed additional strain gage load sensors on the aircraft struts. These sensors were calibrated on the aircraft to calculate individual wheel load to estimate the GW and CG independently from the optical LGLMS system. The remainder of Section 2 provides details on the Epsilon optical LGLMS and reference sensor systems and provides results from the bench test, aircraft calibration, and flight test phases.

2.2.1.1.1 Optical Landing Gear Sensors

The Epsilon optical LGLMS design consisted of a series of Fiber Bragg grating (FBG) sensors installed in a phenolic cylindrical sensor body custom designed to slide into and clamp against the internal diameter of the UH-60 landing gear structure. The sensor body was constrained on both ends by radial clamps that translate structural bending or axial strain to the cylinder. The design of the cylinder was such that the strain of the cylinder was amplified in the central measurement region, allowing Epsilon to improve output from the FBGs. A main landing gear (MLG) outfitted with the optical LGLMS sensors is shown in figure 4, with the tail landing gear (TLG) sensor shown in figure 5. Both sensors are shown partially installed in the landing gear. Figure 6 shows a close-up of the screws that are used to tighten the clamping mechanism to the structure once the sensor is installed.

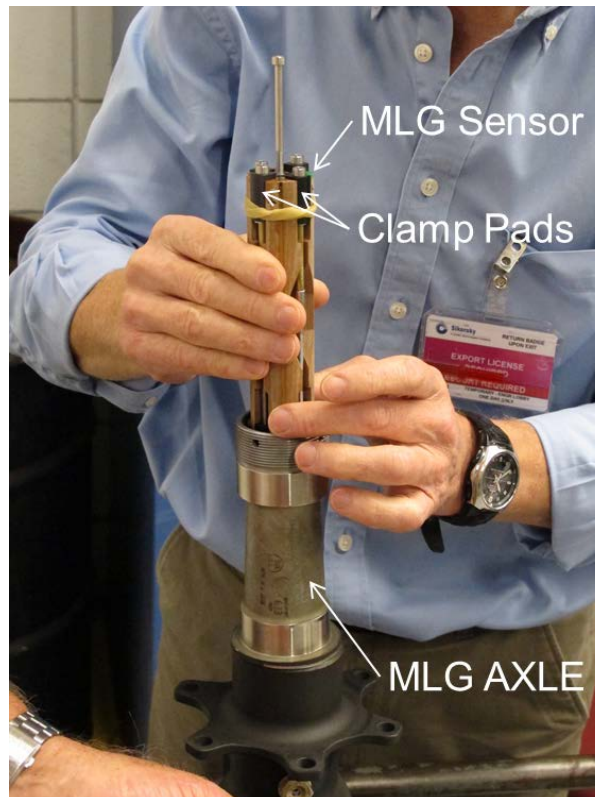


Figure 4. Optical LGLMS UH-60 MLG sensor

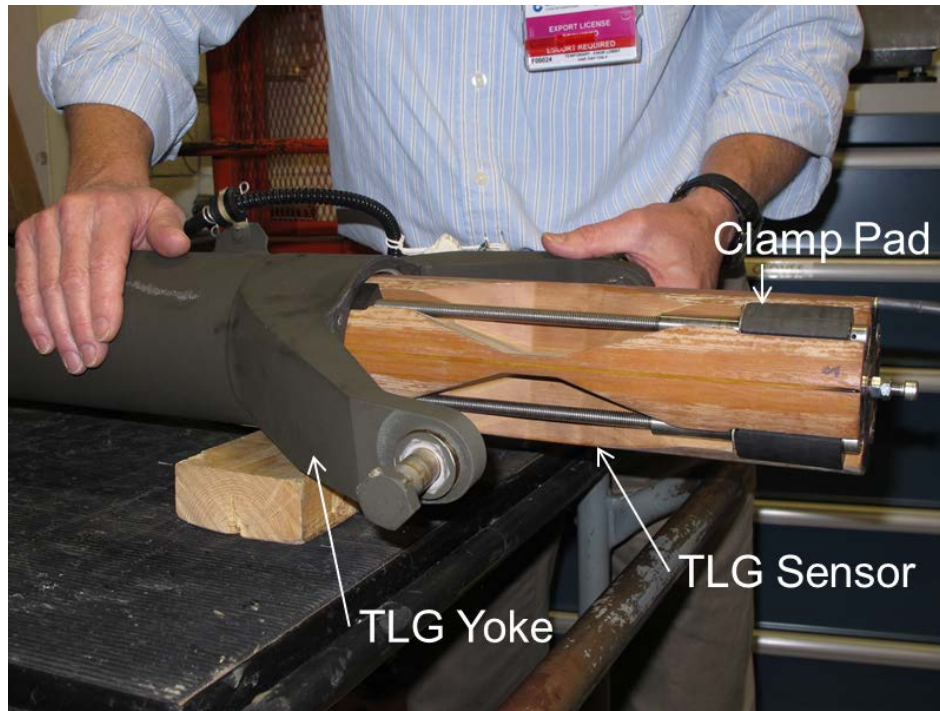


Figure 5. Optical LGLMS UH-60 TLG sensor

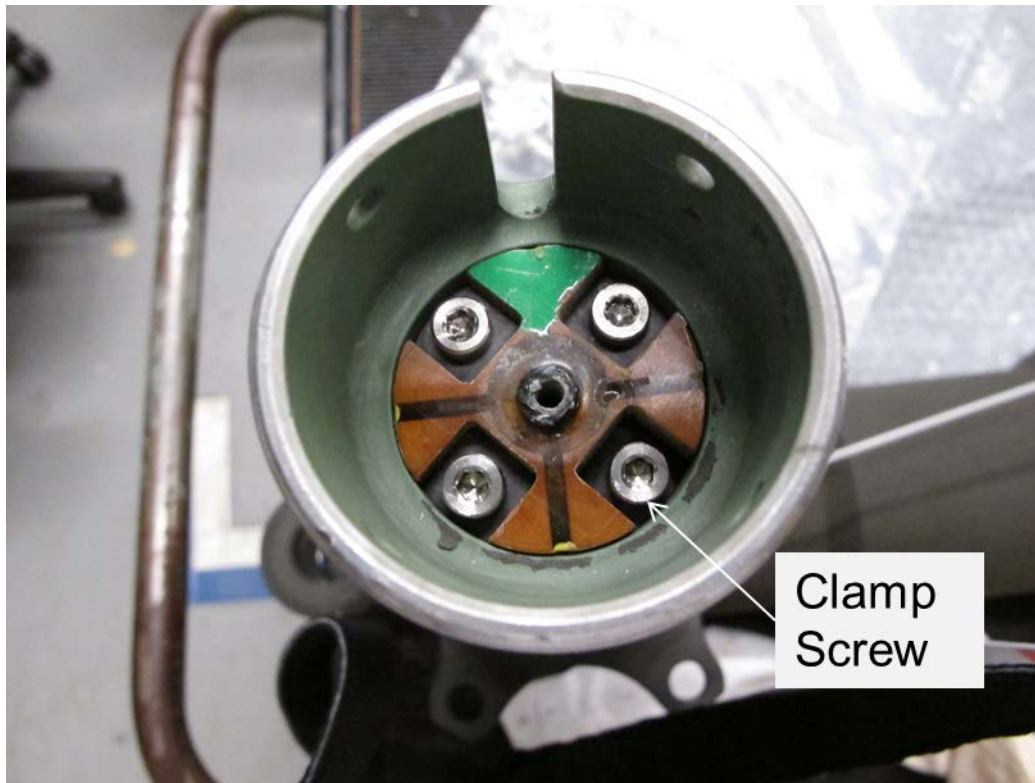


Figure 6. MLG sensor clamp screws

2.2.1.1.2 Reference Sensors

The reference sensors utilize a traditional landing gear load measurement approach of using foil strain gages in a full bridge configuration. Figure 7 shows a diagram of the reference strain gages on the airframe attachment lugs of the MLG shock strut. The TLG shock strut reference measurements were made in a similar location as the MLG shock strut, although sensors were placed on both the upper and lower ends of the TLG shock strut. The shock strut measurement location shown in figure 7 has been used on all UH-60 structural flight load survey tests that have included landing gear load assessments. The measurement captures the axial load component in the strut, which can then be related to the normal load applied to the wheel through knowledge of the strut position or assuming a nominal strut position.

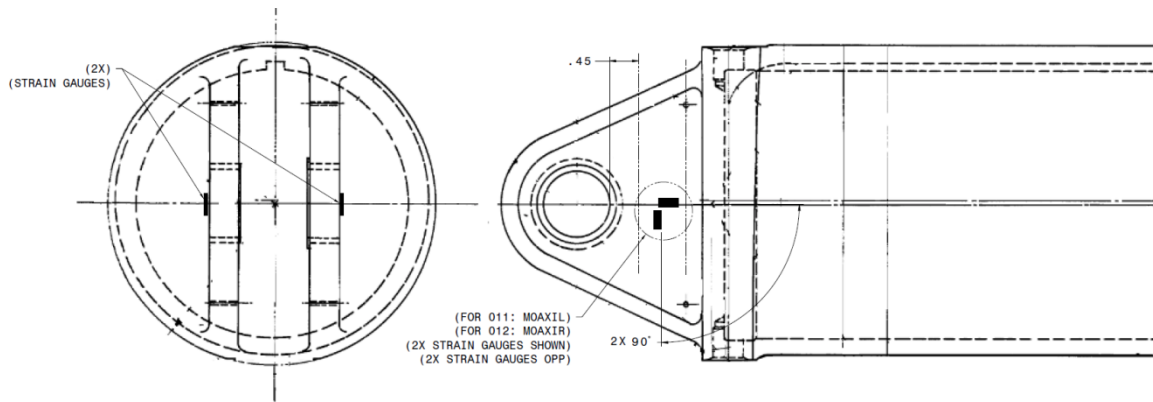


Figure 7. MLG shock strut reference sensor location

2.2.1.2 Bench Calibration

2.2.1.2.1 Optical Landing Gear Sensors

The optical LGLMS sensors were tested in two UH-60 landing gear test rigs. Figure 8 depicts the MLG, while figure 9 depicts the TLG. Bench calibration consisted of applying precise loads in uniaxial directions of the sensor. For the MLG, calibration loads were applied in the positive drag axis and positive and negative vertical axes, as shown in figure 10. For the TLG, calibration loads were applied in the positive vertical direction and positive and negative lateral direction, as shown in figure 11. While it is normally desirable to apply calibration loads to all axes and directions, some directions were not tested due to limitations of the calibration rigs and a condensed schedule allotted to offsite instrumentation and calibration in order to minimize down time for CERDEC aircraft.

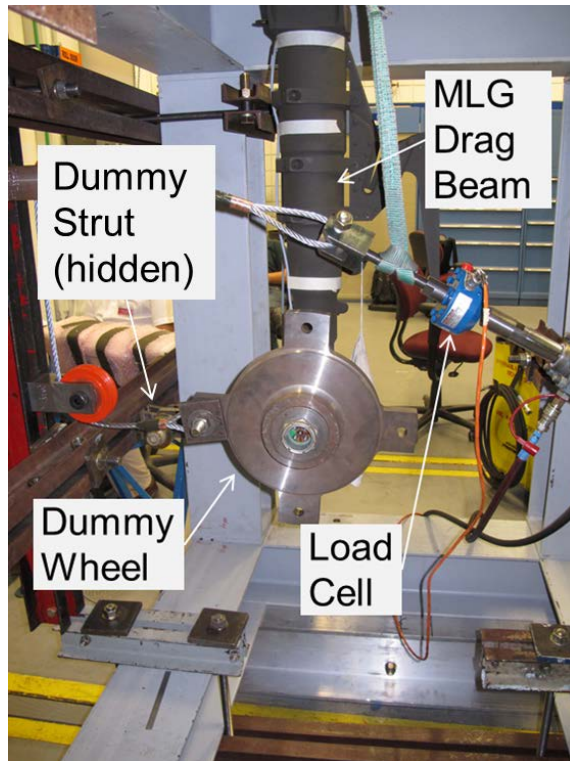


Figure 8. MLG calibration fixture

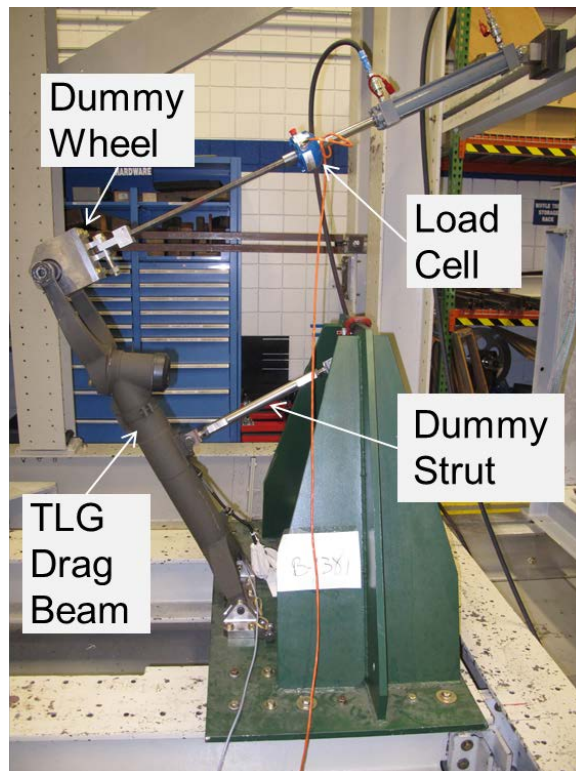


Figure 9. TLG calibration fixture

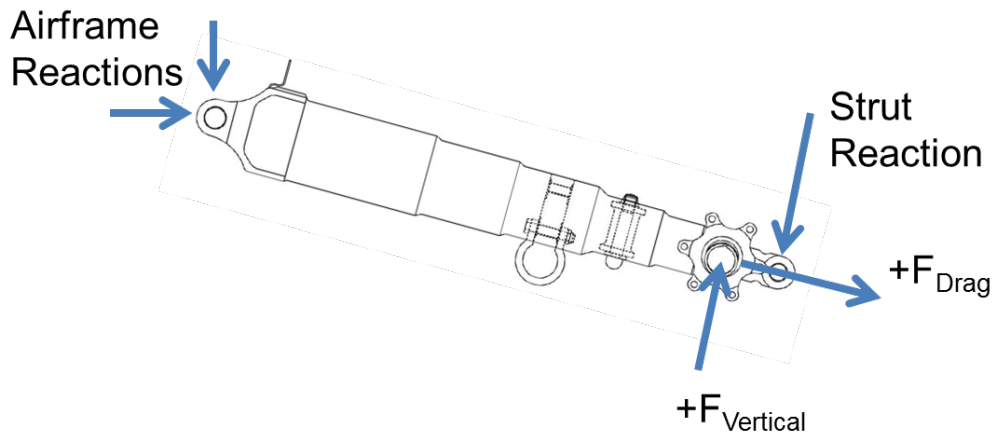


Figure 10. MLG axle calibration loads

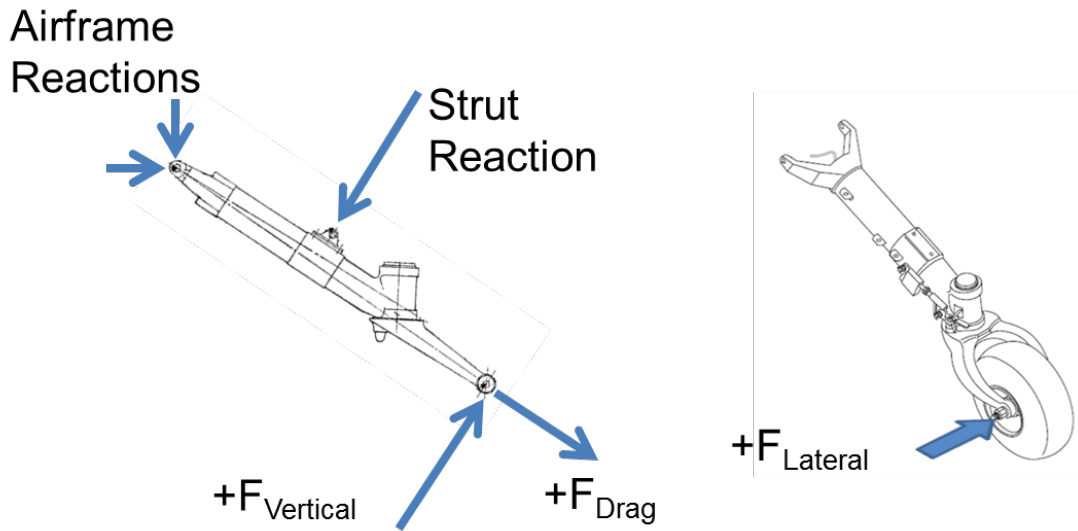


Figure 11. TLG calibration loads

The performance of the MLG sensors is shown in figures 12 and 13, in terms of vertical sensitivity and drag sensitivity, respectively. Two very notable and undesirable features of the sensitivity plots are clearly visible in these figures: 1) the response is nonlinear to load input, and 2) the responses between the right and left side FBG are dissimilar. During the calibration testing, it was also observed on several occasions that the MLG sensor output had a bias shift during the load sequence. These issues and others are discussed in more detail below.

1. The nonlinear response is believed to be due to insufficient clearance in the MLG sensor body relative to the inside diameter (ID) of the axle. The sensor body mechanism is designed to be attached to the ID of the cylindrical structure of the MLG axle or TLG yoke through the clamp pads that are located on each end of the sensor body. Between the clamp pads, the sensor body is designed to float within the cylindrical structure, with clearance between the ID of the structure and the outside diameter (OD) of the sensor body. As bending occurs in the axle structure, the clearance is reduced between the structure ID and sensor body OD. If there is insufficient clearance in the design of the sensor, then the sensor body will contact the structure that will begin to change the strain response of the sensor body and FBGs mounted in the sensor body. This theory has not been confirmed by testing, although the TLG sensor did not observe this non-linear response. It was also believed by Epsilon to have been designed with more than sufficient clearance. Epsilon believed that the MLG sensor was more at risk of contact than the TLG sensor.
2. Dissimilar response between the left and right were observed in the bench testing. The cause of this is unknown. During aircraft calibration, both the left and right sensors displayed similar output. The left sensor displayed consistent output between the bench test and aircraft test, whereas the right sensor did not.
3. The presented bench test calibration plots in figures 8 and 9 were the final test sequences conducted after several trial runs during which adjustments were made to the clamping mechanism in order to tighten the grip of the phenolic cylinder to the internal surface of the axle. These adjustments were made because of observed step changes of the sensor output during or immediately after the application of load. The step changes were always in the direction toward the initial resting strain. Following the step change in output, the load was removed, and the resting output was observed to have shifted significantly. The root cause hypothesis is that the sensor grips had slipped, thus allowing the sensor to return to a relaxed state and instantaneously reducing the strain output from the FBGs. An increase in the clamping force followed by retesting resulted in increased load-carrying capability before the point of slippage. After several iterations of increasing the clamping force, the test was completed to full calibration load without slippage and the sensor output returned to its pre-test value.
4. The FBG system was designed with a fifth unloaded strain sensor channel that would be used for temperature compensation. It was found that the temperature compensation channel was significantly straining with load, rendering this channel unreliable for use with temperature compensation.

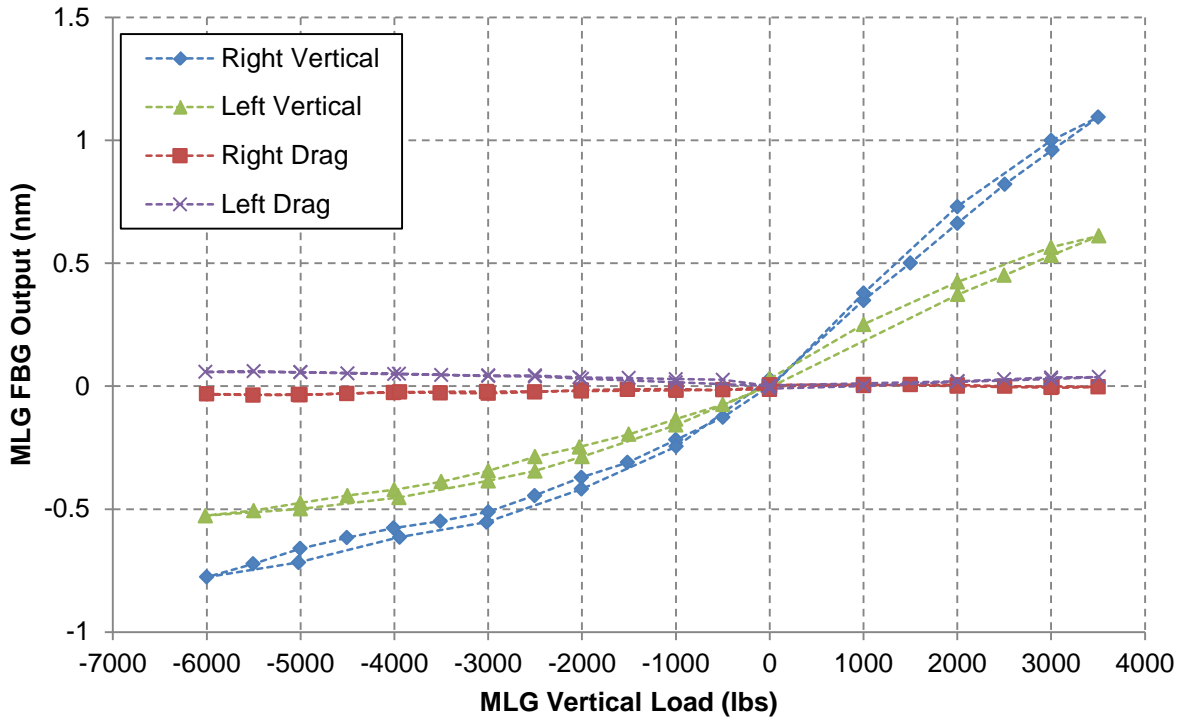


Figure 12. Optical LGLMS vertical sensitivity (right and left MLG)

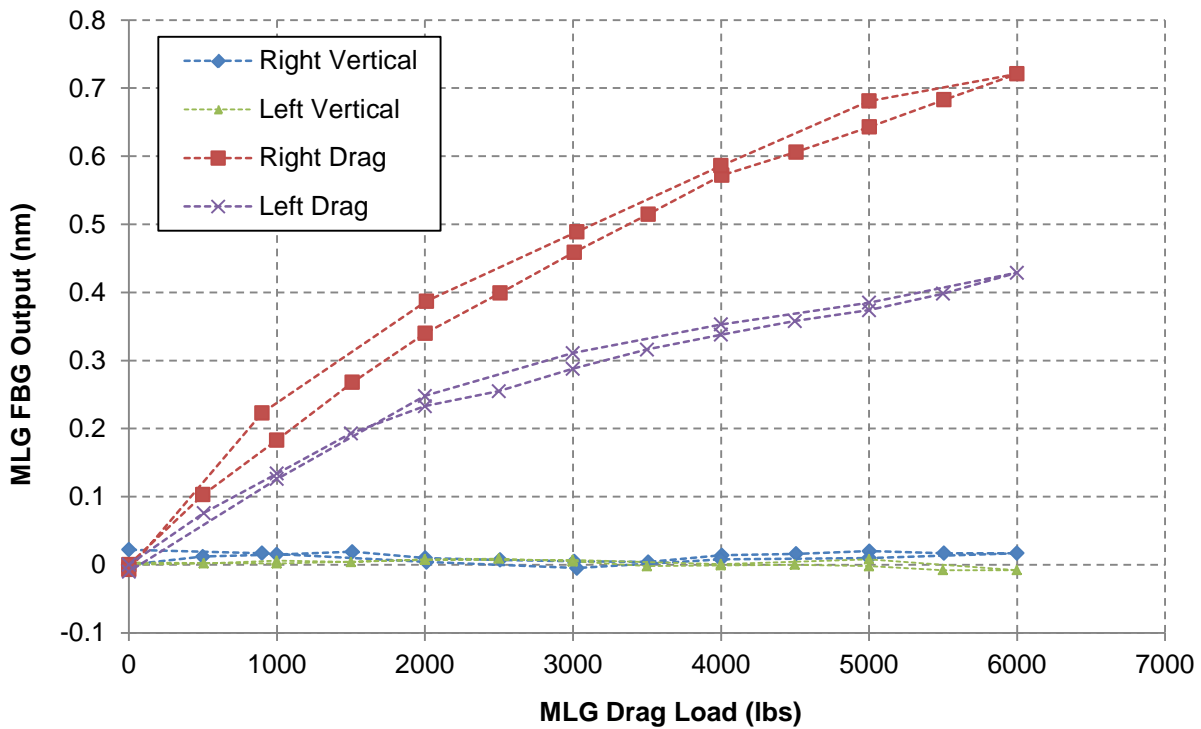


Figure 13. Optical LGLMS drag sensitivity (right and left MLG)

Performance of the TLG sensor during the bench calibration (shown in figure 14 for vertical sensitivity and figure 15 for lateral sensitivity) was excellent in that it displayed linearity in both the vertical and lateral direction. The lateral sensor output was approximately 6% of the vertical strain during vertical load cases, and the vertical sensor output was 6% of the lateral strain during lateral load cases. This symmetry in the cross talk between vertical and lateral directions likely indicates an imperfect sensor alignment relative to the loading axes. The only observed problem with the TLG sensor is that the fifth temperature compensating channel was significantly strained with applied load, rendering this channel unreliable for use in temperature compensation.

The calibration testing provided an opportunity for early risk reduction of the prototype sensors prior to flight testing. The issues that were observed in the MLG sensors would normally be sufficient to warrant a redesign prior to flight testing; however, it was agreed among SAC, Epsilon, CERDEC, and the FAA that the reference foil-gage strut sensors, combined with a functional Epsilon tail FBG sensor, provide enough data to conduct a meaningful flight test to provide insight into sensitivity of GW and CG calculations to various ground conditions (e.g., ground idle, flat pitch) and into dynamic landing loads. The MLG sensors were still installed in the CERDEC aircraft, and aircraft calibration test results for the MLG sensors are provided as well as those for the TLG.

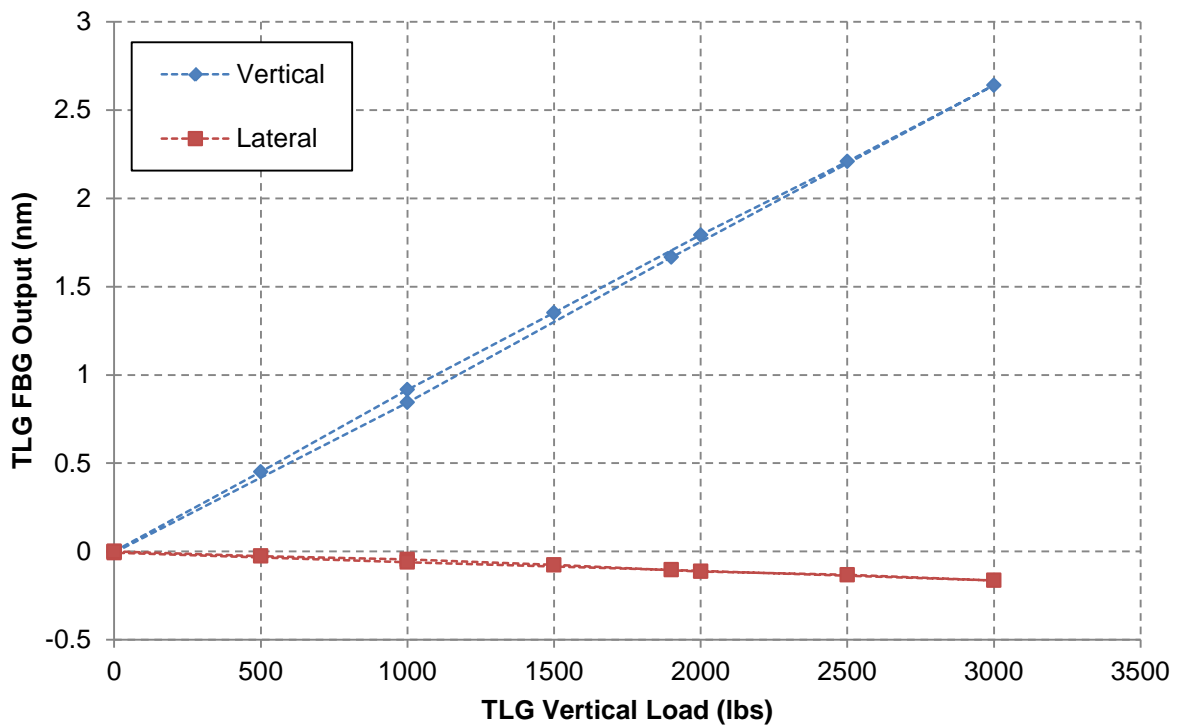


Figure 14. Optical LGLMS vertical sensitivity (TLG)

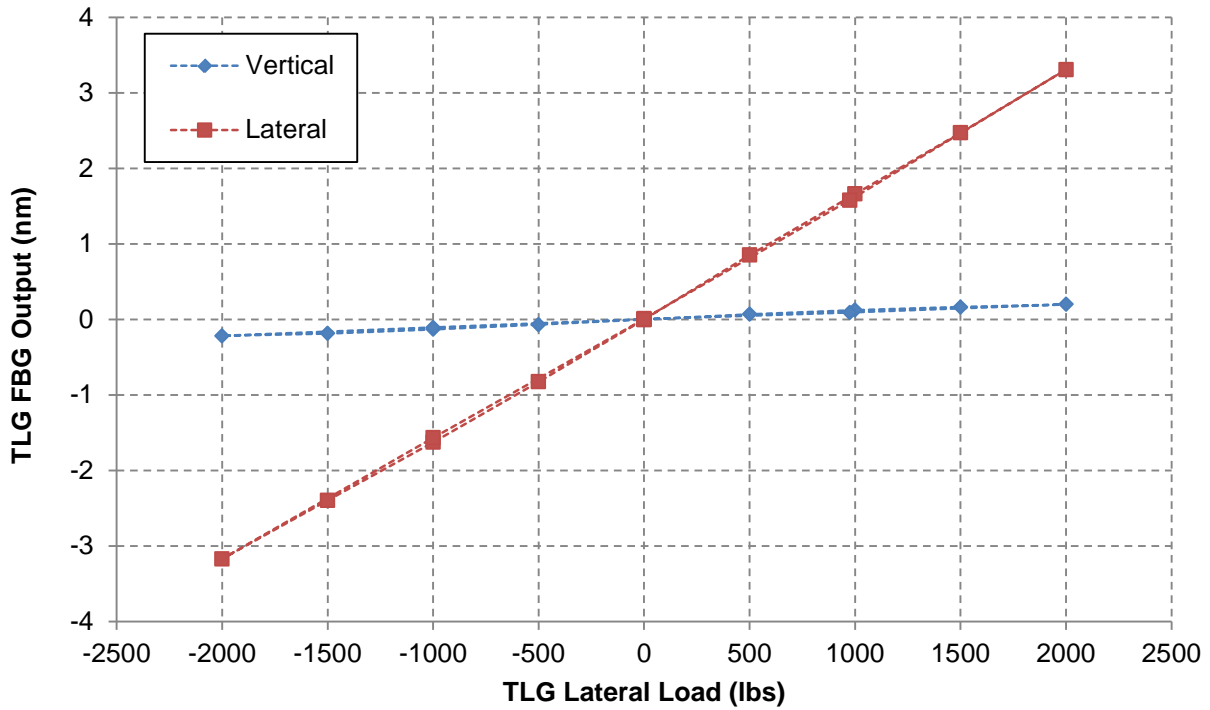


Figure 15. Optical LGLMS Drag sensitivity (TLG)

2.2.1.2.2 Reference Sensors

The reference strut sensors were calibrated in a uniaxial load fixture according to SAC standard work practice specific to aircraft struts. The calibration fixture is shown in figure 16. As part of the calibration standard work, results for commonly calibrated components are compared with results from previous calibrations. The main and tail struts passed this comparison test. Results from the calibration are shown in figure 17 for the left and right main strut sensors and in figure 18 for the tail strut sensors. The MR strut sensors displayed excellent results in linearity, repeatability, and similarity between left and right. The two tail rotor strut load measurements displayed non-linear behavior, but they are consistent with results from previous calibrated landing gear sensors.



Figure 16. Calibration fixture for strut sensors

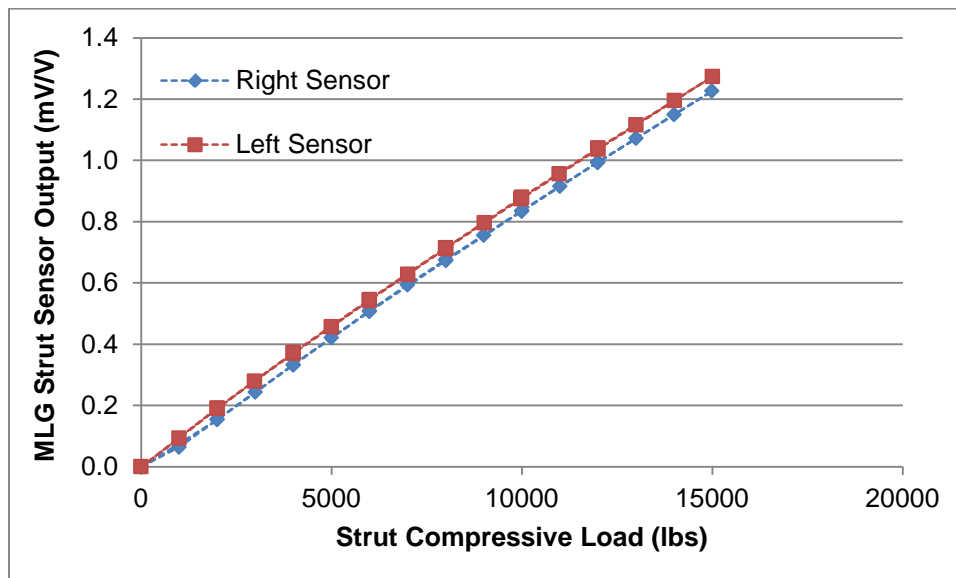


Figure 17. Right and left main strut calibration sensitivity plot

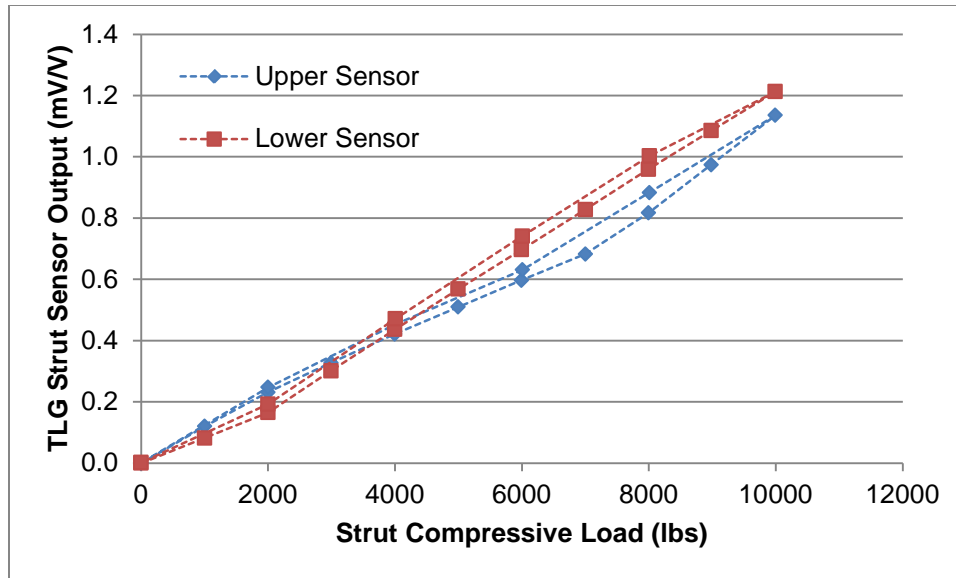


Figure 18. Tail strut upper and lower calibration sensitivity plot

2.2.1.3 Aircraft Calibration

Aircraft calibration of the three landing gears and struts was performed using both platform scales and lifting jacks, as shown in figure 19 and as described in the following procedures:

1. With aircraft weight fully on the scales and at complete rest, a manual record of the displayed weight on each scale was made along with the measured angle of each drag beam relative to the horizontal plane using a digital inclinometer.
2. The aircraft was then jacked up completely off the scales.
3. Once the aircraft was sufficiently at rest, a 5-second data capture was made on the CERDEC data acquisition system to record all sensor outputs from both the optical LGLMS and reference sensors.
4. Each MLG was then jacked down by 1,000 lbs by reading the weight reduction directly from the jack load cells.
5. The TLG was simultaneously jacked down according to a foreman's verbal direction to achieve the required level tolerance as indicated by a plumb bob in the cabin door frame.
6. Simultaneous to, or immediately preceding, step 5, a 5-second data capture was made on the CERDEC data acquisition system to record all sensor outputs from the optical LGLMS and reference sensors.
7. Once the aircraft was sufficiently at rest, a manual record of the displayed weight on each scale was made along with the measured angle of each drag beam relative to the horizontal plane.
8. Steps 3–7 were repeated until the aircraft was fully on the scales, capturing a data point in the WOW position.
9. Reverse procedure was followed until the aircraft was fully off the scales, capturing the last data point in the weight-off-wheels position.
10. The aircraft was lowered back to the scales and a final reading taken on the CERDEC data acquisition system.

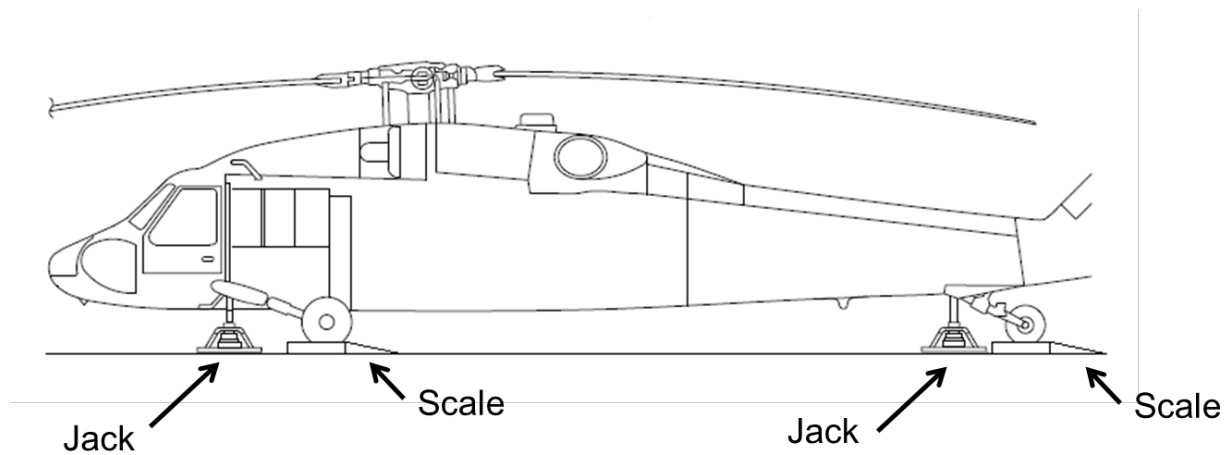


Figure 19. Aircraft calibration setup diagram

The calibration data were analyzed by comparing the measured wheel load versus sensor output for all three optical LGLMS sensors and reference strut sensors. For the optical LGLMS sensors, a comparison of the wheel load to sensor output was only made for the vertical load axis, as this is the primary axis through which the wheel load is applied.

2.2.1.3.1 Optical Landing Gear Sensors

The optical LGLMS MLG output versus applied wheel load is shown in figure 20. A significant bias shift was observed in both left and right MLG sensors between the initial WOW condition and the final WOW condition, which is similar to that observed during the original bench calibration. This behavior is somewhat expected based on the fact that the bench calibration test exhibited this same behavior after several iterations of increasing clamping force. Further, the clamping force was only adjusted to accommodate the calibration loads, which were less than half of the total expected WOW load (based on limitations of the calibration rig). In addition, a hysteresis band of approximately 0.2 nm, or roughly 25% of the full-scale range of 0.8 nm, was observed after the initial bias shift. Based on these results, the MLG sensors were not considered to be a reliable source of landing gear load information during the flight test.

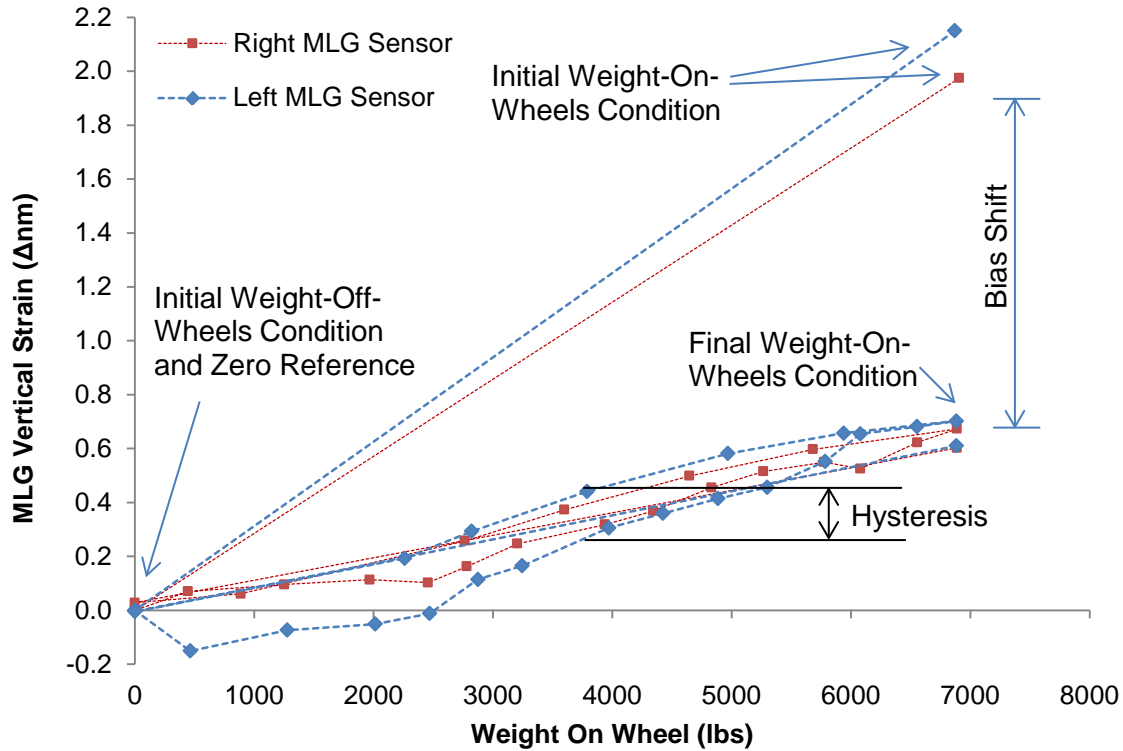


Figure 20. Optical LGLMS MLG A/C calibration sensitivity

The aircraft calibration results for the optical LGLMS TLG sensor are shown in figure 21. The TLG exhibited non-linear behavior not observed in the bench calibration. This is due to the angular displacement of the landing gear during the application of load. The bench calibration was performed with uniaxial loading in the vertical direction, defined as perpendicular to the tail yoke. Because the landing gear angle changes with strut position and load, the angle of the applied load changes as well. To correct for this during the calibration, precise angular measurements were made on the yoke that allow the wheel load to be translated to vertical load in the yoke axis. This translation also allows a direct comparison between the aircraft and bench calibration results, which are shown in figure 22. The corrected load calibration curves are well-behaved. It becomes apparent from these results that knowledge of the strut position can enhance the accuracy of the landing gear sensors, although a performance penalty in terms of accuracy may be acceptable in order to avoid the cost of adding new sensors. Because strut positions were not measured during the flight test phase, the error induced by strut displacement is a main component of the total observed sensor error.

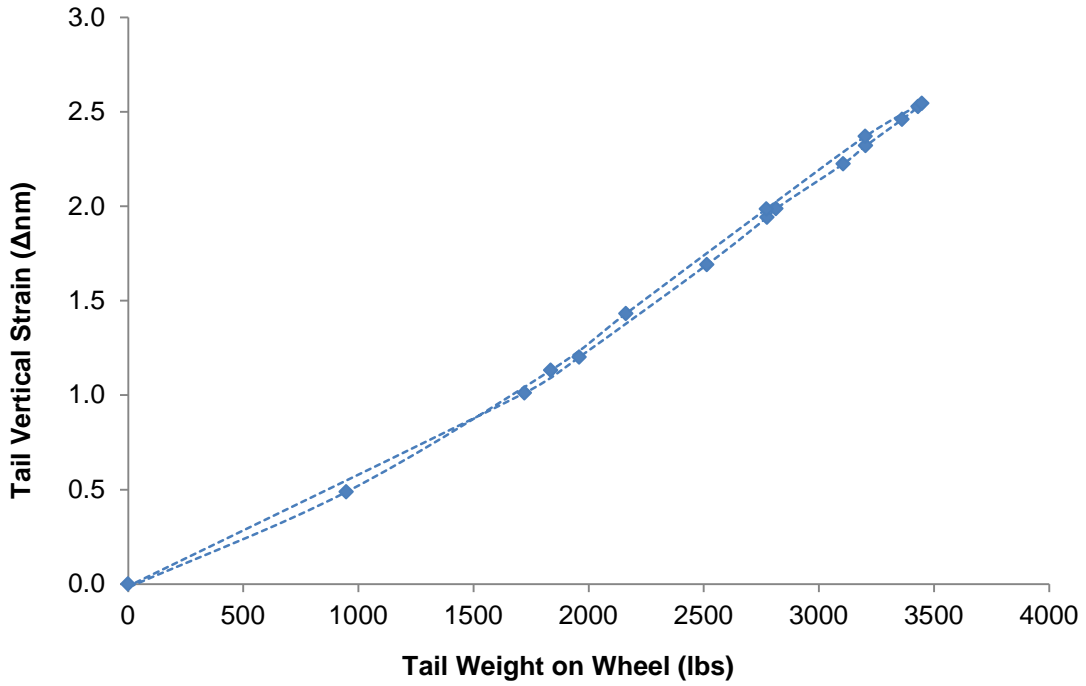


Figure 21. Optical LGLMS TLG A/C calibration sensitivity

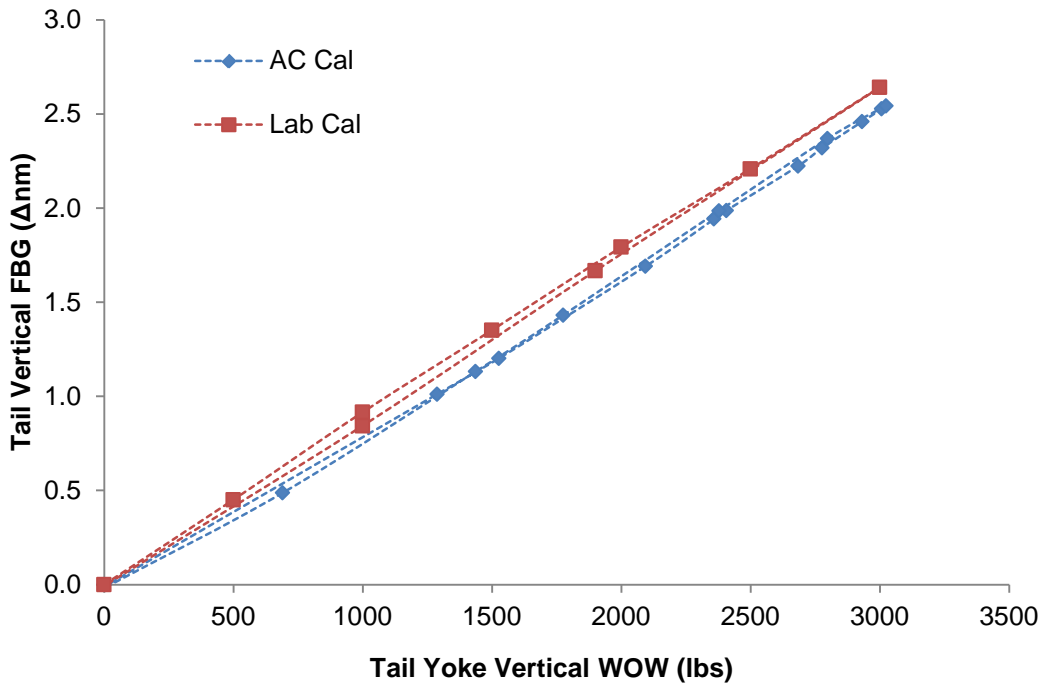


Figure 22. Optical LGLMS TLG A/C calibration sensitivity—corrected to yoke axis

2.2.1.3.2 Reference Sensors

The MLG strut sensitivity results are shown in figure 23, with the TLG results shown in figure 24. During the aircraft calibration, the MLG strut sensors performed similar to how they performed in the bench calibration. Excessive non-linearity in the TLG sensors was observed, which is likely due to a combination of the non-linear effect of strut displacement of the tail and non-linear features observed in the uniaxial bench calibration.

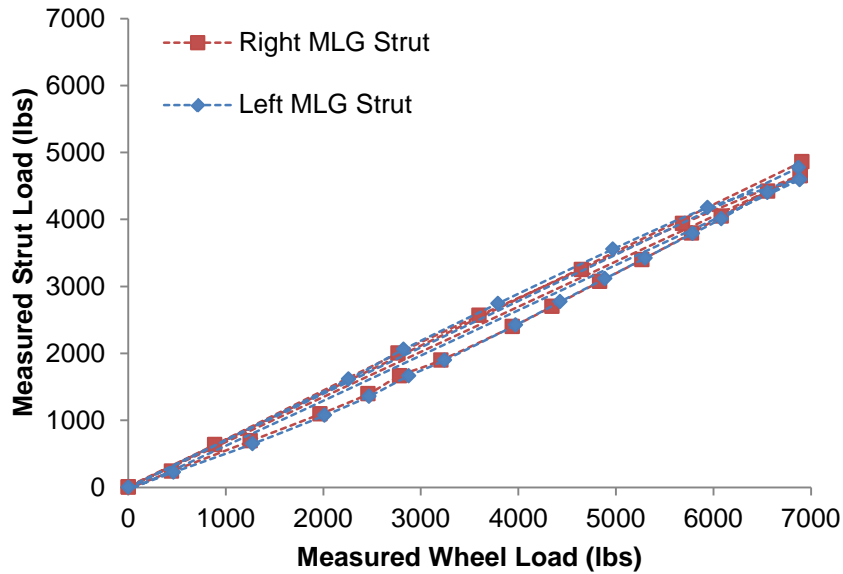


Figure 23. MLG strut sensor A/C calibration sensitivity

2.2.1.3.3 GW/CG Measurement System

The results from the optical LGLMS and reference sensor evaluations indicate that for the purposes of the subject R&D effort, the best combination of sensors to estimate GW and CG is the optical LGLMS TLG sensor combined with the reference MLG strut sensors. For the subsequent analysis of flight test data, GW and CG estimates were performed using this combination of sensors.

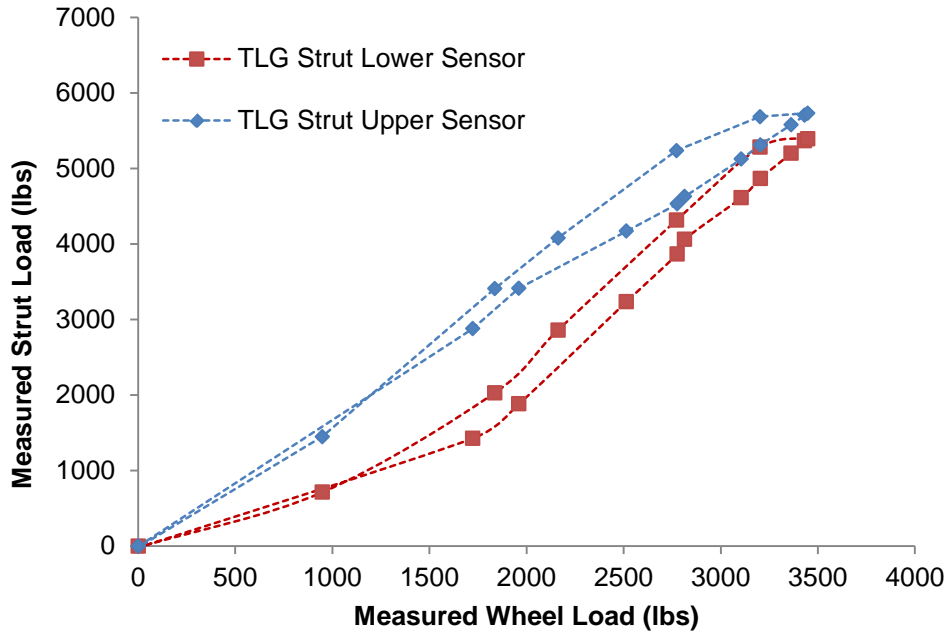


Figure 24. TLG strut sensor A/C calibration sensitivity

2.2.1.4 Flight Test Data

2.2.1.4.1 IVHMS GW Estimation

To evaluate the performance of the GW/CG sensor system during the flight tests, an independent truth GW and CG were required for comparison against the sensor data at various points throughout the flight test program. To accomplish this, the existing IVHMS onboard GW calculator was used, which operates by establishing a starting GW using pilot input and updating GW over time using the fuel tank levels indicated by fuel level gages. The aircraft was precisely weighed on platform scales before and after each flight in order to assess the accuracy of the IVHMS GW estimator. The pre- and post-flight GW and CG values are listed in table 3. Using these data, a quick assessment of the IVHMS GW estimator performance, which is shown in figure 25, was conducted. The IVHMS GW estimator was demonstrated to be excellent at calculating changes in GW, provided the starting GW input by the pilot was accurate. Average error was approximately 100 lbs. for both the pre- and post-flight estimates, which means the estimator is sufficiently trending the GW change over time using fuel consumption as measured by the fuel level gages.

Table 3. Pre- and post-flight GW and CG values

Pre-Flight Values

Flight Number	Date	A/C Calculated GW	LMG Scale	RMG Scale	TLG Scale	Scale GW	Calculated CG
1	11/19/2014	18,003	7,590	7,082	3,342	18,014	362.4
2	11/25/2014	17,189	7,176	6,858	3,134	17,168	361.3
3	12/03/2014	16,355	6,720	6,572	3,064	16,356	363.0
4	12/10/2014	22,080	9,177	9,306	3,578	22,061	354.3
5	12/19/2014	20,509	8,748	8,746	3,300	20,794	353.1
6	12/19/2014	19,358	7,870	8,042	3,242	19,154	356.7

Post-Flight Values

Flight Number	Date	A/C Calculated GW	LMG Scale	RMG Scale	TLG Scale	Scale GW	Calculated CG
1	11/19/2014	16,971	7,072	6,880	2,980	16,932	359.1
2	11/25/2014	16,390	6,840	6,620	2,878	16,338	359.1
3	12/3/2014	15,368	6,265	6,358	2,702	15,325	359.2
4	12/10/2014	20,499	8,420	8,425	3,440	20,285	356.8
5	12/19/2014	19,358	7,870	8,042	3,242	19,154	356.7
6	12/19/2014	17,485	7,288	7,290	3,008	17,586	357.4

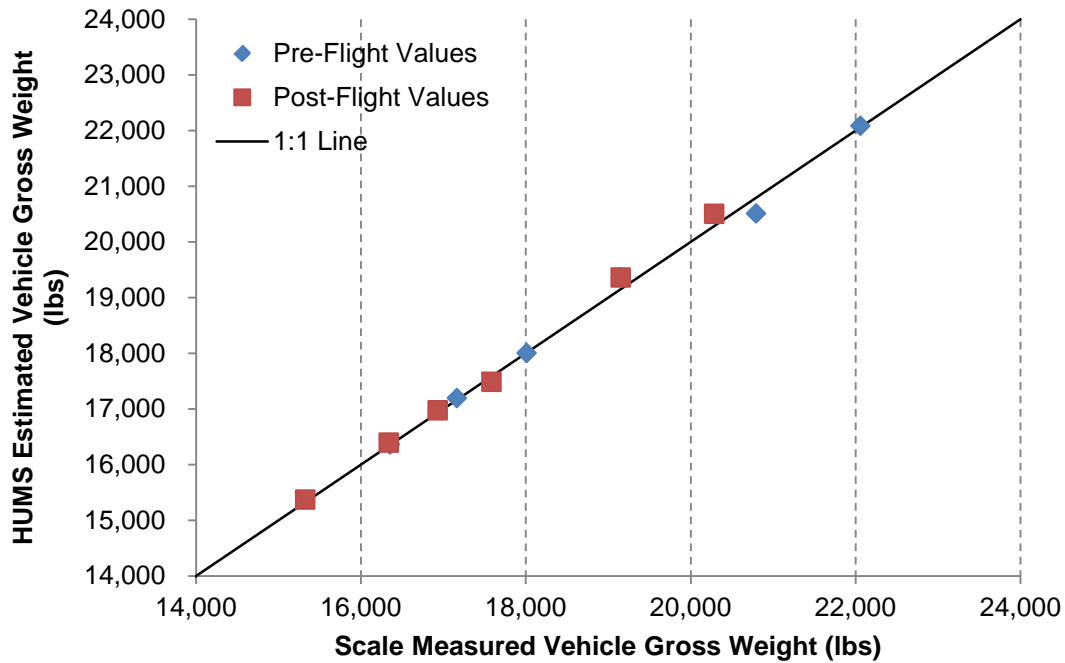


Figure 25. IVHMS GW estimator performance

2.2.1.4.2 GW Measurement

Using the landing gear measurement system, which is composed of the optical LGLMS TLG sensor and the reference MLG sensors, a derived GW parameter was created that can be plotted across time. The derived GW parameter for Flight #1 is shown in figure 26. The plot is organized using color codes to indicate various phases of the flight. The light blue portion represents the rotor off condition before the flight. The light green region shows the ground idle condition when the rotor is operating at roughly 50% rotor speed. The red region is indicates the rotor is operating at 100% rotor speed in a flat pitch condition. The darker blue region indicates when the aircraft is in a taxi condition, which is detected by the WOW sensor and Global Positioning System ground speed data. The grey section indicates when the aircraft is off the ground, defined only by the WOW sensor. The white section indicates when the aircraft does not fall directly into one of the above defined categories.

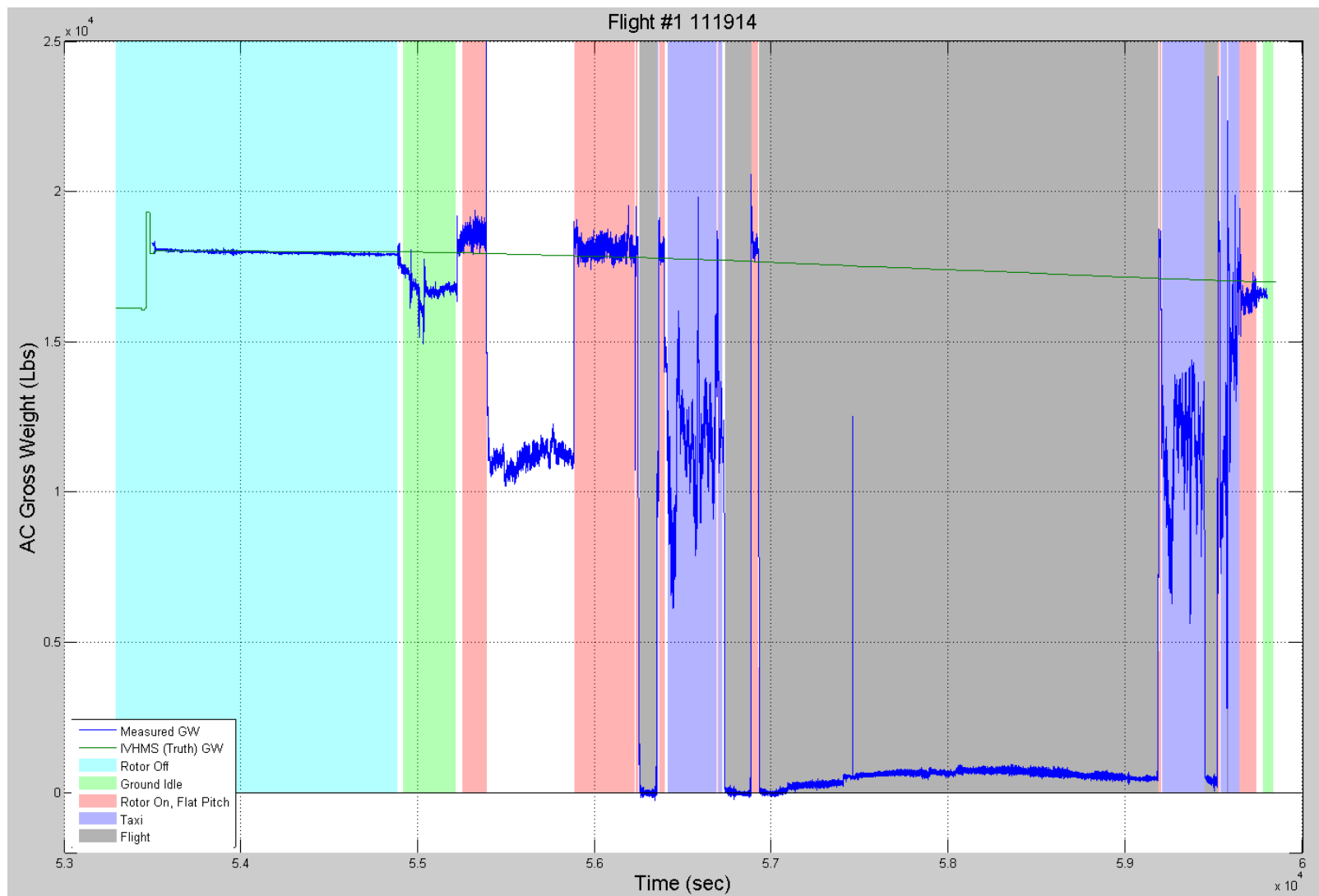


Figure 26. GW derived parameter plot for Flight #1

Several observations can be made from this plot regarding the ability of the GW sensor system to accurately measure the GW of the helicopter. First, the GW measurement is very accurate during the initial rotor off condition. The sensor-based GW measurement is shown by the dark blue curve while the IVHMS GW estimate, which is used as the “truth” or reference GW, is shown by the green curve. As the rotor spins up to ground idle, the sensor-based GW measurement decreases, as if the rotor disk were imparting some amount of lift to the airframe. As the rotor turns up to 100% rotor speed, the GW measurement increases, as if the rotor disk were imparting downward thrust to the vehicle. After review of this behavior with the flight test pilot, it was found that this is the expected behavior of the GW measurement given the normal aircraft start-up sequence. As the rotor spins up to the ground idle condition, the collective blade pitch is raised in order to allow the rotor to fly easier to lift the rotor blades up off the droop stops. As the rotor transitions from ground idle to 100% rotor speed, the collective pitch is simultaneously dropped in order to keep the blades flying in a flat pitch condition, as the centrifugal force at 100% NR is sufficient to keep the blades off the droop stops. After the rotor has been in the flat pitch condition for approximately 3 minutes, the GW estimate suddenly drops by nearly 50%. This is due to the pilot initiating an engine health test, during which the collective is raised to partially load up the engines, which creates a light-on-wheels scenario. These observations are better explained by viewing the GW measurement along with the collective position during the ground conditions, as shown in figure 27. Here, it is observed, as expected, that the measured GW by the landing gear sensors is significantly affected by both the rotor condition (idle versus 100%) and collective position. Achieving an accurate GW measurement from a landing gear sensor while the rotor is turned on will involve monitoring these parameters for appropriately defined measurement capture windows.

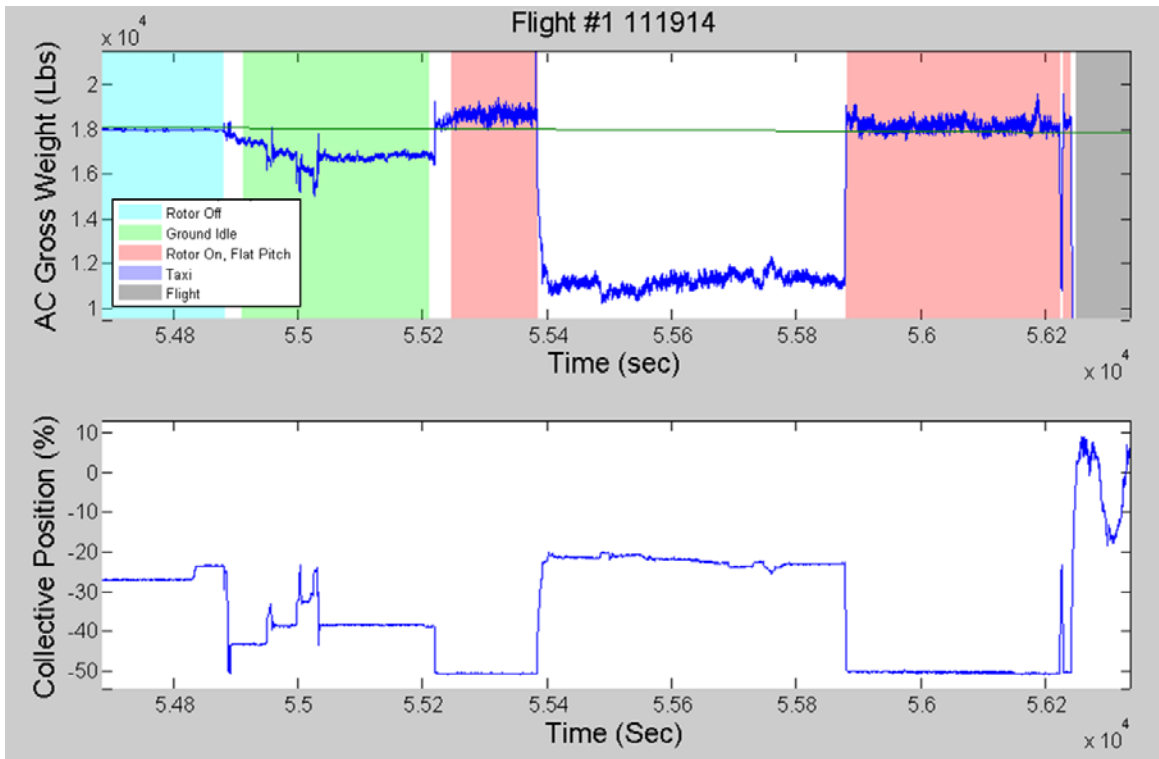


Figure 27. Flight #1 GW sensor output during ground ops

Using the data from the rotor off, ground idle, and flat pitch ground conditions, a correlation plot was created based on the pre-flight and post-flight values from the flight test. The results, shown in figure 28, indicate that the observations from Flight #1 were consistent across all flights. The rotor-off condition was the best condition for accurate measurement of GW, while the ground-idle condition consistently resulted in a lower GW measurement and the flat-pitch condition consistently resulted in a higher GW measurement for the reasons summarized above. Error statistics for each of these three conditions are shown in table 4. The rotor-off condition produced a mean error of -67 lbs and a 1-sigma error of 476 lbs—or approximately 2% of the maximum tested GW of 22,000 lbs. On average, the ground idle condition measurements underestimated by 800 lbs. and the flat pitch condition measurements overestimated by 770 lbs. A holistic GW measurement approach for production use should develop appropriate capture windows and correction factors based on measurements of other aircraft state parameters (e.g., revolutions per minute [RPM], collective) to provide maximum opportunity for measurements and address known uncertainties during various pilot start-up procedures.

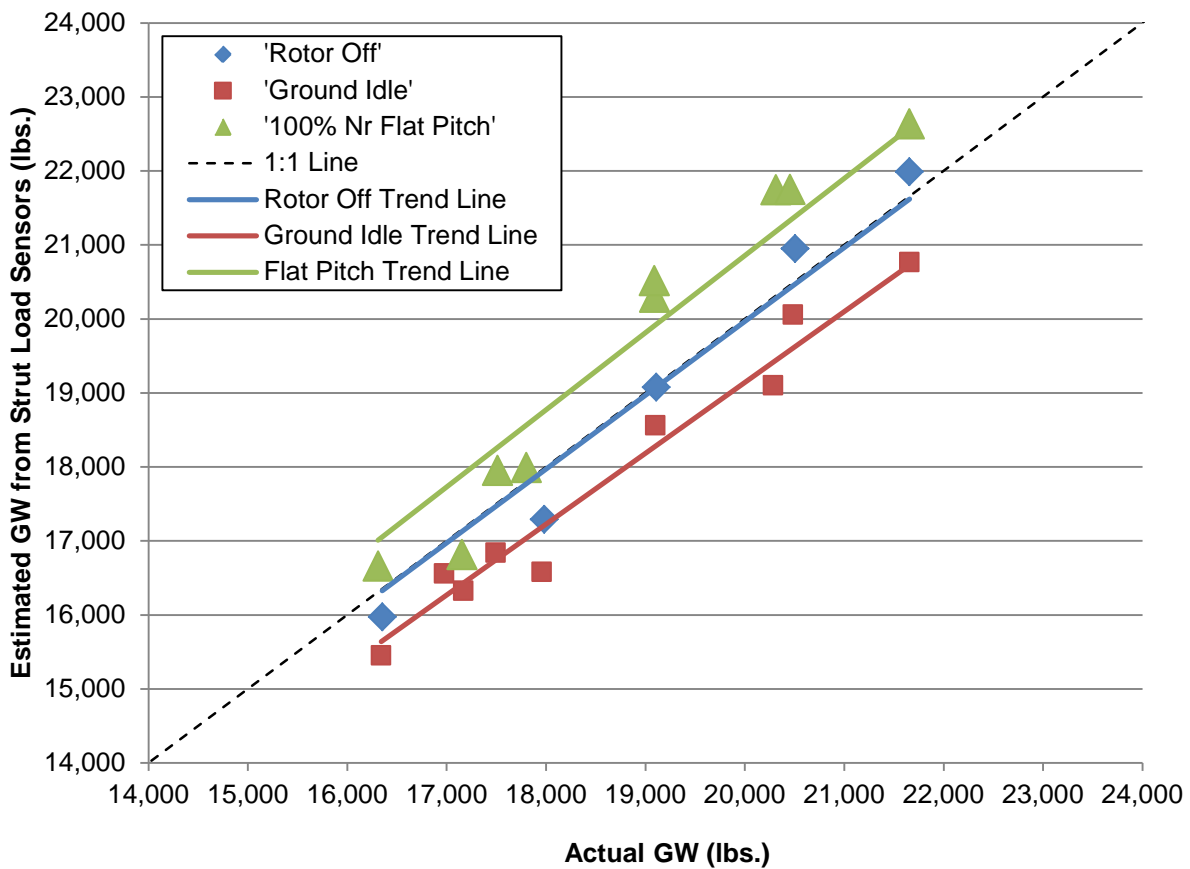


Figure 28. GW measurement performance

Table 4. GW measurement performance metrics

	Rotor Off	Ground Idle	Flat Pitch
Mean Error (lbs)	-67	-802	772
1-sigma Error (lbs)	476	331	634
Max Error (lbs)	691	1,377	1,429

2.2.1.4.3 CG Measurement

The aircraft longitudinal CG was calculated from the landing gear sensor data by assuming nominal wheel positions in the aircraft longitudinal axis, although in reality the position of the wheel on the ground can vary by as much as four inches due to variations in vehicle GW and strut condition. Figure 29 shows the results from the CG measurements made using the landing gear sensors during the rotor-off conditions. The rotor-off condition immediately before each flight was used to measure CG from the sensors because those are the only conditions in which the actual CG is accurately known. Ground-idle and flat-pitch conditions were not considered here because of the known wheel load bias created by the rotor loads.

CG measurements were observed to trend with the known CG using a best fit line, although a 1-sigma error of about 3 inches, or roughly 12% of the total UH-60 CG range of 342–366 inches, was observed. Results for CG measurements are susceptible to more sources of error than the GW measurements due to the assumption of nominal strut positions. Knowledge of the strut positions, derived from accurate measurements in production aircraft, could possibly reduce this uncertainty.

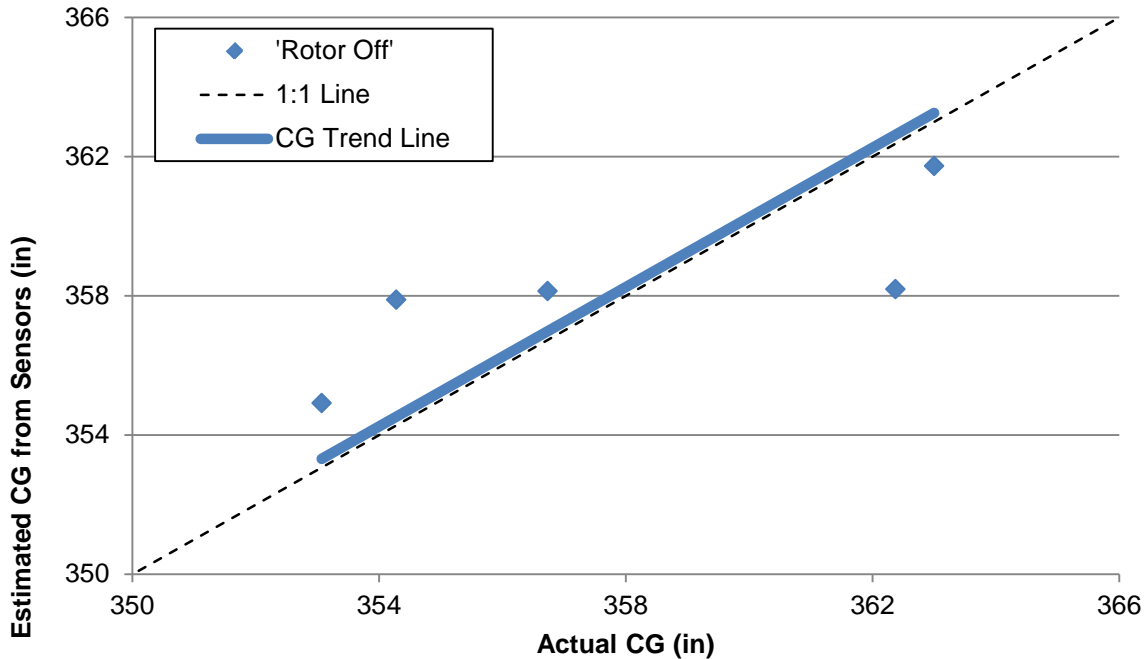


Figure 29. CG measurement performance

2.2.1.4.4 Temperature Sensitivity

Both the Epsilon TLG sensor and reference MLG strut sensors were found to be sensitive to temperature by comparing in-flight sensor output against measured outside air temperature from the aircraft's air data system. This approach to assessing temperature sensitivity is not precise because the air temperature does not equate to the temperature of the landing gear, and the assessed flight conditions (hover and LF) are not true unloaded conditions because the aerodynamics may be applying non-trivial loads to the landing gear. When transitioning from the hangar to the outside, the landing gear may be transitioning from a stable 55° F to the ambient 30° F conditions over a period of roughly an hour. While imprecise, the approach does indicate a linear relationship between sensor output and temperature. Figure 30 shows the reference MLG sensor output for various in-flight conditions plotted versus outside air temperature. An output range of roughly 0.035 MV/V was observed, relative to a full-scale range of at max GW of 0.600 MV/V, which means that the temperature sensitivity of the reference sensors can influence the wheel load measurement by roughly 6% over the range of tested flight temperatures. Figure 31 shows this same data for the Epsilon TLG sensor with a range of roughly 0.35 nm, relative to a full-scale range at max GW of 2.9 nm. The temperature sensitivity of the Epsilon TLG sensor can influence the tail wheel load result by as much as 12%. It should be noted that the SAC reference measurement is made using a full Wheatstone bridge strain gage system, which is designed to cancel temperature effects that equivalently strain the unloaded legs of the bridge. However, the Wheatstone bridge in this application may only be alleviating the effect of temperature variation rather than eliminating it. On the other hand, the TLG sensor data has no temperature mitigation applied to it. As noted in section 2.2.1.2.1, the temperature compensating channel was found to be unreliable and therefore not used to correct the Epsilon TLG strain output for temperature.

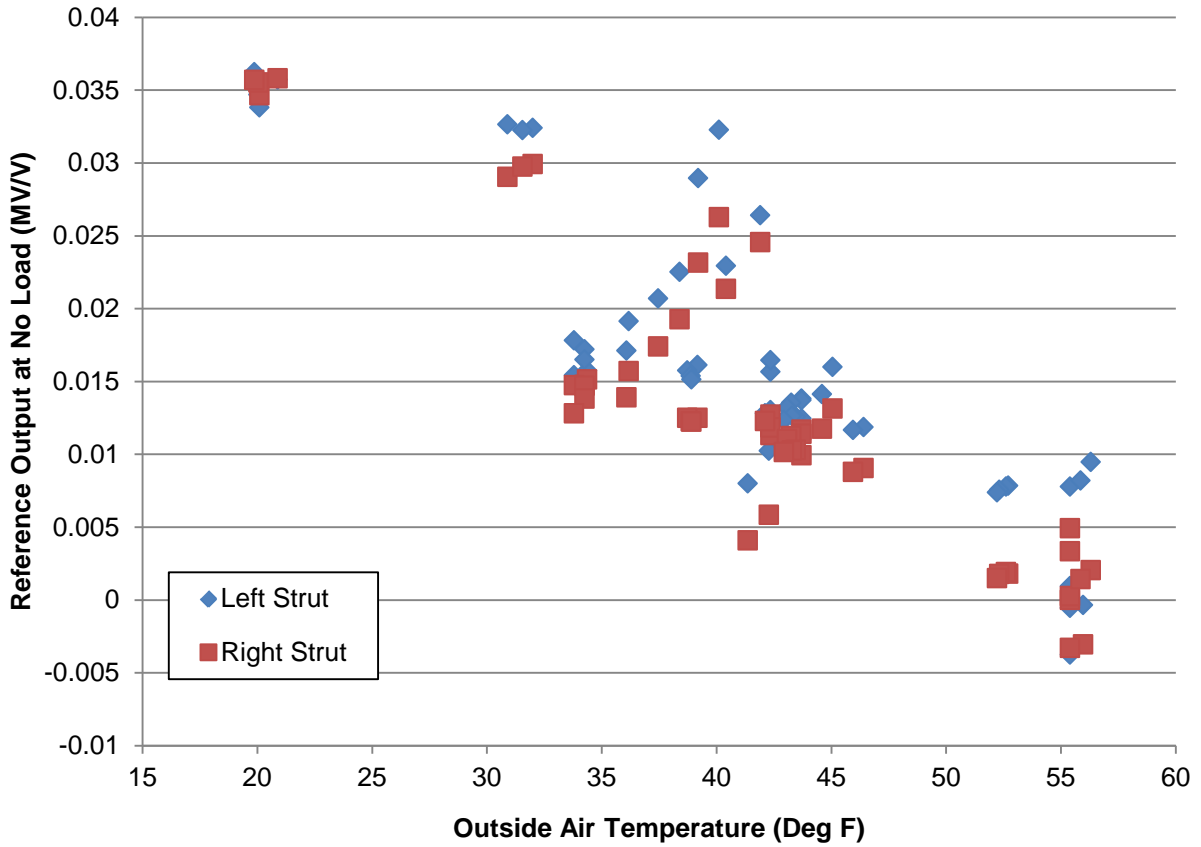


Figure 30. MLG strut in-flight output versus outside air temperature

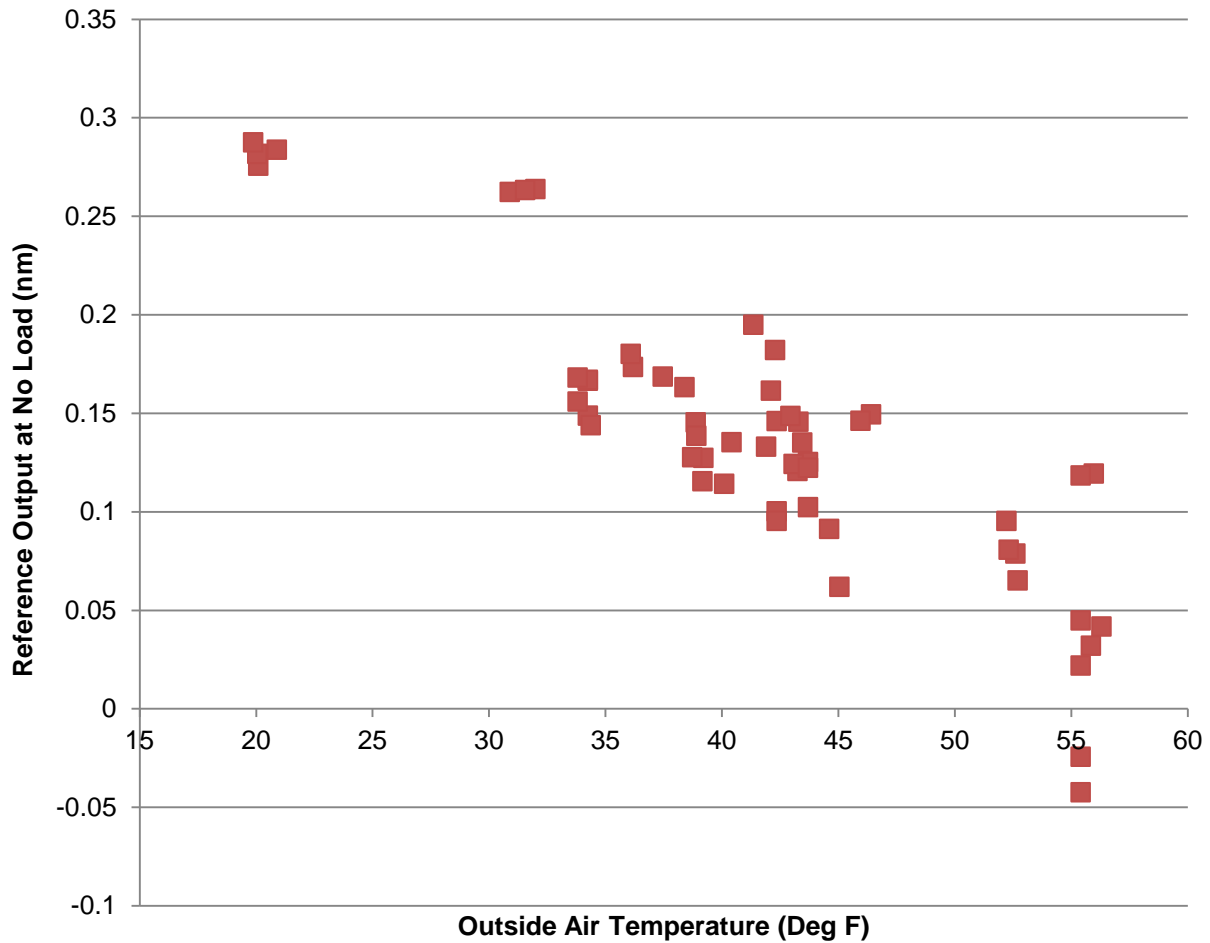


Figure 31. Epsilon TLG in-flight output versus outside air temperature

2.2.1.4.5 Other Applications of Landing Gear Sensors

While the focus of this project was to demonstrate the ability to measure vehicle GW with landing gear sensors, there are several other applications of landing gear sensors that were captured in figure 32 during a heavy landing event. WOW switches are the current standard method for determining if the aircraft is on the ground; however, WOW switches typically require several thousand pounds of force applied to the gear in order to actuate the switch. Future fly-by-wire flight control systems will require knowledge of ground contact well before traditional mechanical WOW switches will actuate. Figure 32 shows that the landing gear load sensors detected ground contact through the tail wheel eight seconds prior to the WOW switch actuating. Load was sensed on all three wheels 3 seconds prior to actuation of the WOW switch. In addition to sensing ground contact, the right wheel load sensor also recorded a peak transient landing load. Detection of load exceedances for specific gear or tracking of fatigue cycles over the lifetime of the gear are additional important capabilities that are enabled by a robust landing gear load monitoring system.

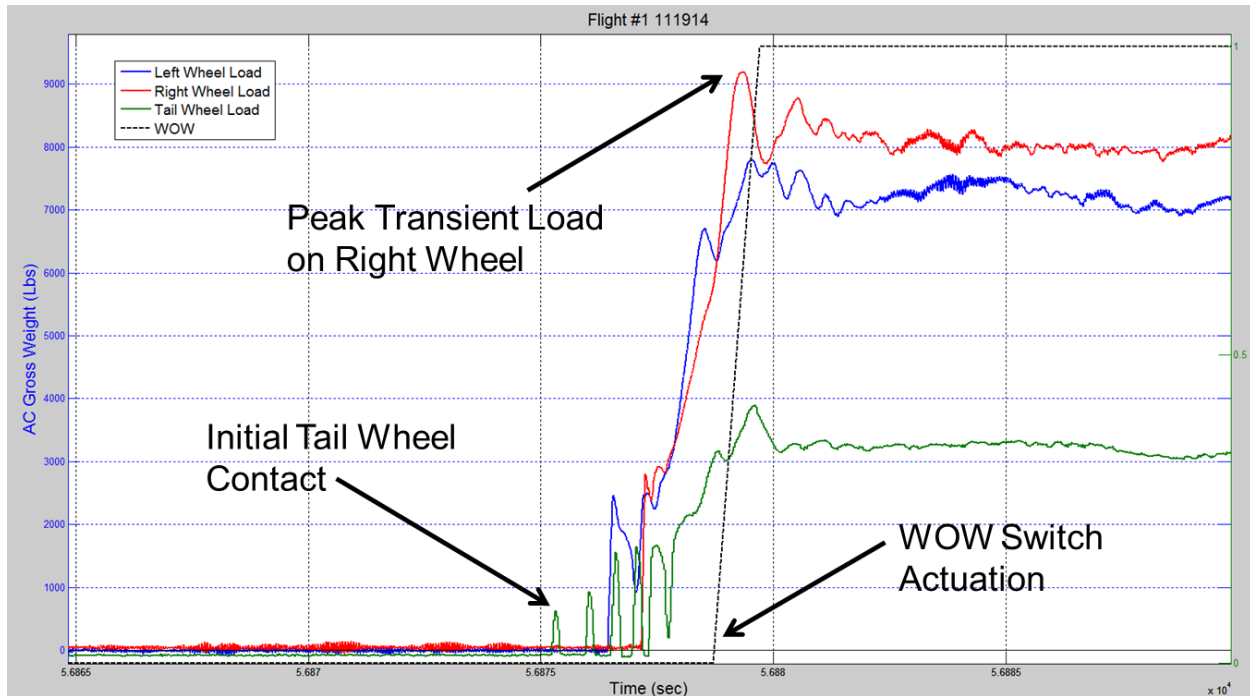


Figure 32. Hard landing event from Flight #1

2.2.2 Direct Monitoring of Loads

The following presents a review of various direct load monitoring design considerations that would need to be assessed in much more detail in the context of certifying a HUMS-based load monitoring approach for the management of the fatigue life of dynamic components in service. The effects of various measurement parameters on the measured load signal and calculated fatigue damage were evaluated through a simulation study that was carried out using S-92 aircraft flight test data and a component fatigue damage model.

Strain sensors are widely used to monitor a load subjected to critical aircraft structures and dynamic components in flight test environments. Because the strain sensor is sensitive to its orientation/location, wiring, and especially thermally induced strain, it is often calibrated and recorded after installation and at the beginning of each test run. The thermally induced strain varies with temperature during flight and can vary from flight to flight depending on when a zero reference strain was recorded and assigned to each strain sensor measurement and the ambient air temperature on the day the zero was recorded. Therefore, the actual loads (or strain/stress) experienced by the structures should be obtained by eliminating the zero reference strains from newly measured strain outputs and implementing standard temperature compensation techniques. This highlights just one unique challenge to strain-based load measurement in a fleet monitoring application where sensor attachment location and orientation can vary slightly even with carefully designed installation techniques.

2.2.2.1 Identification of Measurement Parameters

While temperature has a critical influence on load measurements using a strain sensor, other measurement parameters can also affect the strain output and subsequent load estimate. Table 5 lists a comprehensive set of measurement parameters, which are categorized into attributes and faults. The attribute parameters are configured in the measurement system design/installation processes, whereas any faults are captured during the data acquisition process. A direct use of signals with inaccurate configuration of attribute parameters or in the presence of faults can result in erroneous load measurement. Table 5 also describes possible issues for each parameter, their effects on a signal itself and/or load estimate, recommendations to address the issues, and simulation and detection methods to test and evaluate a sensitivity of load estimation model on each parameter variation. Listed in the last two columns is the complexity of simulating and detecting parameter variation.

For each measurement parameter in table 5, possible issues encountered when using suboptimal parameter settings and their effects on the load estimate are presented, along with recommendations to consider when designing a measurement system for a particular fleet monitoring application.

For production fleet aircraft applications, it would be hard to devise monitoring methods to detect inappropriate configurations of attribute parameters listed as “complex” or “not applicable (N/A)” in the table. Thus, it is important when designing LGLMS that the end-use of the load measurements is known and appropriate attribute configurations are defined to accurately capture loads for these end uses. They should be further validated during flight tests conducted to gather data representative of intended end uses. On the other hand, faults can be detected and isolated through standard signal quality assessment processes not described in this document. Therefore, the following simulation study of parameters variation will be limited to attribute parameters, and the results can be used as initial guidelines on minimum hardware and digital processing requirements for LGLMS and sensors.

Considering the complexity of parameters and variation, methods of detection, and availability of simulation methods, the following three representative attribute parameters were selected for simulation and sensitivity study:

1. **Sample rate:** The Nyquist sampling theorem states that the information of a signal is ideally recovered when it is sampled at a minimum of twice the highest frequency (also called the Nyquist frequency) contained in the signal. Non-ideal sampling rates can result in significant amplitude inaccuracies in the reconstruction of a signal sampled at or near the Nyquist sampling rate. In the typical instrumentation system, if amplitude accuracy is required, it is common to sample at least five times the highest frequency of interest. Even in less than ideal conditions, it is possible to accurately determine the frequency content of a signal sampled near the Nyquist sampling rate. The ability to accurately reconstruct the frequency content of a signal sampled near the Nyquist sampling rate is crucial to the prevention of aliasing. Sampling a signal at less than the Nyquist sampling rate can induce aliasing effects and also loss of useful frequency information contents due to insufficient time resolution.

2. Sensitivity error: Sensitivity is measured by the magnitude of the output signal corresponding to a unit input of the measured signal along the specified sensitive axis and describes a linear relationship between input and output signals, as shown in figure 33. It may be expressed as the ratio of the incremental output to incremental input, which is essentially a gain. The load sensors (or stain gages) should be sensitive enough to measure the smallest amplitude required for the intended application and detect the signal at the specified mounting location of the sensor. Also the sensor's off-axis sensitivity should be 5% or less than the on-axis sensitivity. The sensitivity of a sensor is determined by a calibration process at specified operating conditions and used in converting a measured voltage signal to an engineering unit. However, it can be affected by multiple factors: miscalibration, output signal exceeding sensor limits, and system or sensor nonlinearity.

3. Sensor bandwidth (or useful frequency range): The bandwidth of a sensor is defined as the frequency range over which the magnitude of the ratio of the output to the input does not differ by more than ± 3 dB from its nominal value, as shown in figure 33. To ensure sufficient sensor response, the bandwidth or useful frequency range of the sensor should exceed the frequency range of interest for the components being monitored. The signal levels for measurements outside the bandwidth could be very inaccurate. This means that a linear relationship between excitations and sensor responses can be changed into a non-linear relationship.

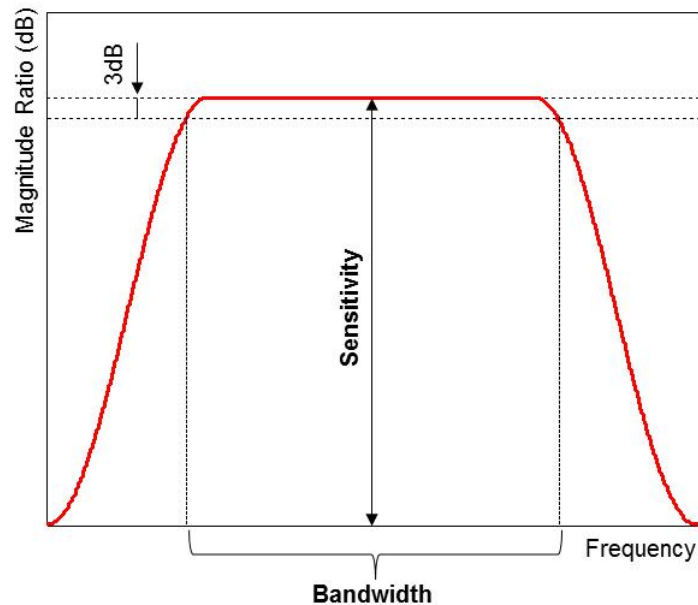


Figure 33. Sensitivity and bandwidth

Table 5. Identification of measurement parameters

Category	Parameter	Possible Issues	Effects on Signal and Load Estimate	Recommendations	Level of Simulation	Level of Detection
Attribute	Sample rate	Low sample rate	Insufficient time resolution, aliasing, and loss of useful information	<ul style="list-style-type: none"> • Increase sample rate to at least 2.56 times of anticipated max frequency 	Moderate. Combination of filtering and interpolation	Complex. Should know max frequency and resulting error (or aliasing) frequency
Attribute /fault	Sensitivity	System nonlinearity and miscalibration of measurement system	Signal magnitude change and erroneous information signal	<ul style="list-style-type: none"> • Correct calibration and check measurement system linearity 	Simple. Multiplication of scale factor	Complex. Generation of a load signal with other measurements and comparison with a direct load measurement
Attribute	Sensor bandwidth (useful frequency range)	Frequency of interest exceeds bandwidth	Nonlinear signal output and erroneous information signal	<ul style="list-style-type: none"> • Select proper sensor with bandwidth exceeding frequency range of interest 	Complex. Combination of Fourier analysis, transfer function, and exponential function (or lowpass filtering)	Complex. Should know expected signal level to compare the level with actual signal level at specific frequency
Attribute	Data length	Limited data length	Insufficient frequency resolution and loss of information signal	<ul style="list-style-type: none"> • Determine data length and sample rate to catch frequency components of interest 	Simple. Trim data points	Simple. Check data length or frequency resolution
Attribute	Synchronization	Time gap between DAQ channels	Erroneous load estimation	<ul style="list-style-type: none"> • Synchronize data recording 	Moderate. Combination of Fourier analysis and exponential function	Moderate. Only if commensurate signals available. Use cross correlation function

Table 6. Identification of measurement parameters (continued)

Category	Parameter	Possible Issues	Effects on Signal and Load Estimate	Recommendations	Level of Simulation	Level of Detection
Attribute	Signal amplification (gain)	Wrong gain setting	Out of signal range, coarse dynamic resolution, and erroneous information signal	<ul style="list-style-type: none"> • Proper gain setting considering signal range and dynamic resolution 	Simple. Multiplication of scale factor	Complex. Generation of a load signal with other measurements and comparison with a direct load measurement
Attribute	Dynamic resolution	Insufficient dynamic resolution or higher resolution than sensitivity at given DAQ bit and signal range	Quantization error, uniformly distributed noise power over entire frequency spectrum, and loss of useful information	<ul style="list-style-type: none"> • Increase DAQ bit or decrease signal range 	N/A Matter of ADC	N/A
Attribute	Installation error	Poor bonding, misalignment, off-positioning, isolation, and ground loop	Sensor drift, signal nonlinearity, and erroneous information signal	<ul style="list-style-type: none"> • Check sensor installation/wiring and calibrate sensor 	N/A	Complex. Trend analysis with linear fit
Attribute	Configuration parameters	Incorrect configuration parameters setting	Erroneous information signal and load estimation	<ul style="list-style-type: none"> • Check and correct configuration parameters 	N/A	N/A
Attribute	Windowing	Wrong choice of window function	Smearing or magnitude change, and erroneous information signal	N/A	N/A	N/A

Table 7. Identification of measurement parameters (continued)

Category	Parameter	Possible Issues	Effects on Signal and Load Estimate	Recommendations	Level of Simulation	Level of Detection
Attribute	Hysteresis	Mechanical hysteresis	Signal nonlinearity and erroneous information signal	<ul style="list-style-type: none"> • Right choice of sensors and installation 	N/A	N/A
Fault	Random error	Electrical and mechanical noises	Masking information signal and erroneous information signal	<ul style="list-style-type: none"> • Proper ground & insulation & wiring, matching sensor/test structure materials • Apply noise reduction methods and minimize the noises 	Moderate. Combination of deterministic signal with specific frequency harmonics and random number generation	Complex. De-noising technique or frequency analysis/peak picking
Fault	Signal range	Out of signal range	Signal clipping, modulation, and loss of useful information	<ul style="list-style-type: none"> • Increase range for capturing expected excursion in signal • Remove clipped points and interpolate the points from good sample points 	Simple. Clipping some sets of data samples	Simple. Check clipped samples

Table 8. Identification of measurement parameters (continued)

Category	Parameter	Possible Issues	Effects on Signal and Load Estimate	Recommendations	Level of Simulation	Level of Detection
Fault	Missing data points	Missing data samples in dynamic sensors and A/C parameters	Loss of actual information signal	<ul style="list-style-type: none"> • Check all measurement system from sensors to DAQ system and remove snapshots with missing data points • Evaluate how much data can be replaced or removed before too much error is introduced, or reliability is affected 	Simple. Substitution of NaN (i.e., Not a Number) or Inf (i.e., infinite) points	Simple. Logical and data length
Fault	Signal jump, scatter increase	Measure system damage	Signal transition and erroneous information signal	<ul style="list-style-type: none"> • Check and replace measurement system • Detect jump points and remove a bias or balance segments before/after jump • Detect scattering points and discard the scattered points or all points 	Moderate. Multiplication of step function	Moderate. Statistical change detection

Table 9. Identification of measurement parameters (continued)

Category	Parameter	Possible Issues	Effects on Signal and Load Estimate	Recommendations	Level of Simulation	Level of Detection
Fault	Linearity	Miscalibration, sensor damage, and out of operating ranges	Sensitivity error and erroneous information signal	<ul style="list-style-type: none"> • Correct calibration • Use sensor within operating ranges • Isolate and subtract nonlinearity from signal 	Moderate. Multiplication with nonlinear function	Moderate. Trend analysis with linear fit
Fault	Sensor drift	Output signal change independent of measured property	Sensitivity error, sensor nonlinearity and erroneous information signal	<ul style="list-style-type: none"> • Use half- or full-bridge strain sensors to minimize the effects of operating conditions and replace sensor before a sensor starts drift by aging • Isolate and subtract linearity or nonlinearity from signal 	Moderate. Linear trend	Moderate. Trend analysis with linear fit
Fault	Bias error	Signal output when measured property is zero	Gauge factor change and erroneous information signal	<ul style="list-style-type: none"> • Common ground of sensor and measurement system, zero setting before measuring property, and use half-or full-bridge strain sensors 	Simple. Addition of scale factor	Simple. Mean

2.2.2.2 Test Matrix

Table 6 is a test matrix that was used to generate simulation data for variations of the selected attribute parameters using the simulation methods defined in table 5. It also includes the levels of each parameter variation and basis/rationale for level selection. The simulation data were then fed into a load estimation model for sensitivity study. The estimated loads were correlated to levels of matching parameters to evaluate the effects of variations in the selected attribute parameters on direct load monitoring accuracy.

Table 10. Test matrix for simulation and sensitivity study

Parameter	Level	Basis/Rationale
Sample rate	(0.75, 1, 1.5, 2, 3) × anticipated maximum frequency (or Nyquist frequency)	A key reason of optimal sample rate selection is to avoid aliasing and reconstruct an original waveform. Because a minimum required sample rate is 2.56 times the Nyquist frequency and higher sample rates over 2.56 result in almost the same waveform reconstruction, limit a level of the highest sample rate to 3 times and drop the sample rates to 0.75 times the Nyquist frequency.
Sensitivity	Nominal sensitivity ±5 steps (2% sensitivity change per step)	A sensitivity (or GF) of strain sensor can be changed from a reference (or nominal) value according to miscalibration, installation errors, operating conditions, and sensor/system nonlinearity. The sensitivity is typically determined with a tolerance of less than 1%. Considering the sensitivity variation of the sensor itself and other influences, extend the tolerance up to ±10% for the sensitivity study.
Sensor bandwidth	Nyquist frequency-10 steps (5 Hz change per step)	When a frequency response of the component being monitored exceeds a sensor bandwidth (or useful frequency range), a measured sensor signal would be distorted or exaggerated. Considering an anticipated maximum frequency (or Nyquist frequency), simulate a sensor response with bandwidths of less than the Nyquist frequency.

2.2.2.3 Simulation of Parameter Variation

As described in table 5, for simulation of sample rate variation, a polyphase implementation method is used to resample the data at a modified sample rate, and an anti-aliasing filter is applied to the data during the resampling process. A default filter order is 10. For sensitivity variation, a scale factor corresponding to a sensitivity error is directly multiplied to an original data signal. For sensor bandwidth, a linear phase lowpass filter using least-squares error minimization is used to limit the bandwidth. A signal out of band will be distorted or exaggerated.

Based on the test matrix defined in table 6, the simulations were performed on each variation level of the parameter. An MR right servo load sampled at 172 Hz from S-92 aircraft flight tests was used as reference data for the simulation. Figure 34 shows a simulation result of sample rate variation. The top plot includes the original 172 Hz (blue line) and resampled 65 Hz (red line). The 65 Hz is calculated by multiplying 0.75 by the Nyquist frequency. There is a big difference between the signals; this is much clearer in the bottom plot depicting the difference between the two signals. Figure 35 is an example of 10% sensitivity error. The top plot shows the original and simulated signals, the bottom plot the difference between the signals. It can be shown that the signals are close to each other. The top plot of figure 36 shows the original and lowpass filtered signals with a cutoff frequency of 36 Hz, while the bottom plot shows a clear difference between the signals. The original signal components above the cutoff frequency were filtered out or highly suppressed.

In summary, it can be inferred that the sample rate and sensor bandwidth variation would highly affect load estimation, but the sensitivity error of below 10% would have relatively minor effects on load measurement. The effects on fatigue damage assessment are discussed next.

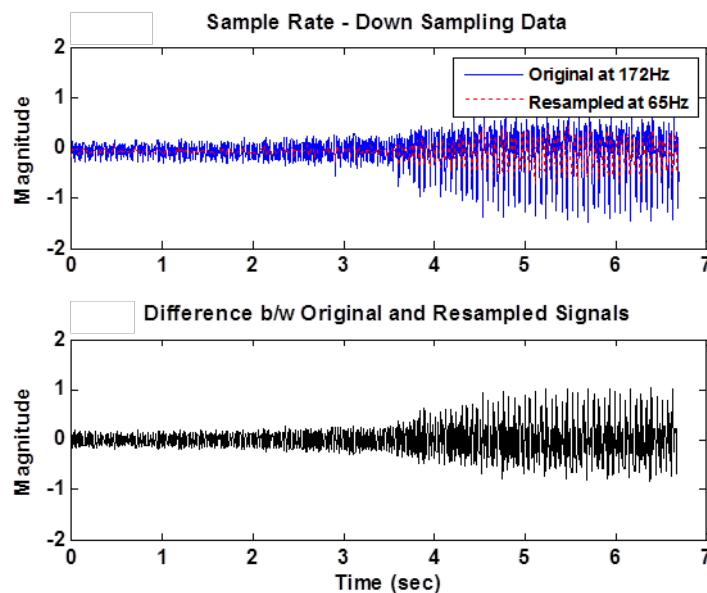


Figure 34. Example of sample rate variation—down sampling signal

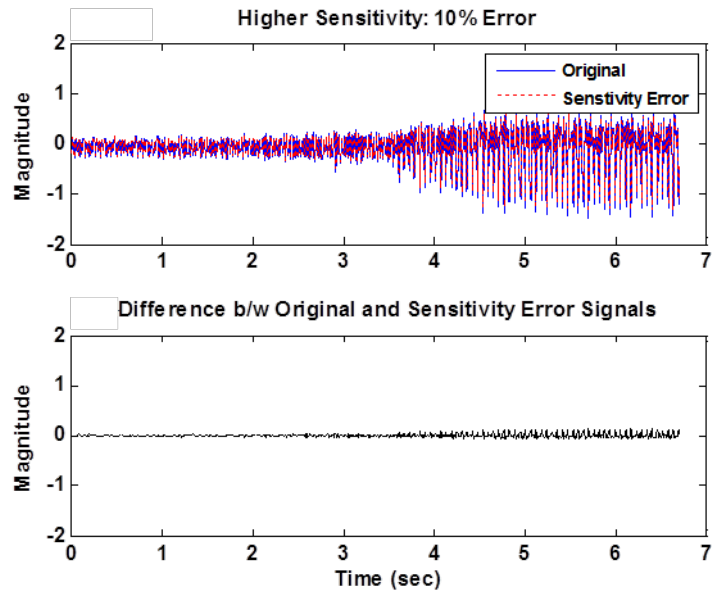
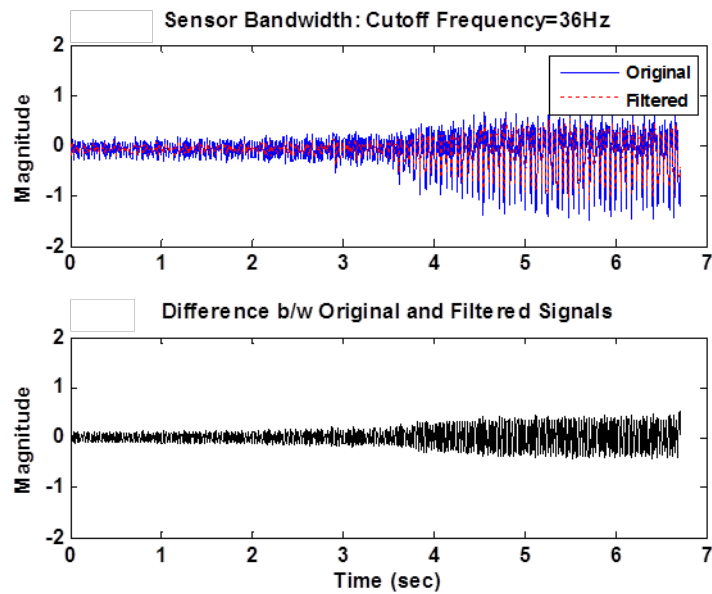


Figure 35. Example of sensitivity error—10% higher sensitivity



**Figure 36. Example of sensor bandwidth variation—
lowpass filtering with cutoff frequency of 36 Hz**

2.2.2.4 Effect of Parameter Variation on Damage Calculation

As described in section 2.2.2.2, damage accumulation model results were used as a test case for simulating the effects of variations in load signal data. An MR right servo load was used as a reference load for the simulation in conjunction with a CRT calculation for the MR stationary swashplate assembly. The existing CRT provides a ground-truth damage fraction for comparison against the output of the damage accumulation model when the simulated variable data are used as input. Both a damaging steady-state and damaging transient flight-test maneuver were selected for the simulation analysis. The damage accumulation model was developed and verified against the reference CRT outputs for the two damaging flight-test maneuvers prior to using the simulated variable data inputs.

The damage accumulation model was executed for all levels of measurement parameter variation (as previously defined in table 6) across both sample test maneuvers for each of the three parameters under investigation: sample rate, sensitivity error, and sensor bandwidth. The resulting damage fraction calculations were tabulated and plotted, as shown in figures 37–39.

Of interest is the effect of load variability both within a maneuver as well as across maneuvers. Sampling rate and sensitivity error results suggest the effects share similar trends across the two test maneuvers; however, sensor bandwidth results present nearly inverse trends across the maneuvers. Additionally, within each maneuver, the effects of the three tested parameter variations show no correlations. This suggests one would need to study each type of parameter variability before making generalized statements about the effects of all variabilities across, as well as within, maneuvers.

In addition, the percent change in damage fraction from the baseline for each level of parameter variation was calculated. The following conclusions were drawn:

1. Sample rate variability showed a profound effect when decreasing from the commonly accepted minimum required sample rate of 2 times the Nyquist frequency. A drop from 2 times to 1.5 times the Nyquist frequency resulted in a reduction of more than 50% in the damage estimation result for both regimes.
2. Sensitivity error variability showed a much less abrupt change with each level of variability. A 2% change in sensitivity error resulted in less than a 20% change in the damage estimation from baseline. However, both regimes exhibited a greater than 85% change from the baseline when sensitivity variation levels reached 10%.
3. Sensor bandwidth variability did not produce a monotonic relationship between parameter variability levels and the resulting damage estimation results. While the percent change from baseline never exceeded 60% for all levels of bandwidth variability for Regime 59, the effect appears to be unpredictable. Regime 18 demonstrated an even greater effect, with a similarly unpredictable relationship.

In summary, it can be inferred that the sample rate and sensor bandwidth variation are difficult to model and would highly affect load estimation. In contrast, low levels of sensitivity error variability influence the damage state estimation less dramatically and more predictably. Furthermore, known uncertainties in sensitivity could be accounted for by including uncertainty models and conservative uncertainty compensation when using loads to calculate damage for production aircraft.

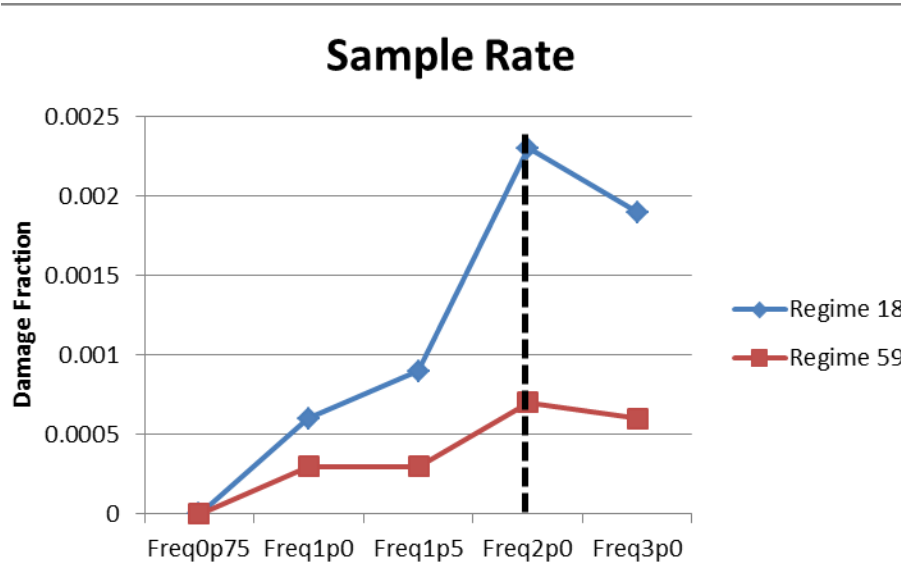


Figure 37. Effect of sample rate variation of load data on the damage fraction

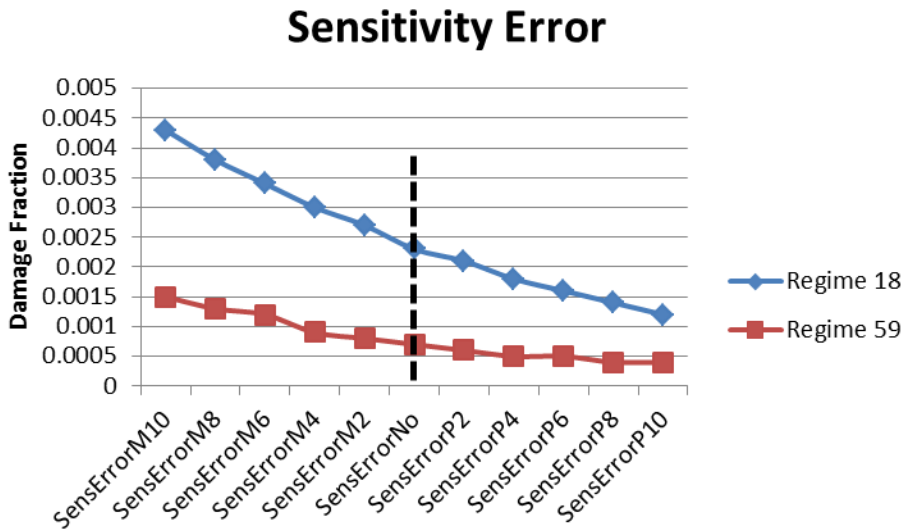


Figure 38. Effect of sensitivity error variation of load data on the damage fraction

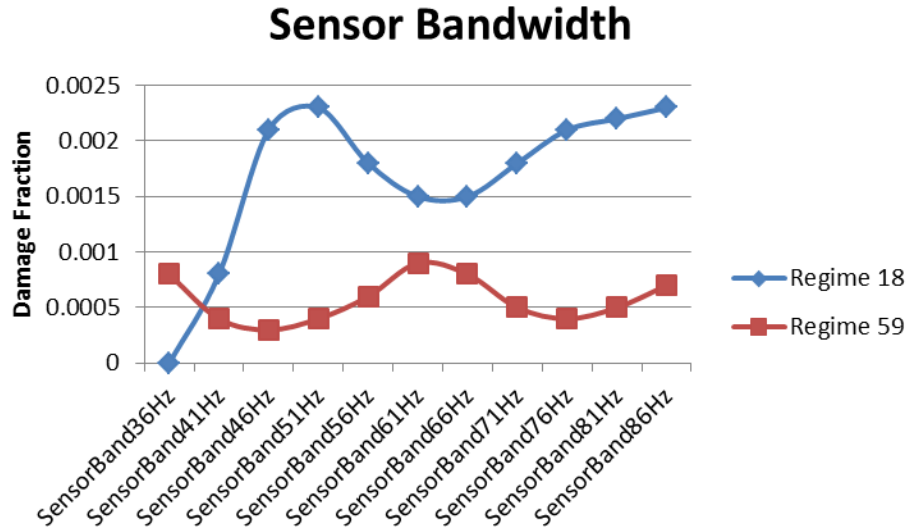


Figure 39. Effect of sensor bandwidth variation of load data on the damage fraction

2.3 RELIABILITY FRAMEWORK

2.3.1 Background

The process of calculating component RTs is often considered somewhat of an art due to the limited availability of information about flight loads, strength, and usage—especially in the development phase. Flight testing provides maneuver loads data but is often limited to the edge of the envelope configurations due to cost/schedule constraints. Full-scale component testing is performed on multiple specimens, but these tests can produce as many suspensions as failures, resulting in “demonstrated” fatigue strength limited by test constraints, or cost/schedule limitations rather than maximum potential fatigue strength limited by the component itself. Usage spectra are derived from a combination of legacy specifications, pilot surveys, and the limited use of fleet data. These key RT inputs are typically known in terms of fleet population statistics but are treated as unknown at the specific serial number level for a fielded part. To provide a high level of fatigue reliability for each component failure mode, RTs are calculated with an extreme combination of low strength (assumed 0.1 percentile, or 100–99.9), CWC usage (assumed 90th percentile), and top of scatter flight loads (assumed 99th percentile). The probability of an individual serial number simultaneously exceeding all of these extreme input values is one in a million, resulting in an expected fatigue reliability of approximately six -9s (0.999999)—a fairly well-accepted industry reliability goal for fatigue life limited components.

The traditional process described above is one way to achieve the reliability goal for a part number. Part number reliability means that the reliability goal for the part number is achieved, on average, when considering the entire population of fielded parts and can be expected to be achieved by any individual serial number as long as the particular combination of loads/strength/usage information remains uncertain at the serial number level. That last condition is important to note because the part number reliability approach is premised on the condition that loads/strength/usage cannot be observed in service and therefore treats loads/strength/usage

as uncertain at the serial number level even if some elements of historical usage are known from fleet data.

It is logical to assume that if usage data were entirely known, or the important aspects of usage for a particular component were known (such as GAG rates for a rotor hub), then the reliability of each serial number part will vary depending on how the aircraft is being flown. In the rotor hub GAG example, helicopters flown at the highest GAG rate will have less than the average reliability, while helicopters flown at the lowest GAG rate will have more than the average reliability. If the GAG statistics still obey the original usage assumptions (such as 90th percentile in the usage spectrum), then the part number reliability goal may still, on average, be achieved; however, it is only achieved by averaging out the lower serial number reliabilities with higher serial number reliabilities. This should not be a surprise, as it is expected that actual usage varies by aircraft, just as strength varies by component. The only difference is that usage data are measurable in the field, whereas component strength is not.

To understand how usage data influence the calculated CRT of a particular component, one might simply substitute the CWC (90th percentile) usage statistic with the actual measured/recorded/calculated usage metric for a particular serial number and recalculate the life using the traditional RT calculation process. The problem with this approach is that the traditional calculation achieved a part number reliability by applying a generally conservative assumption to the usage metric. That conservative assumption is eliminated when substituting the 90th percentile usage with known usage. To take that concept further, if all the inputs (loads/strength/usage) were known precisely, then the traditional calculation process would have no conservatism applied and would result in an expected failure time rather than a six-9's reliable safe life.

2.3.2 Defining a Failure Model

To understand fatigue reliability when dealing with known usage data, fatigue failure must be modeled within a probabilistic framework that accounts for uncertainty of loads/strength/usage holistically rather than by allocating a reliability-based margin to individual input parameters. This process starts by defining a failure model (defined in the form of a limit state function), a set of input assumptions (a combination of uncertainty distributions and fatigue properties), and solving for the reliability at a prescribed lifetime using a probabilistic solver (such as Monte Carlo or the first-order reliability method [FORM]). This approach can flexibly model the traditional part number reliability as well as the serial number reliability based on fleet data if the inputs are properly defined and can do so while conserving reliability. It is important that the probabilistic approach is consistent with the traditional approach in terms of the failure model and input assumptions, such that the results from each process can be directly compared. For example, the traditional part number RT calculation can be used as a cross-check to compare the result using the probabilistic approach. To be tractable, it is also important that the failure model be a simplified model such that the number of random variables is minimized to a practical set of key variables and any simplifications of the model be conservative. The use of a simplified model means that any resulting failure probability should not be treated as a true probability of failure but rather as a conservative best estimate based on appropriate assumptions.

To explain how the traditional failure model can be used in a probabilistic framework, consider the example in equation 1, which shows a simplified fatigue failure model that is used to calculate an RT with six-9's reliability. The term inside the square brackets is the familiar Miner's rule of cumulative damage, where the regime usage (n) is defined as a rate per flight hour, which results in the cumulative damage term being defined as damage per flight hour. The function $f(S_i, E)$ is based on a stress cycles fatigue curve (S-N curve), where the flight load (S) intersects with a cycles-to-failure curve set by the component fatigue endurance strength (E) determined from lab testing and material parameters. The inverse of the damage per flight hour term is the number of flight hours when damage equals 1. By allocating "9s" to each input, this method approximates the six-9's RT. To solve for the probability of failure at a given RT using a probabilistic approach, this equation must be translated into a limit state function. A limit state function has the property where the function value is negative for a failed state and positive for a safe, un-failed state. The limit state function that is consistent with the traditional failure model is shown in equation 2. Here, the first term is the failure time model borrowed from equation 1, and the second term is the desired RT. This function has the property where g is negative when the RT exceeds the failure time (failed state), while g is positive when the failure time exceeds the RT (safe state). The probability of failure is then the probability that $g < 0$. By solving for the probability of failure for a range of input RTs, a life versus reliability can be plotted to determine the RT associated with a desired reliability.

$$RT_{6-9s} = \left[\sum_R^{i=1} \frac{n_i}{f(S_i, E)} \right]^{-1} \quad (1)$$

$$g = \left[\sum_n^{i=1} \frac{n_i}{f(S_i, E)} \right]^{-1} - RT \quad (2)$$

n_i = 90th percentile usage for regime i , in units of seconds or counts per flight hour

S_i = 99th percentile or top of scatter flight load for Regime i

E = 100 – 99.9th (0.1) percentile component strength

R = total number of Regimes

2.3.3 Input Assumptions

2.3.3.1 Strength

Three 9s of reliability are often attributed to the reduction traditionally applied to an S-N curve to arrive at a reduced-strength or working curve for use in CRT analysis. This working curve represents a strength reduction of 3-sigma (roughly three 9s). In a probabilistic framework, the test based mean fatigue strength and 3-sigma reliability reduction can be applied to model the component's fatigue endurance strength as a random variable. This can be accomplished by a normal distribution that has the same mean and standard deviation as is assumed in the traditional fatigue analysis.

Consider an S-N curve with a mean endurance limit of 11,600 lbs and a 61% working endurance limit of 7,077 lbs. The mean endurance is set as the mean of the normal distribution. The working curve knockdown of 39% (100–61%) represents 3-sigma, so 13% of the mean represents the standard deviation of strength (39/3 = 13%). For a normal distribution, the mean and standard deviation sufficiently define the probability density function and can be used in the probabilistic analysis to represent random fatigue strength that obeys the assumptions in the traditional fatigue substantiation analysis methodology.

2.3.3.2 Load

Two- 9s are often attributed to the use of top-of-scatter flight loads from flight tests. Modelling loads from flight tests as a distribution of random variables is very difficult due to the number of factors that influence load within a given regime (such as airspeed, GW, CG, control input rate, and altitude). There are rarely enough flight test data points to control for these factors when considering the large number of combinations of factors that would need to be considered. Rather, the peak flight test load from all occurrences and combinations of factors within a given regime is assumed to occur for all occurrences of the regime in CRT analysis. It is assumed in standard fatigue methodology that this top-of-scatter load achieves at least the 99th percentile peak fatigue load. The Weibull random variable distribution is commonly used for this application with a shape parameter that can be estimated from flight test data or assumed based on experience. Values of 2–10 were used in a similar probabilistic analysis documented in a paper by Zhao and Adams [8], with lower values indicating a higher degree of variation in the random loads. Specific studies may be carried out to refine the Weibull shape parameter based on flight test data, although flight test data rarely provide a random sampling of peak fatigue loads achieved in normal fleet operations due to the edge-of-envelope configurations of the flight test aircraft. As an example, consider an MR pushrod top-of-scatter vibratory flight test load of 11,300 lbs during a moderate pullout at 0.8 V_{NE}, and shape parameter of four. Equations 3 and 4 can be used to solve for the Weibull scale parameter, which will sufficiently define the random load distribution for use in fatigue reliability modeling:

$$F = 1 - e^{-\left(\frac{x}{\eta}\right)^\beta} \quad (3)$$

$$\eta = \frac{x}{\left[-\ln(1-F)\right]^{1/\beta}} \quad (4)$$

F = cumulative probability of flight test top-of-scatter fatigue load = 0.99 (two--9s)

x = flight test top-of-scatter fatigue load = 11,300

β = Weibull shape parameter = 4

η = Weibull scale parameter

The missing distribution scale parameter for this random load distribution can now be solved as η = 7714. Using this approach, the load distribution can be modeled analytically in a way that is consistent with the assumptions in the traditional fatigue substantiation analysis methodology and leveraged in a probabilistic analysis tool.

2.3.3.3 Usage

One-nine is often attributed to the CWC usage spectrum. In the absence of usage monitoring, distributions of usage across a fleet are typically not well understood, especially for a new aircraft or customer. It is commonly assumed in reliability studies that the usage parameter varies as a Weibull parameter with a shape parameter β of 2 [8], although these parameters can now be better estimated from fleet data using RR. By setting the regime usage metric (either maneuvers per 100 hours or % time) from the CRT as the 90th percentile usage as an anchoring point, a distribution can be attained for model random usage. The derivation of the Weibull scale parameter is the same, as shown in the load example. Consider an example CRT where the moderate pullout $0.8 V_{NE}$ has a CWC usage of 90 maneuvers per 100 hours. Using equations 3 and 4 in the load example, the Weibull scale parameter $\eta = 59.3$. Using these Weibull distribution parameters, the usage distribution can now be modeled in a probabilistic tool.

2.3.4 Probabilistic Solver

Having defined the physics of failure model, the next step is to choose a probabilistic approach to estimate the probability of failure. Over the years, there have been numerous documented approaches. The most widely used approach is the Monte Carlo simulation method, due to its relatively intuitive and straightforward implementation. A major disadvantage of Monte Carlo occurs when estimating very small probability of failure ($<1E-6$) combined with a large number of input variables because it requires a very large number of simulations to obtain an acceptable level of accuracy. For example, the number of samples needed for achieving an accurate probability of failure that is equal to $10E-6$ is 10 million. In general, to estimate the total number of samples required is obtained by using the following approximation:

$$N \cong \frac{10}{p_f} \quad (5)$$

Where N corresponds to the total number of Monte Carlo simulations, and p_f is the required probability of failure estimate.

Fast reliability integration methodologies have been introduced within the past three decades with the purpose of providing more efficient approaches to estimate probability. The FORM is the approach that has been chosen to estimate structural reliability of rotorcraft components [8]. This particular approach is purely analytical and requires the physics of failure model to be converted into a limit state function. The limit state function, defined as the boundary separating the safe region from the failure region, as described above, is shown notionally for a 2-dimensional function in figure 40.

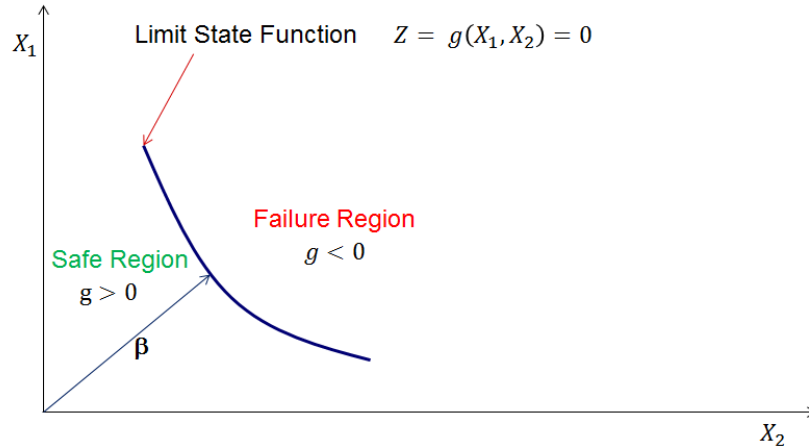


Figure 40. 2D case limit state function

In the general case, the limit state function is derived from the performance function, which is described as:

$$Z = g(X_1, X_2, \dots, X_n) = D_{\text{critical}} - D_{\text{current}} \quad (6)$$

Where X represents the set of input random variables. D_{critical} is the critical damage threshold where the component is treated as failed, and D_{current} is defined as the current damage estimate. The limit state function is considered a special case of the performance function, specifically when:

$$Z = 0$$

The probability of failure can be defined in the following integral:

$$p_f = \int \dots \int_{Z < 0} f_X(x_1, x_n, \dots, x_n) dx_1 dx_2 \dots dx_n \quad (7)$$

Where $f_X(x_1, x_n, \dots, x_n)$ is the joint probability density function for the random variables $X_1, X_2 \dots X_n$.

The integration is evaluated over the failure region $Z < 0$.

Although the integral above is the general representation of probability of failure, it cannot be solved directly. In order to estimate probability, analytical approximations were introduced, and one of them was the FORM. There are multiple variations of FORM and each of them can be applied under specific assumptions. The method used in this case is named FORM 1 [9]. In the general case, the main objective of FORM is to estimate the minimum distance to the limit state function in a standardized coordinate system. The minimum distance is also known as the distance to the most probable failure point and is defined with the symbol β . The worst

combination of the stochastic input variables will lead to the most probable point of failure. In order to calculate β , the approach is structured as a gradient-based optimization method:

$$\begin{aligned} \text{Minimize } D &= \sqrt{x'^t x'} \\ \text{With constraint } g(x) &= g(x') = 0 \end{aligned} \quad (8)$$

Where x' is the coordinate evaluated on the limit state function evaluated in the reduced coordinate system. The minimum distance is calculated using the method of Lagrange multipliers:

$$\beta = \frac{\sum_{i=1}^n \left(\frac{\partial g}{\partial X'_i} \right)^*}{\sqrt{\sum_{i=1}^n \left(\frac{\partial g}{\partial X'_i} \right)^{2*}}} \quad (9)$$

The design point in the reduced space is calculated as follows:

$$x'_i{}^* = -\alpha_i \beta \text{ for } i = 1, 2, \dots, n \quad (10)$$

Where α_i is defined as the directional cosine along the axis X_i and is calculated as:

$$\alpha_i = \frac{\left(\frac{\partial g}{\partial X'_i} \right)^* \sigma_{X_i}^N}{\sqrt{\sum_{i=1}^n \left(\frac{\partial g}{\partial X'_i} \right)^* \sigma_{X_i}^N{}^2}} \quad (11)$$

Where $\sigma_{X_i}^N$ is the standard deviation at the design point in the equivalent normal distribution. One important detail about this approach relates to the type of input distributions used for the random variables; if the distributions are not normal, they must be converted into equivalent normal.

The optimization procedure is summarized in the following steps:

1. Define the limit state function
2. Assume an initial value for β and initial values for the design point coordinates: x'_i , $i=1, 2, \dots, n$
3. Transform non-normal variables into equivalent normal, and compute mean and standard deviation
4. Compute directional cosines
5. Compute updated value for β
6. Repeat steps 1–5 until β reaches convergence

Once β is calculated, the probability of failure is calculated by using the standard normal cumulative density function defined as:

$$p_f = 1 - \varphi(\beta) \quad (12)$$

Where φ is the standard cumulative density function.

In summary, FORM is very efficient at estimating small probability of failures and capable of handling a large number of input variables. The algorithm converges rapidly within five to 10 cycles, depending on the complexity of the limit state function. Unfortunately, there are cases where convergence to a β solution is not always guaranteed. When convergence is an issue, the selection of initial conditions, based on knowledge of the physics of failure model and how the input variables influence output, becomes very important.

In the mock certification section that follows, this methodology is applied to independently validate the use of Usage Monitor Reliability Factors (UMRFs) in recurring serial number life calculations. The probabilistic framework is applied and demonstrated to provide reasonable results as validated against the baseline component RTs detailed in section 3.5.3.3.

3. MOCK REGIME-BASED UBM CREDIT CERTIFICATION

3.1 CREDIT DEFINITION

A UBM credit application must define the component(s) affected, specific type of credit (e.g., RT extension, serial number versus part number extension, one-time versus continuous credit calculations), usage and load parameters required to calculate the UBM credit, and HUMS method or algorithms required to calculate and substantiate the credit. A moderately complex UBM credit application involving the extension of the RTs for individual serial numbers for a selected life-limited part number, which requires regime monitoring of two or more critical regimes, was selected as the focus of the mock credit application documented herein. It was also decided to develop an approach that could be successively applied for a given component serial number. This representative application was deemed to be a significant step beyond the “crawl before your walk” rotor hub credit previously approved by the FAA for the S-92 aircraft, which required monitoring of min-max values of only one aircraft state parameter (i.e., MR RPM) during each flight. Based on the recent progress achieved in refining and validating regime clustering, the selected credit focus was deemed to be achievable in practice and ready for near-term credit applications using only data already recorded by HUMS/IVHMS, where there was no need for additional physical sensors. While the application of virtual estimation of GW and loads also fall into this category of credits, it was decided to focus on a regime-based “walk before you run” application for two reasons. First, a regime-based application is readily understood by various stakeholders. Second, it is also a tractable application that could be completed within the allocated budget and schedule of the FAA program. The addition of virtual monitoring of GW and/or CG would only moderately increase the complexity but would require additional socialization to obtain concurrence from various stakeholders because the S-92 aircraft usage spectrum does not currently apply GW prorates. The use of VML estimated loads is achievable for an appropriate application but would be outside the comfort zone for many stakeholders in the near-term.

Both the component and UBM method(s) were selected based on a thorough review of the S-92 fatigue substantiation report. The entire list of S-92 aircraft dynamic components was evaluated and prioritized based on various quantitative and qualitative criteria, as described herein. The most appropriate UBM credit methodology was determined based on individual component details. Initially, all components with unlimited RT were eliminated from the list. Next, all attachment components—such as bolts, fasteners, and other components of low value or interest—were eliminated, resulting in high-value life limited candidate components for further consideration. The list of candidate components down-selected for more detailed assessment is provided in table 7.

Life sensitivity analysis was performed on the down-selected candidates in order to understand each component’s life sensitivity to both usage and loads. Sensitivity metrics were calculated for each component, as discussed in the next section.

Table 11. High-value, low-lifetime S-92 dynamic components

Components
Main rotor stationary swashplate
Main gearbox housing
Swashplate bearing retainer
Damper piston rod
Main rotor hub assembly
Tail rotor torque tube/blade
Tail rotor flexbeam
Tail rotor horn assembly
Tail gearbox housing

3.1.1 Life Sensitivity Analysis

A life sensitivity analysis Excel table was constructed from information extracted from an internal Sikorsky report. In this table, all pertinent information regarding the damage calculations of the candidate components was collected and organized in a manner that aided in conducting quantitative sensitivity analyses. Focusing mainly on usage monitoring applications, this information included several useful parameters for all candidate components. The approach used was similar to the life sensitivity analyses conducted for the UH-60M to support a component selection task under DO-1, as documented in Beale and Davis’ FAA report [2].

Parameters that were required to perform the life sensitivity analysis include the list of damaging regimes and loads, calculated damage for any damaging regime, and CWC usage. Capturing the effects of each individual regime on component damage was essential in identifying potential “low-hanging fruit” regimes as initial usage monitoring candidates, as well as determining the overall sensitivity of lifetimes with usage. Because the life sensitivity table allows regimes to be

easily sorted on a number of categories and is set up for computational analysis, it was the primary tool for all sensitivity analyses.

In order to investigate which of the components should be targeted for RT extensions, two metrics were defined and calculated: Life Sensitivity with Usage and Life Sensitivity with Load. These metrics, coupled with analyses of the component life as damage calculation parameters change can aid in quickly prioritizing where additional investigation into potential HUMS fatigue life benefits can be obtained.

The sensitivity of the calculated lifetime to both the regime load and the usage at that load are defined as sensitivity factors. These parameters can be interpreted as the percent change in lifetime given a 1% change in load/usage. Using these parameters, all regimes can quickly be scanned to determine which might provide a larger benefit for small changes in usage when compared with others.

The calculation of both sensitivity factors flows from a generalized derivation of component RT. Equation 13 shows this derivation begins with a typical formula that is often used to represent material or component fatigue (S-N) curves:

$$N = \left[\frac{\beta}{\left(\frac{S}{E}\right)^{\gamma} - 1} \right]^{1/\gamma} \quad (13)$$

In this formulation, S is the load, E is the endurance limit, N is the number of cycles to the initiation of a crack, and β and γ are material constants that are defined for each structural material. This curve shape can be used for the vast majority of materials considered in aircraft substantiations, including titanium, steel, aluminum, fiberglass, graphite, and most adhesives.

The second step in the derivation is to invoke Miner's rule of damage summation often used for metallic materials. This rule allows the damage from each regime to be calculated based on a single S-N curve, then linearly summed together to obtain a total damage. The part is assumed to reach the end of its useful life when this damage summation is equal to 1. Note that damage calculations presented herein use a baseline of 100 hours. This means that the number of cycles or occurrences provided in the CWC table of a damage calculation is really the number of cycles/occurrences per 100 flight hours. With this modification the calculated lifetime of a part can be calculated as in equation 14 below:

$$L = \frac{100}{\sum_i D_i} \quad (14)$$

Where L is the CRT and D_i is damage for regime i . The damage for a single regime can be calculated from the generalized S-N curve shape as follows in equation 15:

$$D_i = \begin{cases} \frac{t_i \cdot \omega / 10^6}{\left[\frac{\beta}{\left(\frac{s_i}{e} \right) - 1} \right]^{1/\gamma}} & \text{for steady state regimes} \\ \frac{O_i \cdot L_i \cdot \omega / 10^6}{\left[\frac{\beta}{\left(\frac{s_i}{e} \right) - 1} \right]^{1/\gamma}} & \text{for transient regimes} \end{cases} \quad (15)$$

In the first of these two formulations, t_i is the number of seconds spent within a regime per 100 flight hours, s_i is the regime load, and ω is the loading frequency (1/rev Main, 4/rev Tai, etc.). Note that the total number of cycles is divided by one million, as the S-N curve constants are derived with this scaling. The second formulation, which is used for transient maneuvers, calculates the number of seconds per 100 flight hours by multiplying the occurrences per 100 flight hours (O_i) by the length of each occurrence (L_i).

The final step in the sensitivity calculation is to evaluate the derivative of the single regime damage with respect to both time per 100 hours (t_i) and regime load (s_i). These are presented below in equations 16 and 17.

$$\frac{\partial D_i}{\partial t_i} = \frac{\omega / 10^6}{\left[\frac{\beta}{\left(\frac{s_i}{e} \right) - 1} \right]^{1/\gamma}} \quad (16)$$

$$\frac{\partial D_i}{\partial s_i} = \frac{(t_i \cdot \omega / 10^6) \cdot \left(\frac{s_i}{e} - 1 \right)^{1/\gamma - 1}}{\gamma e \beta^{1/\gamma}} \quad (17)$$

Two additional parameters, the Maximum Life Change % and Absolute Maximum Life Change (in hours), provide the potential life change if all damage associated with a given regime were taken away. When observing the sensitivity factors, it is essential to monitor the maximum benefit for a given regime as well, as some high-sensitivity regimes might be sensitive over small changes but may not provide benefit over a large range.

A Pareto chart showing the output of the component life sensitivity to load analysis for each component is presented in figure 41.

Life Sensitivity to Load by Component

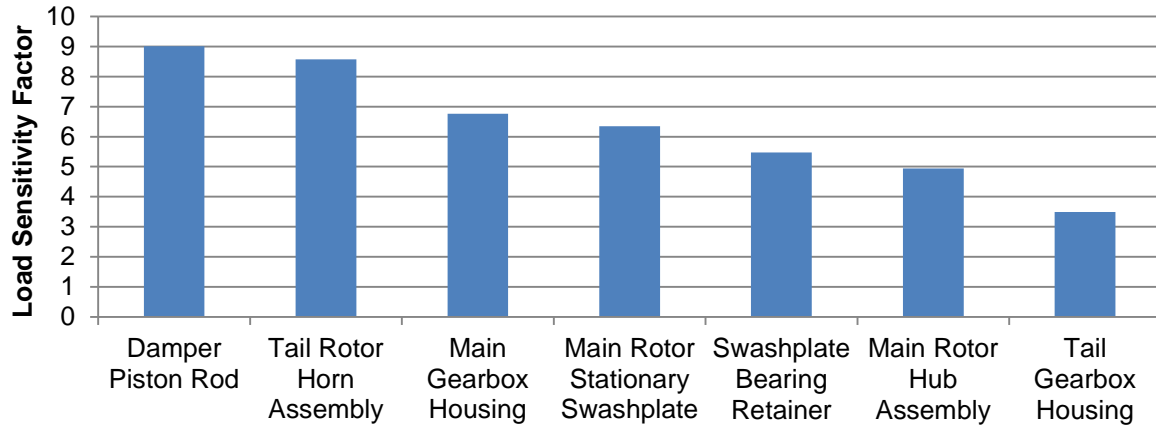


Figure 41. Component life sensitivity to load

3.1.2 Component Selection

The down-selection from the final list of candidate components to one component was performed by combining the results from the sensitivity analyses with independent qualitative feasibility and benefit scores provided by subject matter experts (SME). Four semi-qualitative metrics were developed to support the down-selection process, which are described below:

- Feasibility of regime monitoring
 - Based on a combination of the component regime sensitivity quantitative metrics and the feasibility of monitoring the components damaging regimes
- Feasibility of load monitoring
 - Based on a combination of the component load sensitivity quantitative metrics and the feasibility of monitoring the substantiating load for the component
- Feasibility of serial number tracking
- Potential benefit of life extension

Each metric was scaled from 0–5, with 5 being the most favorable. A final score was developed for each component by summing all four metrics together for a total possible score of 20. This analysis resulted in a clear top 10 list of candidate components, which are listed in table 8, along with the total score. The final component selected was the stationary swashplate, which is the item that scored the highest in table 8. It is noted that the top two components are both assembled into the swashplate assembly but are separate components with different tracked RTs and, for the most part, are affected by the same core set of regimes. The third through fifth components are all in a similar load path and affected by the same set of regimes. Out of the 10 components listed, a small number of HUMS-based UBM credit strategies may cover the majority of the list. The process that is documented herein for the stationary swashplate will be applicable to many of these components, even to the degree that the monitored critical regimes are common among the components. The stationary swashplate scored the highest due to both high life sensitivity and SME-perceived feasibility of monitoring the usage in terms of flight regimes. The functionality of the stationary swashplate is described in detail in section 3.5.2.1.

Table 12. Top 10 component list

Component	Total Score	Dominant Regimes	Critical load	UBM Approaches
Stationary swashplate	18	Turns (90%) Pullouts (10%)	Servo load	RR for turns/pullouts VML for servo load
Stationary swashplate bearing retainer	18	GAG (7%) Turns (84%) Pullouts (9%)	Servo load	GAG counting RR for turns/pullouts VML for servo load
MGB housing	18	GAG (30%) LCF (69%)	Foot stress	GAG counting VML for stress LCF GW monitor
MR hub	17	GAG (38%) LCF (58%)	MR torque	GAG counting VML for LCF MRQ GW monitor
MR shaft	16	GAG (58%) LCF (42%)	MR torque	GAG counting VML for LCF MRQ GW monitor
Rotating swashplate bearing retainer	15	GAG (23%) Turns (59%) Pullouts (18%)	MR push rod	GAG counting RR for turns/pullouts VML for pushrod load
MR servo assembly	15	GAG (24%) Turns (65%) Pullouts (12%)	Servo load	GAG counting RR for turns/pullouts VML for servo load
TGB output housing	15	GAG (90%) LCF (9%)	TGB output housing stress	GAG counting VML for stress LCF
MR blade	15	GAG (97%) LCF (2%)	Blade station 21% corner spar strain	GAG counting VML for stress
MR shaft nut	15	GAG (78%) Pullouts (22%)	MR shaft bending	GAG counting RR for pullouts VML for bending

3.2 DEFINITION OF END-TO-END PROCESS

An end-to-end process was mapped out and organized into components (presented in figure 42) that align with the sections in the FAA’s Advisory Circular (AC) 29-2C MG15 [10]. The end-to-end process is mapped in terms of the flow of information, which starts with the onboard system (OBS), flows through the ground-based system (GBS), then into the rotorcraft OEM analysis environment where the data are stored, analyzed, and distilled into an actionable CRT adjustment. Customer maintenance records also are used to acquire component flight hours, aircraft installation history, and relevant maintenance repair history. The credit hazard and criticality analysis described in section 5 is performed in the context of this end-to-end process.

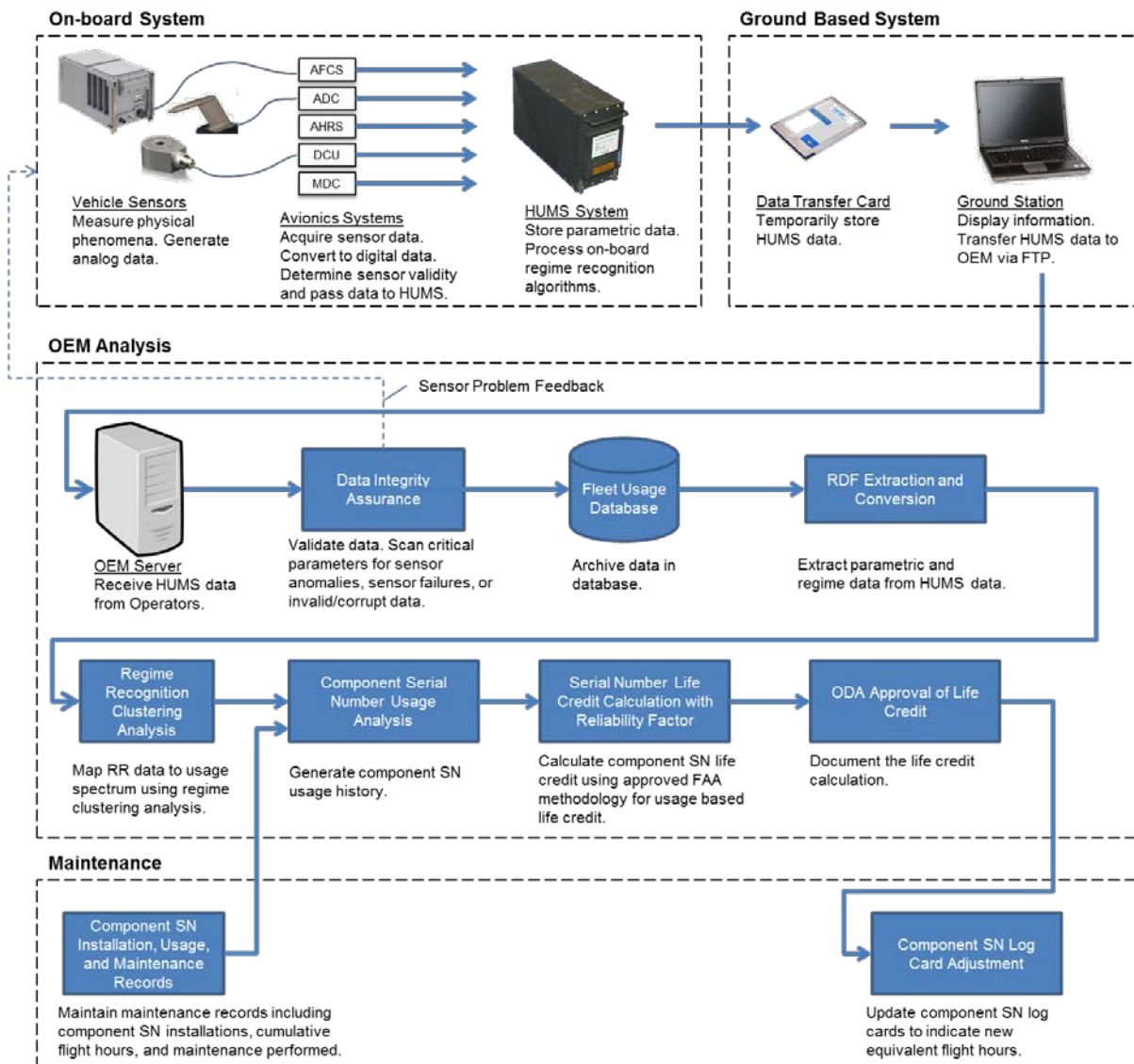


Figure 42. End-to-end regime recognition credit process

3.3 CREDIT HAZARD AND CRITICALITY ANALYSIS

The objective of the UBM credit in this study is to adjust the RT for a flight-critical, life-limited dynamic component while maintaining the baseline risk (or reliability) that was in place before usage monitoring was applied. The end-to-end HUMS UBM process (see figure 42) begins with the acquisition of airborne data and ends with the adjustment to the component cumulative flight hours via a usage credit. A Functional Hazard Assessment (FHA) was performed for this HUMS-based UBM credit as implemented through the entire end-to-end process. Because the end-to-end process spans multiple domains, providing different levels of functionality (e.g., OBS, GBS, OEM, and maintenance from figure 42), it is not practical to assign a single worst-case hazard level to the entire process. Rather, criticality is assigned to the individual systems. The hazard analysis for each system is evaluated based on the function(s) executed by the system, although failure mode effects and criticality may be dependent on functionality implemented by other systems. For example, failure modes of the onboard HUMS system must be evaluated with consideration to how the OEM analysis process uses the HUMS data. Each failure mode is classified using the hazard criticality categories listed in table 9, which are extracted from a combination of AC 29-2C MG15 [10], SAE-ARP4761 [11], and DO-178B [12].

Table 13. Functional hazard criticality levels

Failure Condition Category (Criticality)	No Effect	Minor	Major	Hazardous/ Severe-Major	Catastrophic
Effect on rotorcraft	No effect on operational capabilities or safety	Slight reduction in functional capabilities or safety margins	Significant reduction in functional capabilities or safety margin	Large reduction in functional capabilities or safety margins	Loss of rotorcraft
Allowable probability per flight hour	1.0 (Frequent)	10^{-3} (Reasonably probable)	10^{-5} (Remote)	10^{-7} (Extremely remote)	10^{-9} (Extremely improbable)
Required DO-178B software level	E	D	C	B	A

Before addressing the FHA for the HUMS UBM process, it is important to understand the relationship between a component RT and component criticality. RTs are assigned to components with fatigue failure modes that have nominally a 10^{-6} probability of failure within the design life of the aircraft. Fatigue failure modes of dynamic components are assigned criticality levels using Failure Modes, Effects, and Criticality Analysis (FMECA), which considers the merits of both the design and any compensating provisions—such as design redundancy or inspection or maintenance requirements—that can reduce the criticality of the failure modes. In the fatigue analysis of a dynamic component, a single RT is set based on the lowest individual RT for all fatigue failure modes, regardless of criticality.

Criticality for fatigue failure modes can be anywhere from minor to catastrophic. While the RT for a dynamic component is a means to ensure an extremely remote probability of failure, an RT does not eliminate or reduce the criticality of the associated failure mode. Likewise, an erroneous RT does not increase the criticality of the component failure mode established in the component FMECA; it only changes the risk or structural reliability of the component. In very rare circumstances, a gross error in the RT may increase the risk of failure to the point that failure may be reasonably probable during the life of the component. This type of error could occur if a very low strength part were assigned an erroneously long RT. In this case, a large reduction in structural reliability may exist, but the hazard criticality associated with the HUMS monitoring system cannot be more severe than the component failure mode criticality. On the other hand, small errors in the RT cannot significantly affect the risk of failure and therefore present no hazard to the rotorcraft. Most failure modes for a generic UBM process will fall somewhere in between these two extremes. By ensuring that gross errors are not possible, certain attributes (e.g., credit cap, rigorous data validation, or use of pilot reported flight hours) of a UBM process can be imposed, as appropriate for specific credits, to limit the severity of an erroneous RT. In these cases, the worst case effect of a large reduction in structural reliability may be claimed, which results in the Hazardous/Severe-Major failure condition shown in table 9. As an example, an RT credit is inherently limiting because it can only give back a percentage of the RT.

For reasons described above, criticality is dependent on the component and UBM process details and must be evaluated for each HUMS application. The AC 29-2C MG15 [10] explicitly does not address applications with a corresponding failure category of catastrophic; however, it does state in paragraph f.(1)(i)(A) that:

The intended application can range from systems that acquire data for proof of concept only to a system that acquires and processes data to determine if a life-limited part should be replaced. This range of applications will have a corresponding range of criticality for the systems from No Effect to Hazardous/Severe-Major.

The UBM credit application described herein falls into the expected range of applications covered by the AC.

The FHA for the HUMS UBM process documented herein is approached by providing a functional description of the end-to-end process, review of the existing FMECA for the target component (stationary swashplate), and FMECA assessment for the HUMS UBM end-to-end process for each of the four domains of the process (i.e., OBS, GBS, OEM, and Maintenance). The assessment for each potential failure mode in the HUMS UBM process includes a description of worst-case failure effect at the aircraft level and resulting criticality. In general, failures can be described as loss of functionality, erroneous/misleading functionality, or degradation of the function. Each possible failure has an associated worst-case effect on the rotorcraft system as classified in the failure condition categories listed in table 9. The following steps provide a general framework for conducting a hazard analysis for a HUMS UBM process.

1. Review/conduct FMECA of target component:
 - a. Identify component failure modes that are managed by maintenance protocols that are affected by the UBM credit (e.g., RT).
 - b. Review/analyze component failure mode effects and hazard level after mitigation, which may include design features (e.g., redundancies and damage tolerance) and/or maintenance actions (e.g., inspections) to achieve desired/acceptable component and/or subsystem hazard level.
2. Conduct FMECA of UBM credit process:
 - a. Identify UBM process failure modes.
 - b. Analyze UBM process failure mode effects in the context of relevant component failure mode effects and UBM process details.
 - c. Analyze UBM process hazard level, assuming that component design/maintenance mitigations still apply except for those that are to be managed, modified, or replaced by the UBM credit.
 - d. Determine whether HUMS onboard and ground-based software Design Assurance Level (DAL) is commensurate with UBM credit process hazard level.
 - e. If not, investigate whether UBM credit process changes or other mitigating actions can be used to reduce determined hazard level associated with the UBM credit process.

3.3.1 Functional Description

The end-to-end mock UBM credit process will accumulate time and number of occurrences for defined flight regimes to account for all ground/flight operations. This HUMS UBM process requires the aircraft parametric data recorded from various onboard sensors and the sequence of identified regimes resulting from the onboard RR algorithm processing of these state parameters. Both the parametric data and regime sequences are sealed with an error-checking protocol and written to a data card by the onboard Data Transfer Unit (DTU). The data are transferred to the rotorcraft OEM for evaluation of helicopter usage and calculation of accumulated fatigue damage and UBM flight-hour credit. Regime and parametric data are analyzed by the OEM to independently assure data quality and then used to assign time and occurrences of select critical CWC regimes to each tail number and/or component serial number. The time and occurrences of select critical CWC regimes are then used to calculate usage-based flight-hour credits for specific serial number components based on a conservative calculation of cumulative fatigue using reliability factors. Usage-based flight-hour credits are applied to the component log card by adjusting the “total time since new” for a given serial number.

3.3.2 Component FMECA

The S-92 aircraft swashplate is a flight-critical component with multiple failure modes of various levels of criticality. The swashplate was designed with significant inherent load carrying redundancy to reduce the immediate consequences of initial degradation of the component. Further, the RT is established for fatigue failure modes that are a function of usage and loads. The component has other failure modes that are not as deterministic in nature. Therefore, specific

maintenance actions (e.g., daily inspections and RT removal) and dedicated bearing monitoring have been employed to ensure that swashplate degradation is detected before failure. The swashplate is an assembly of the rotating and stationary swashplate subassemblies that are joined through a duplex bearing. Each of these components has its own failure modes and associated RTs. The fatigue failure modes of the stationary swashplate range in severity from major to catastrophic; however, all catastrophic failure modes have been analyzed previously to meet the requirements for an unlimited RT. The worst-case failure mode associated with the limiting RT of the stationary swashplate has a criticality of Hazardous/Severe-Major.

3.3.3 HUMS UBM FMECA

The FMECA for the HUMS UBM process is listed below and organized into the OBS, GBS, OEM analysis, and Maintenance domain, as presented in figure 42.

3.3.3.1 OBS Failure Modes

1. Potential failure mode: Complete loss of HUMS airborne system functionality.
 - a. Worst-case failure effect: Loss of the airborne system functionality results in gaps in the usage history for a particular aircraft. These gaps are identified during OEM analysis by comparing the calculated HUMS flight hours to operator-logged flight hours. The difference between operator-logged flight hours and calculated HUMS flight hours can be caused by a number of things, such as HUMS not installed or being non-functional, data loss, data corruption, or conservative estimation of flight hours by pilots/operators. Gaps are treated conservatively to cover any possible sources of error that are due to system/process failures by assigning the worst-case damage rate during the period of time not covered by HUMS data.
 - b. Failure condition category (criticality): No effect.
2. Potential failure mode: Erroneous sensor data detected.
 - a. Worst-case failure effect: Sensor failures are detected and flagged onboard, resulting in invalid regime data that are flagged and treated in this mock UBM credit application as a complete loss of HUMS airborne system functionality.
 - b. Failure condition category (criticality): No effect.
3. Potential failure mode: Erroneous sensor data undetected.
 - a. Worst-case failure effect: It is possible to erroneously record and process sensor data that the airborne system uses to calculate regimes. Most sensors used by the HUMS RR algorithms deployed on the S-92 aircraft are also used by the aircraft flight control system and, as such, sensors are redundant—which provides detection capability. However, there is one sensor (an accelerometer that measures aircraft load factor) that is used only by HUMS RR algorithms. Any sensor anomalous data patterns not caught and rectified by the operator are

expected to be detected during OEM data integrity analysis shown in the end-to-end UBM process (see figure 42). SAC has developed comprehensive data integrity algorithms to automatically identify known sensor failure characteristics and resultant anomalies in usage patterns. However, it may still be possible for sensor faults (subtle changes in calibration) and resultant errors in regime sequences identified onboard to remain undetected and be propagated into the OEM analysis of the helicopter usage data. Short duration sensor faults (less than a few flight hours) not detected onboard are more difficult to detect by the OEM analysis but would have a negligible effect on the Fatigue Usage Spectrum metrics. Long duration sensor faults (greater than 100 flight hours) not detected onboard are more easily detected by OEM analysis. If left undetected, they would have a significant effect on the resulting recommended adjustments to the component flight hours or RT. If this error is then in the unconservative direction, it can result in a component being left on the helicopter longer than the appropriate RT. If this error is also significant in magnitude, and still undetected, the erroneous UBM credit can result in a large reduction in structural reliability or safety margins.

- b. Failure condition category (criticality): Hazardous/severe-major.
4. Potential failure mode: Erroneous onboard calculation of regimes.
- a. Worst-case failure effect: The erroneous calculation of regimes in the OBS can only have a significant effect on the resulting life credit if the erroneous calculations occur on a sustained systemic basis for many hundreds or thousands of flight hours. Such systemic errors are unlikely given RR algorithm validation and software qualification. In the unlikely event that a software error did occur, such a significant systemic error in calculated regimes would likely result in odd regime usage patterns for the fleet or a particular aircraft that could be easily detected during OEM analysis as well as fleet and aircraft usage audits. Parametric data can then be used to assess the validity of onboard regime sequences. Detected systemic errors in onboard regime sequences would be mitigated through the elimination of suspicious usage data and its replacement with worst-case damage rate assumptions. However, undetected errors in the calculated regimes could result in large reductions in structural reliability or safety margins.
 - b. Failure condition category (Criticality): Hazardous/severe-major.

3.3.3.2 Ground-Based System

1. Potential failure mode: HUMS data are not transferred to OEM (i.e., loss of data).
 - a. Worst-case failure effect: HUMS data are expected to be transferred to the OEM on a regular basis to aggregate usage statics over the cumulative life of an airframe and calculate component UBM credits. An audit to identify missing data is part of the UBM process. Missing HUMS data are detected and dealt with as described in Potential Failure Mode 1.1.
 - b. Failure condition category (Criticality): No effect.
2. Potential failure mode: Corruption of HUMS data during transfer from OBS to OEM server.
 - a. Worst-case failure effect: Data corrupted during the transfer to the OEM are extremely unlikely to be corrupted in a way that is undetectable by state-of-the-art data integrity checks. Data recorded onboard the HUMS system include encapsulated error bits based on established error-checking protocol (e.g., Checksum or CRCs). These data are then transmitted to the OEM through a multistep process. First, the onboard HUMS data are transferred to a Personal Computer Memory Card International Association (PCMCIA) card by the onboard DTU. Then, the PCMCIA card is hand-carried from the aircraft to the operator ground station and uploaded to a HUMS ground station. Next, the data are transferred via a local network to an operator server. Lastly, the data are transferred over the Internet via File Transfer Protocol (FTP) to an OEM server, where it is written to a hard drive. The error-checking protocol is then conducted by the OEM to validate the integrity of the data as recorded by the OBS. Any error bit failure results in categorization of the associated packet as invalid. Any parametric and usage data corruption detected is addressed in the same manner as loss of data (Potential Failure Modes 1.1 and 1.2).
 - b. Failure condition category (criticality): No effect.

3.3.3.3 OEM Analysis

1. Potential failure mode: Erroneous analysis of component usage, calculated fatigue damage accumulation, and UBM credit from HUMS data.
 - a. Worst-case failure effect: Analysis of component life using HUMS data must follow an FAA-approved methodology or process that is submitted as part of the aircraft design certification package. This analysis is carried out by SME engineers using the same analytical software tools, standard work, and engineering reviews and approvals used to calculate the original component life. Results of this analysis are documented in technical reports that are then subject to an engineering review and approval process. The calculation of UBM credits is subject to even greater rigor as a result of the process established as part of the

end-to-end UBM credit process to monitor usage trends for individual aircraft, operator fleets, and the total S-92 fleet. Detection of unusual usage patterns or UBM credit results that are inconsistent with usage statistics will trigger further SME audit and analysis. UBM credit approval is contingent on the aforementioned engineering checks, balances, and audits being passed. If an unlikely analysis error passes through undetected, it could produce erroneous UBM credits that may result in large reductions in structural reliability or safety margins.

- b. Failure condition category (criticality): Hazardous/severe-major.

3.3.3.4 Maintenance

1. Potential failure mode: Erroneous maintenance data provided by operator.
 - a. Worst-case failure effect: The worst case failure scenario is for the operator to provide an erroneous component log card that underrepresents the component flight-hour history. This failure mode is not unique to the HUMS UBM process, as this would be a risk to any component in the field not managed by a HUMS UBM process. The risk is reduced by the UBM process because any significant discrepancy between HUMS recorded and operator-recorded flight hours triggers an audit. Differences must be reconciled before a UBM credit will be granted.
 - b. Failure condition category (Criticality): No effect.

3.3.4 FHA Summary

The above assessment of eight potential failure modes for the specific mock UBM credit application yields the worst-case criticality of the end-to-end process of Hazardous/severe-major. However, as stated previously, it is more useful to assign criticality to each domain of the process as this has further implications for software certification requirements. By assigning criticality based solely on the functions provided by each domain, the results of the FHA are shown in table 10.

Table 14. UBM process FHA results

UBM Process Domain	Worst Case Criticality	Software DAL
Onboard system	Hazardous/severe-major	DAL-B
Ground-based system	No effect	DAL-E
OEM	Hazardous/severe-major	N/A (see Section 3)
Maintenance	No effect	N/A (No S/W)

It is recommended that the onboard software for parametric data acquisition and RR be designed and qualified/certified to DAL-B for this mock HUMS UBM process. The ground station can be designed to DAL-E or any good software development standards, as it is used only for data pass through in this end-to-end mock UBM credit process. OEM data assessments and calculations can be performed using the same methods and software tools used for aircraft design and lifing certification. The S-92 aircraft has an integrated HUMS that was certified to DAL-B. If the HUMS were less than DAL-B, other mitigating actions not employed in the end-to-end process defined herein may be required. Potential mitigating actions include implementing a UBM credit cap or limiting the number of UBM credits that can be applied to a given component over its life.

3.4 INSTALLATION QUALIFICATION

Installation qualification addresses approval of systems and equipment that acquire, store, process, and display HUMS data. The degree of qualification of the installed equipment is commensurate with the hazard level assigned in the functional hazard and criticality analysis. However, some elements of the end-to-end process described in figure 42 are not allocated to the installed HUMS equipment, as they are performed through OEM data analysis. This presents a challenge in understanding certification requirements for a credit process that is not entirely contained within the installed HUMS equipment. Certification requirements for these two domains are addressed in Sections 3.4.1.1 and 3.4.1.2.

3.4.1 Installed HUMS Equipment

3.4.1.1 Airborne Equipment

The S-92A installed HUMS equipment consists of an onboard main processing unit (MPU), DTU, data transfer card, and ground-based Ground Support System (GSS) computer. The MPU acquires, processes, and stores data from a host of systems as well as dedicated HUMS and shared sensors (refer to figure 43 for an overview of the system and its interfaces). Flight regimes are calculated within the MPU using a set of parameters that originate from multiple aircraft systems. Each parameter is fault-detected and validated by the source computer prior to sending data to HUMS. Along with parameter values, the data validity bit is received by HUMS, which indicates whether the parameter value is valid or invalid. An invalid bit can indicate that the sensor failed or the source computer is not functional—among other possible issues. When any parameter required to perform RR is invalid, HUMS declares the regime as “Undetermined.” The raw parametric data, validity bits, and regime classification data are transferred from the MPU onto a data card using the DTU located in the right-hand avionics rack. These data are written onto the data card as a data packet and stored with an error-checking protocol.

The airborne HUMS system and accompanying GSS have previously been FAA-approved as a usage data recording, display, and archiving system. The approval for DAL “B” for both airborne software and hardware is commensurate with the intent to use HUMS parametric and regime data for component RT adjustments, including the mock UBM credit documented herein.

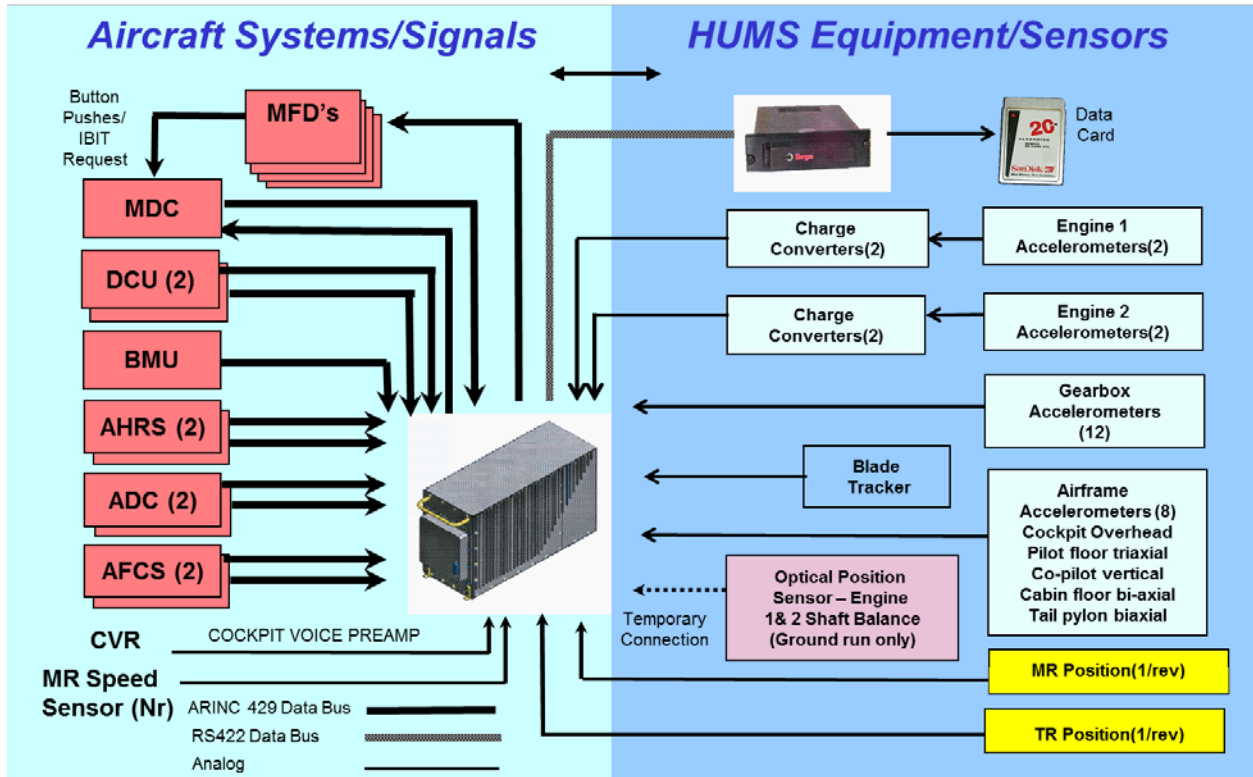


Figure 43. S-92 HUMS system overview

3.4.1.2 HUMS Ground-Based Equipment

The data stored on the data card are transferred to the operator-maintained GSS computer, where the operator can view, but not manipulate, usage data stored on the GSS. The data are then transferred to the operator server, via local area network, where it is stored in a data repository. Finally, the data are transferred to the OEM server over the Internet via FTP. Note that the S-92 aircraft sales agreement requires that the customer provide SAC with all HUMS data. Most operators use an automated script provided by SAC for doing this on a regular basis, typically once or twice a day for larger operators.

When determining qualification requirements for subsystem components, consideration is given to functional allocation among the various components of the UBM process. This means that the criticality level for a given subsystem or hardware component is based on the functional hazards that the subsystem or hardware component presents to the end-to-end process. Based on the credit hazard assessment in section 4, there is no functionality in the HUMS GSS that presents a functional hazard to the end-to-end mock UBM credit process. Therefore, there are no additional requirements for the certification HUMS GSS beyond that used to certify the overall HUMS onboard and GSS system. At that time, the AC 29-2C MG-15 direct evidence methodology was utilized to validate the use of the GSS as a device for uploading and displaying usage data from the PCMCIA card. For the mock UBM credit process, the GSS is only used to upload the data and transfer it to an operator server, which in turn transmits it to the OEM server.

3.4.2 OEM Analysis

The AC explicitly provides qualification guidance for HUMS airborne and ground-based equipment. Qualification requirements that apply to installed equipment serve to provide a level of integrity commensurate with the defined hazard criticality to ensure that hardware and software deployed in the field will operate and carry out processes reliably and autonomously without reliance on human supervision. Not addressed in these guidelines, however, are elements of an end-to-end process not hosted by the HUMS airborne or ground-based equipment. The end-to-end process for the mock HUMS credit application defined herein extends back to the rotorcraft OEM, which processes the usage data and calculates the UBM credit. This process leverages data generated from previously qualified HUMS equipment and involves engineering analysis of HUMS data to arrive at a maintenance intervention action. This part of the process is labeled “OEM Analysis” in figure 42. It is conceivable that many near-term HUMS credit applications will have process elements that are not entirely contained within the installed HUMS equipment.

Many of the engineering analysis software tools used in this domain are not unique to the HUMS credit application but are the same or similar engineering analysis tools used in the original establishment of component RTs. Examples of the most common analysis tools include MATLAB[®] scripts or functions, Microsoft Excel spreadsheets, and custom-developed structural analysis tools and/or RT calculators. A common element among all of these tools is that they are non-autonomous and employed by SMEs in an engineering support role. The certification burden for this aspect of the credit process should not be focused on the specific software support tools used but rather on the procedures and methodologies employed for calculating component life and RT (such as an FAA-approved fatigue methodology report), resulting analysis reports and documents, and oversight/review processes. The specific procedures that modify or add to already approved fatigue methodology procedures and are used to arrive at component RT adjustments using HUMS data are subject to the credit validation guidelines of the AC. The results of engineering analyses that are the basis of HUMS-based component UBM credits will be published in a technical report and subject to an independent technical review process before being further reviewed and approved by airworthiness authorities. The UBM credit process uses the existing, approved procedures and technical review and approval processes already in place to ensure the highest level of process integrity in an engineering environment where safety critical decisions are made routinely. There is no need to impose additional qualification requirements on the OEM analysis, review, and approval procedures.

3.5 CREDIT VALIDATION

The AC describes the key requirements for credit validation as follows:

- Description of application and associated credit
- Demonstration that the physics involved is well understood
- Validation methodology
- Controlled introduction to service
- Continued airworthiness and synthesis of credit

This section follows the format above as much as possible in order to directly address the guidelines in the AC.

3.5.1 Description of Application and Associated Credit

The stationary swashplate on the S-92 aircraft has a published RT of 14,000 hours. This RT is predicated on operation of the helicopter within all flight and maintenance parameters, as required by current manuals and applicable Federal Aviation Regulations. As the replacement time is not predicated on any specific monitored usage profile, a CWC usage spectrum is assumed in the analysis of the component failure times. This CWC spectrum assumption is one piece of a larger fatigue life methodology that achieves a reliability goal of six- 9s for individual fatigue failure modes in the rotorcraft.

The intent of the HUMS application and associated mock UBM credit is to use RR technology to count occurrences and/or duration of key damaging flight regimes, determine the percent of fatigue life consumed for the stationary swashplate, and calculate a usage credit that adjusts the cumulative flight hours of the installed serial number component. The mock UBM credit application described herein does not change the published RT of the component. It is not limited in the number of times a component may be evaluated for usage credit or by a cap in the life credit amount. The credit hazard and criticality analysis for this application is described in Section 4.

3.5.2 Physics of the Application

3.5.2.1 Stationary Swashplate Fatigue Analysis

The S-92 MR swashplate assembly consists of an inner stationary swashplate assembly and an outer rotating swashplate assembly, as shown in figure 44. The stationary and rotating swashplates are interfaced by a duplex bearing assembly that allows for rotation of the outer assembly, which is directly connected to the four-blade pitch control rods. The stationary swashplate transfers collective and cyclic MR blade pitch commands from three flight control servos that are mounted to both the main gearbox and stationary swashplate. Collective pitch moves the swashplate vertically along a swashplate guide and cyclic pitch controls the angle and direction of the swashplate tilt. The combined collective and cyclic pitch of the swashplate controls the MR blade pitch around the rotor azimuth. Aerodynamic blade pitch moments are translated to the pitch control rods, down through the swashplate, and reacted by the servos.

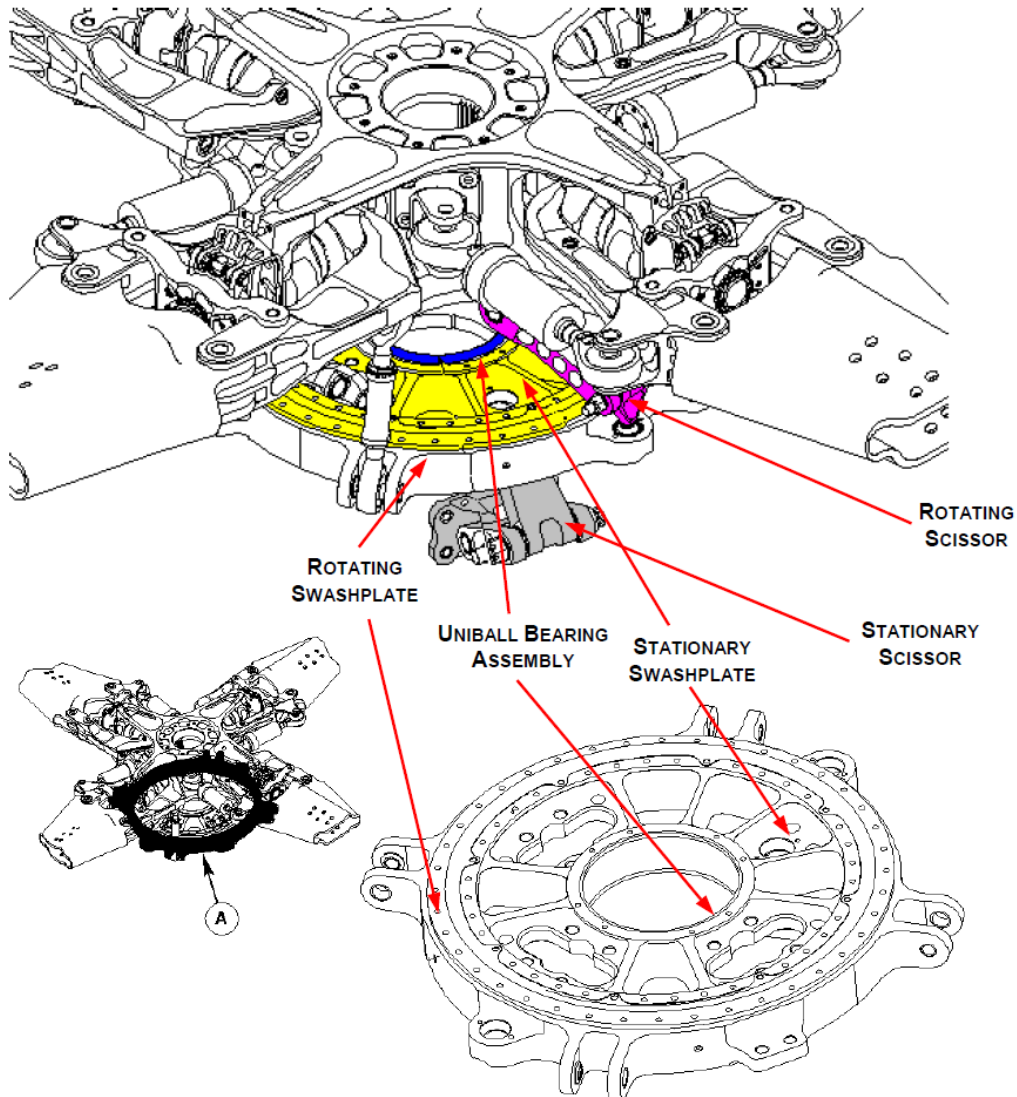


Figure 44. S-92 main rotor swashplate

During the S-92 aircraft development phase, multiple stationary swashplate specimens were fatigue-tested in a specialized rig that allows for controlled test loads to be applied to servo attachment regions and reacted by the four-pitch control rods. While only two fatigue failure modes were generated from this test program, multiple potential failure modes were considered in the RT analysis based on known high-stress regions. In total, six fatigue failure modes were considered in the RT analysis, as listed in table 11. As shown in this table, the life-limiting mode for the stationary swashplate is at the servo trunnion attachment hole, with a CRT of 14,000 hours.

Table 15. Stationary swashplate fatigue failure modes

Component Region	Fatigue Mode	Damage Rate (per 100 hours)	Calculated Retirement Time (hours)
MR servo trunnion attachment region	Trunnion attachment hole, chafing	0.0073	14,000
	Potential, non-chafing	0.0009	120,000
Uniball bore region	Potential, chafing	0.0062	16,000
	Uniball bore, non-chafing	0.002	50,000
Stationary scissors attachment region	Potential, chafing	0	Infinite
	Potential, non-chafing	0	Infinite

It is important to note that the servo trunnion attachment hole is not the only life-limiting fatigue mode for the stationary swashplate. The uniball bore region is also fatigue life-limited to 16,000 flight hours. In this case, both the servo trunnion mode and uniball bore mode are sensitive to the same set of flight regimes, which means that they will always trend together in terms of changes in life due to changes in usage. In other words, the uniball mode cannot be more life-limiting than the trunnion mode, given only a change in the usage spectrum. Detailed results for the uniball mode are not addressed in this report but would need to be verified in a formal certification analysis.

The fatigue test program described above does not solely determine the RT for a component. The key output of the fatigue test program is an S-N curve for each of the evaluated fatigue modes. This curve defines the expected cycles-to-failure for a continuously applied load at given vibratory amplitude. A notional example of such an S-N curve is shown in figure 45. In this figure, a “mean strength curve” is fit to the full-scale test data, which represent the true strength of the fatigue mode. A “working curve” defined from material-specific reliability factors is used when calculating fatigue damage and comparing against flight loads. Figure 45 also shows how flight loads are compared against the fatigue strength. Three reference lines are shown, representing the maximum flight test fatigue load for GAG (maximum GAG load cycle), maximum load of all in-flight maneuvers, and maximum load for all LF conditions. These reference lines indicate roughly which maneuvers are critical in the fatigue analysis. For example, the maximum LF load from all flight test data is below the endurance limit and non-damaging, which means that LF does not contribute to the fatigue damage of this component. On the other hand, GAG and at least one maneuver have the potential to contribute to fatigue damage.

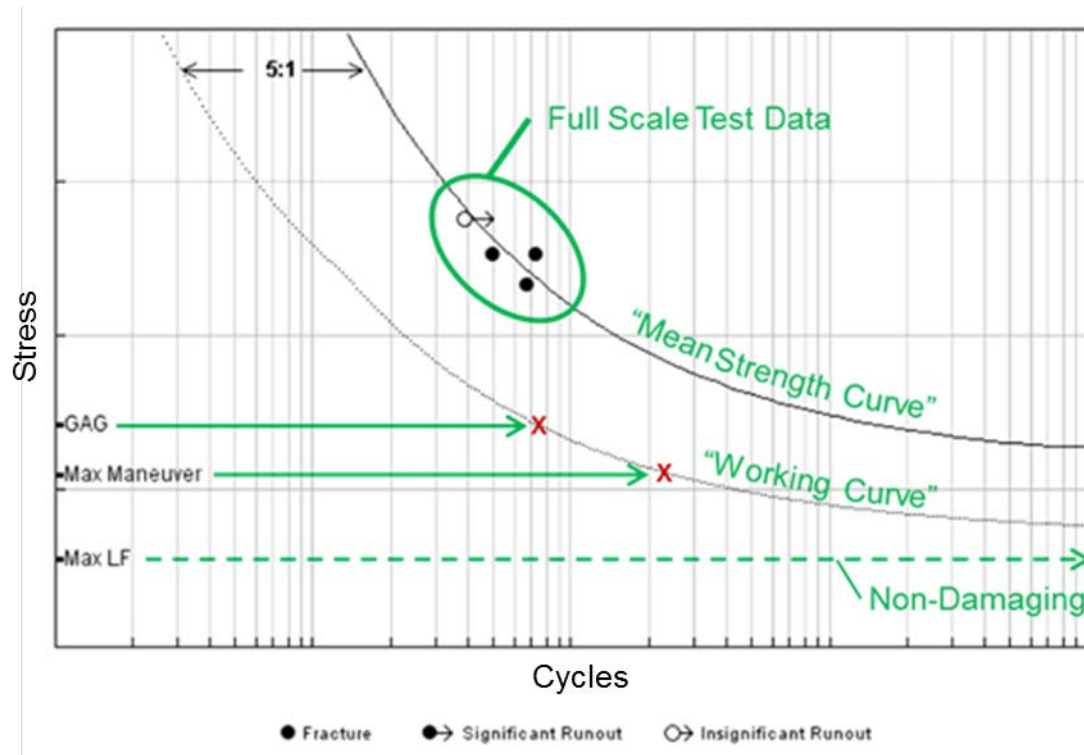


Figure 45. Sample S-N curve for stationary swashplate

The fatigue damage rate for each regime is established through analysis of the flight test loads associated with each regime in relationship to the S-N working curve. Once the list of potentially damaging regimes is established, a regime damage rate is computed using the regime occurrence/duration metrics contained in the CWC usage spectrum. The damage rates for all damaging regimes are summed together to arrive at a total fatigue damage rate for the component fatigue mode. A simplified summary of the final RT calculation for the life-limiting mode of the stationary swashplate is shown in table 12.

Table 16. Damage calculation summary for stationary swashplate life-limiting mode

Reg	Regime Name	Regime Type	Damage/100 Hr
18	LT TRN 45 V_{NE}	Steady state	0.0023
20	RT TRN 45 V_{NE}	Steady state	0.0023
25	DIVE 1.1 V_{NE}	Steady state	0.0000
26	E&R DIVE 1.1 V_{NE}	Transient	0.0000
47	LONG REV LF V_{NE}	Transient	0.0000
51	COLL REV LF V_{NE}	Transient	0.0000
54	E&R LT TRN 30 & 45 V_{NE}	Transient	0.0007
55	E&R RT TRN 30 & 45 V_{NE}	Transient	0.0006
57	SYM PULLOUT MOD V_{NE}	Transient	0.0000
58	SYM PULLOUT SEV V_{NE}	Transient	0.0000
59	SYM PULLOUT MOD 0.8 V_{NE}	Transient	0.0007
60	SYM PULLOUT SEV 0.8 V_{NE}	Transient	0.0000
61	SYM PUSHOVER V_{NE}	Transient	0.0000
62	SYM PUSHOVER 0.8 V_{NE}	Transient	0.0000
72	GAG	Quasi-static	0.0006
102	COL REV LF 0.8 V_{NE} - CARGO	Transient	0.0000
105	E&R PPD - CARGO	Transient	0.0000
			Total Damage/100Hr = 0.0073
<div style="border: 1px solid black; padding: 2px; display: inline-block;">Highlighted = Critical regime</div>			Calculated Retirement Time = 14,000

The most critical regimes that contribute the most to the fatigue damage are determined from fatigue damage calculation tables based on a combination of the level of potential damage that the maneuver can induce, and maneuver rate of occurrence or percent time. The results for the stationary swashplate are presented in figure 46, where the percent contribution to the total damage rate for each of the damaging regimes are plotted in descending order of contribution. While there are a total of 17 regimes that have the potential to cause fatigue damage, 98% of the fatigue damage that produces a 14,000-hour RT is attributed to six critical regimes.

One key feature of the UBM credit approach described herein is that it is not necessary to monitor all damaging regimes for a particular component. Practical considerations for determining which regimes to monitor include the ability or inability to accurately detect various regimes with RR and their relative contribution to fatigue damage and resultant RT. It is always assumed that the CWC usage spectrum is conservative for any particular regime and, therefore, the CWC damage rate is attributed to any non-monitored regimes. The mock UBM credit approach for the stationary swashplate is to monitor only the top six critical damaging regimes with RR, while allocating CWC damage rates to the bottom 11 regimes. The specific calculations used for calculating fatigue damage for monitored and unmonitored regimes will be shown later in the context of calculating the usage credit for a specific serial number component. In this particular case, if the top six damaging regimes were removed from the analysis, the residual damage induced by the remaining 11 regimes with their CWC usage assumptions would be small enough to eliminate the stationary swashplate RT associated with this failure mode. In reality, most of the top six regimes will occur at some non-zero usage rate. Although the actual usage rate on an individual tail number, which is monitored on a regular basis, can be significantly lower than the CWC usage spectrum. This difference can either be due to large variations in the maneuver usage rate across the fleet or a large disparity between the usage spectrum and the actual fleet's worst-case metrics. In either case, the application described herein can take full advantage of this difference in actual versus assumed usage. It is noted, however, that where the latter case dominates, significant HUMS benefit could be achieved through a CWC spectrum update that results in new replacement times for the entire fleet—also termed a part-number credit—which is not the focus of the mock UBM credit application.

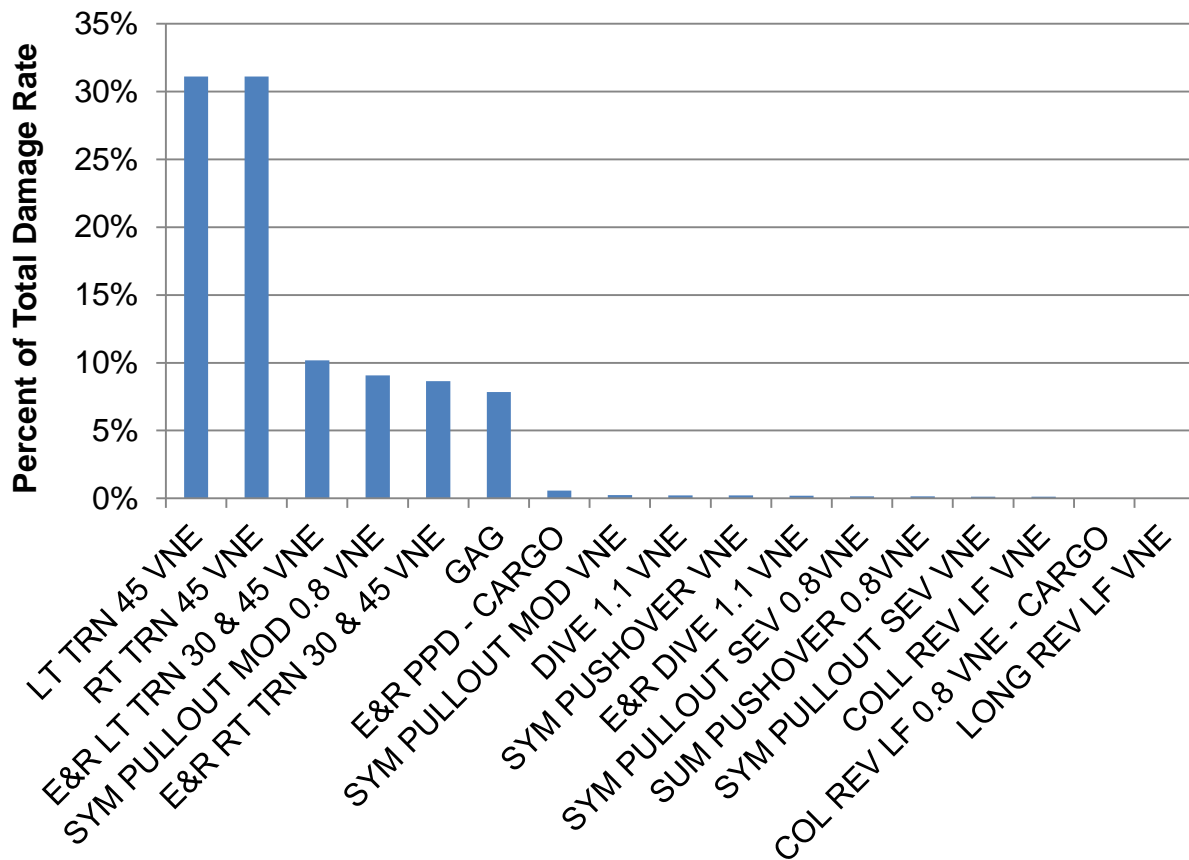


Figure 46. Stationary swashplate damage regimes

3.5.2.2 Regime Recognition Monitoring Technique

The key to the HUMS RR monitoring technique used for the current mock UBM credit is to reliably and accurately track the most damaging usage spectrum regimes that drive the stationary swashplate life analysis. The S-92 aircraft usage spectrum assumptions for the top six damaging regimes are listed in table 13. Within these six regimes, there are three types of maneuvers: steady state, transient, and quasi-static. Steady state regimes, such as LF or hover, are quantified in terms of percent time because the applied fatigue load within a single occurrence is fairly constant, and the accrued fatigue cycles are based on the total time spent in the maneuver. On the other hand, transient regimes such as symmetric pullouts are quantified in terms of occurrences because the transient nature of the maneuver typically causes a single peak fatigue load at some point during the maneuver. Because transient regimes are typically very short duration events, it is difficult to characterize them by duration when there is rarely a distinct start and end to the maneuver. In both steady state and transient regimes, the usage metric is converted to a fatigue cycle rate based on standard assumptions, such as the predominant load frequency, in the fatigue analysis. The quasi-static GAG regime is a single fatigue load cycle that occurs over an indeterminate duration and is caused by the maximum and minimum peak loads that occur across a flight. While RR tracks the in-flight steady state and transient maneuvers, GAG events are counted by the OBS by using the WOW parameter to track landing/takeoff cycles.

Table 17. Stationary swashplate critical regime usage

Regime Name	Regime Type	CWC Usage Rate	Units
Left turn, 45° V _{NE}	Steady state maneuver	0.15	Percent time
Right turn, 45° V _{NE}	Steady state maneuver	0.15	Percent time
Entry/recovery left turn 30° & 45° V _{NE}	Transient maneuver	95	Occurrences per 100 hours
Entry/recovery right turn 30° & 45° V _{NE}	Transient maneuver	95	Occurrences per 100 hours
Symmetric pullout, moderate, 0.8 V _{NE}	Transient maneuver	90	Occurrences per 100 hours
GAG	Quasi-static event	450	Occurrences per 100 hours

The RR clustering/prorating approach described in Section 2.1 is applied in order to reliably track these critical regimes. The regimes that result from the clustering/prorating process are directly aligned with the S-92 aircraft usage spectrum for turns, pullouts, and pushovers and can then be used to track the usage within the context of the usage spectrum. Figure 47 shows a single occurrence of a 22-second duration, 45° right turn at V_{NE} airspeed that was accurately captured in the validation flight test data after the application of the clustering/prorating method. To track fleet usage against the usage spectrum, this single turn occurrence counts as 22 seconds against the right turn, 45° V_{NE} steady state regime as well as two occurrences of the entry/recovery (E&R) right turn 30° & 45° V_{NE} transient regime.

The single turn contributes two occurrences to the transient regime because the turn contains both an entry and a recovery event on either side of the turn. Because HUMS RR does not explicitly detect the transient E&R portion of the turn, the total HUMS RR time of 22 seconds includes a portion of these events. A simplifying conservative assumption in the fleet analysis is to count the entire 22 seconds against the steady state turn regime. While this assumption is very conservative, it eliminates the need for a more rigorous methodology to explicitly capture the beginning and end points of the entry, steady state, and recovery segments of a turn. Another example is shown in figure 48 for a moderate pullout at 130 knots. In this case, HUMS RR, with the clustering/prorating post-processing method, detected a moderate pullout, 0.8 V_{NE}, which is the correct airspeed prorated for the maneuver. This maneuver contributes one occurrence to the symmetric pullout, moderate 0.8 V_{NE} regime in the usage spectrum. While the duration of five seconds is captured, for reasons discussed earlier, duration is not necessary to monitor the usage for this regime.

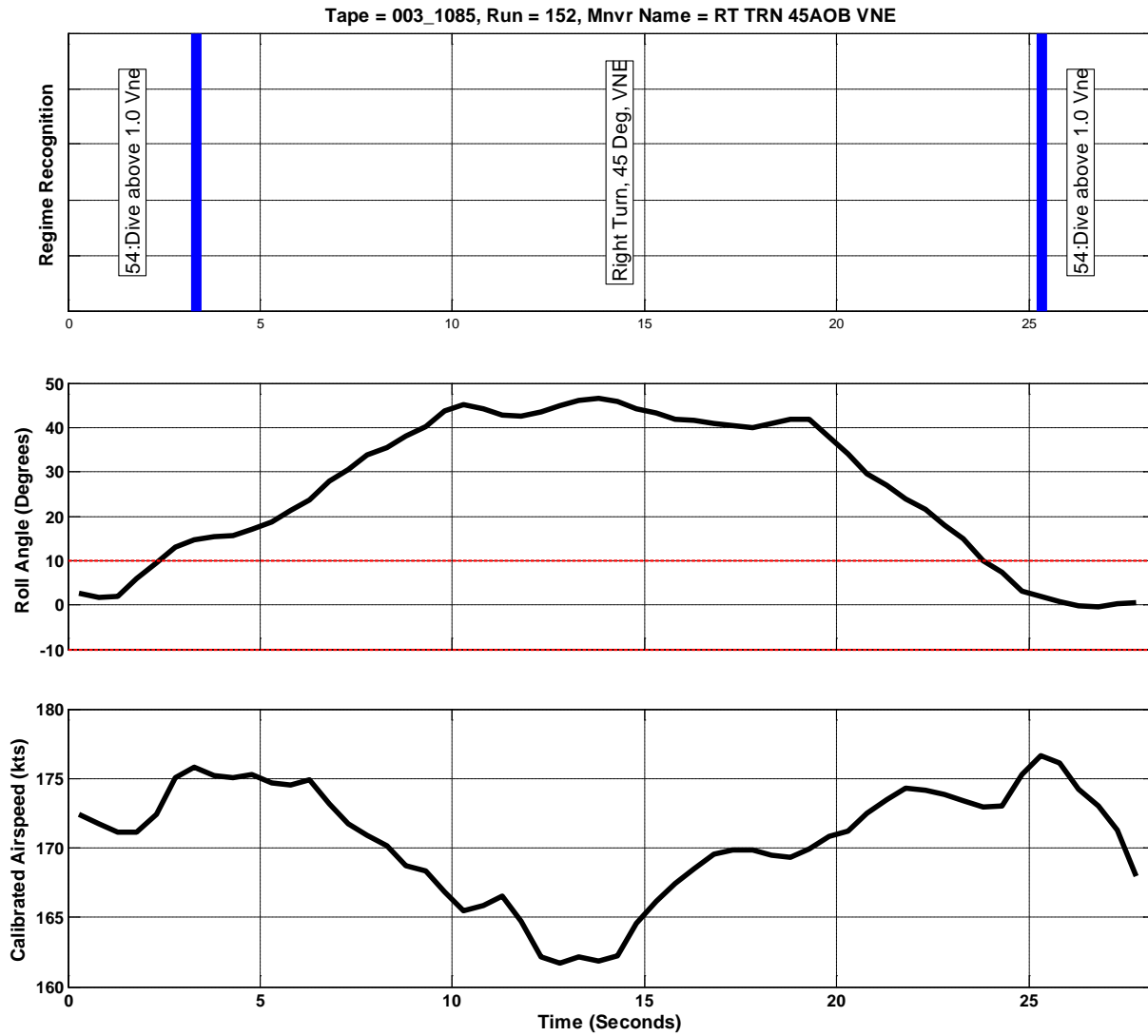


Figure 47. Regime recognition of right turn, 45° V_{NE}

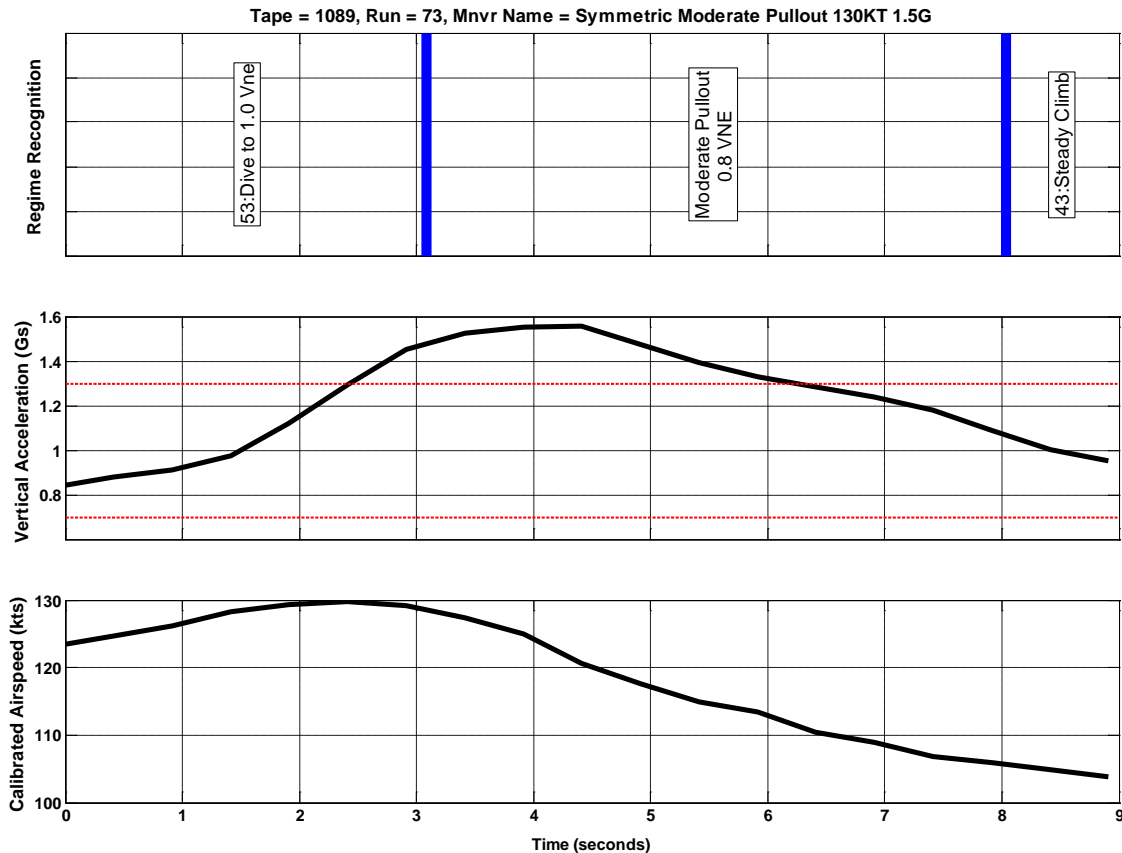


Figure 48. Regime recognition of moderate pullout, 0.8 V_{NE}

3.5.2.3 Data Quality Assessment

Data quality assessment is a necessary step to eliminate data quality issues from the usage analysis results that are used to determine HUMS-based UBM credits. The presence of data quality issues in the HUMS system does not reflect poorly on the integrity of the HUMS system. In fact, most of the data quality issues are detected and mitigated by the HUMS system before the data are transferred offboard. These issues are inevitable given the massive amount of HUMS data generated by the S-92 rotorcraft fleet every day and accumulated over years of operation.

For the successful assessment of data quality, it is important to understand all the types of quality issues that are present in the data set. Even though most of these issues are dealt with onboard, they have to be specifically removed from analysis off board. Further, it is not expected that all data quality issues can be conceived of during the initial development of the OBS. Therefore, it is necessary to continue to monitor and assess fleet data in order to gain a deeper understanding of the quality issues that remain in the fleet database so they can be filtered out from the usage analysis. Table 14 contains a listing of types of data quality issues and a description of how and where these issues are detected and handled in the end-to-end process. Pervasive issues are flagged for engineering analysis, correction, and/or disposition before a specific UBM credit is considered and approved.

Table 18. HUMS usage data quality issues

Quality Issue	Potential Cause(s)	Detection Method(s)	Corrective Action
Unrecognized maneuver	Aircraft maneuver state not mapping to a preconfigured regime	Onboard HUMS checks input data against preconfigured regime list to determine the current regime. Unrecognized maneuvers cannot be mapped to a regime.	RR classifies the regime as “Unrecognized” when the parametric state data cannot map to a regime.
Missing sensor data	Sensor source computer not functioning or not installed	Onboard HUMS continuously verifies that all necessary RR signals are received by the source avionics system.	RR classifies the regime as “Undetermined” when one or more required RR parameters are either unavailable or declared invalid by the source avionics system.
Erroneous sensor data	Degradation of sensor performance	Detected onboard: The sensor source avionics system performs validity tests. Some redundant systems can isolate faults and continue to provide valid data with minimal impact to HUMS. Other systems will declare the sensor data as invalid. Signal validity checks are continuously provided to HUMS by the source computer.	
		Detected offboard: Sensor quality issues not detected onboard can be detected offboard. Errors are identified through engineering analysis of sensor data relative to expected trends. Validation tests are developed based on known erroneous behavior.	Validation tests are performed on RR parameters for each flight data file. Test failures are mitigated by setting a flag during the failed period or by removing the entire flight data file from the analysis.
Incomplete data	Not following the proper procedure to remove the HUMS data card	Parametric data are checked to verify each HUMS data file starts and ends with the aircraft on the ground.	Depending on the application, incomplete data may or may not affect results. For this application, proper GAG analysis requires complete HUMS data. Incomplete data are flagged and removed from analysis during offboard usage processing.

3.5.2.4 S-92 Rotorcraft Fleet Regime Usage Results

The regime clustering analysis was performed on the entire S-92 rotorcraft fleet for all usage data captured in 2013. Note that this assessment is not required for the mock UBM credit application but was conducted to assess fleet usage statistics relevant to the mock credit and to select a representative aircraft that would result in significant usage credit benefit. In total, 127,324 flight hours from 200 aircraft tail numbers were extracted from the HUMS database for this regime usage study. Figure 49 shows the total 2013 HUMS flight hours in descending order by tail number. High utilization aircraft flew about 2,000 flight hours in 2013, which is equivalent to roughly 5.5 flight hours per day. The average utilization in 2013 for aircraft delivered prior to 2013 was 818 hours, or 2.2 hours per day. Also shown in figure 49 are the total operator-logged flight hours since inception for each aircraft. It is noted here that several high-utilization aircraft have flown over 14,000 hours, which is the RT of the stationary swashplate.

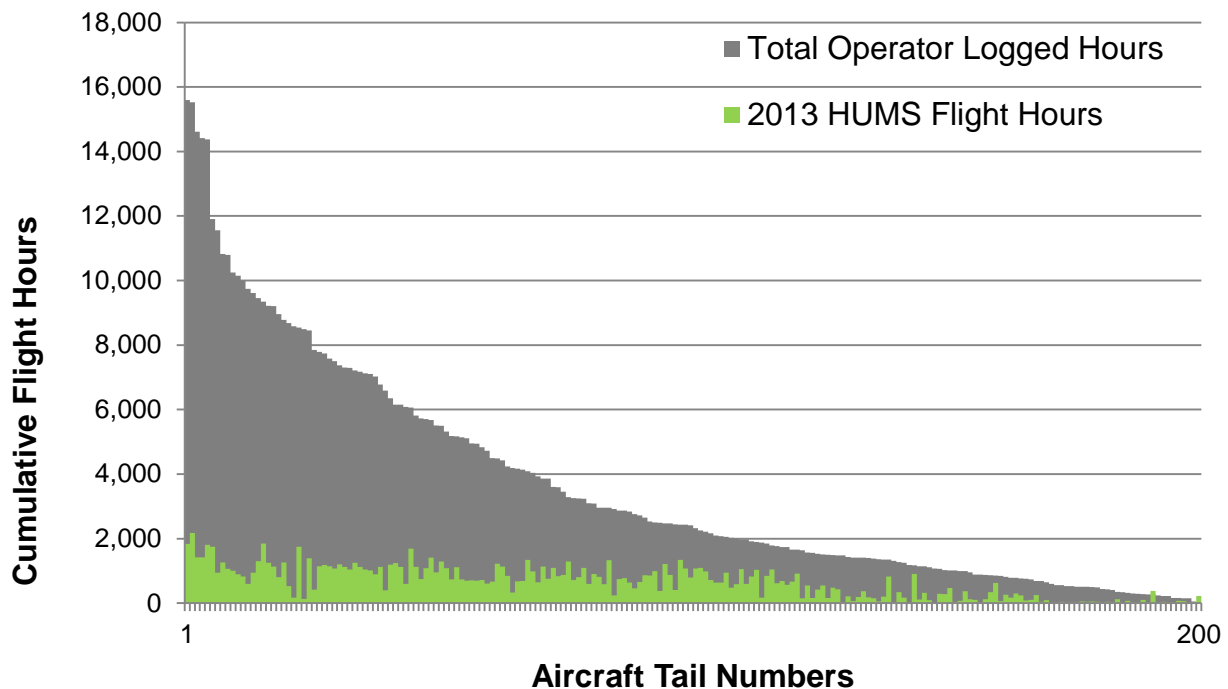


Figure 49. Total 2013 HUMS flight hours by tail number

The data integrity assessment described in Section 3.5.2.3 was performed on the 2013 HUMS data and results are shown in figure 50. In total, only 3% of the 2013 fleet usage data was filtered out for having fallen into one of the four categories above. Note in this figure that both onboard detected erroneous sensor data and missing data were categorized as “Undetermined.” It is possible to determine the causes of Undetermined through further processing of parametric data; however, that analysis was not carried out under this project. The offboard erroneous sensor data detections are noted in the legend with “OB.”

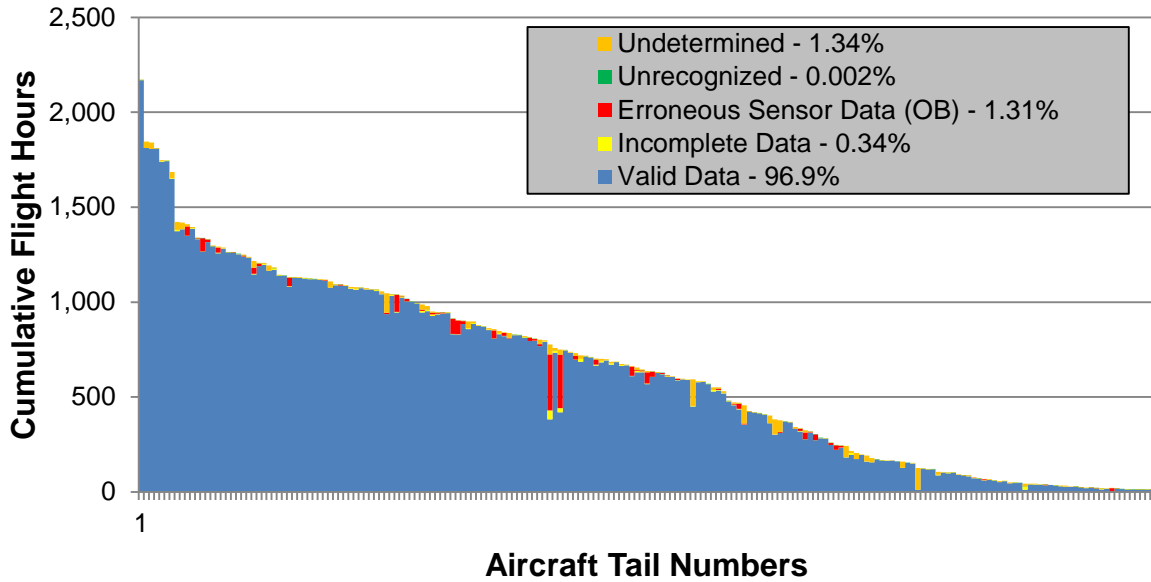
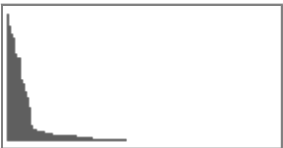
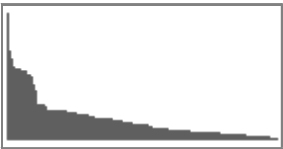
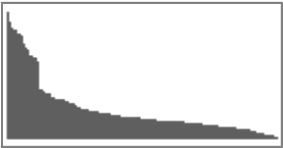
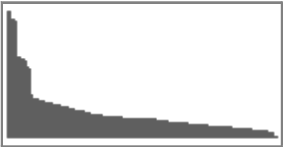


Figure 50. HUMS data integrity assessment results

Prior to processing the fleet data for regime usage analysis, the data set was filtered further to ensure the legitimacy of the results. All aircraft that had no customer-logged hours prior to 2013 were removed to ensure that any infant stage flight activity, such as production acceptance flights, initial customer checkout, and/or customer training flights were not included in the 2013 usage analysis. This filtering step removed 43 aircraft from the usage survey population. In addition, very low utilization aircraft, which flew less than 100 hours in 2013, were removed. This resulted in 33 additional aircraft being removed from the usage survey population. After completion of the data quality assessments and the tail number filtering steps described above, 93,168 flight hours from 124 fleet aircraft remained in the fleet usage survey population.

The regime usage analysis was then performed on this population of fleet data. RR results for the six stationary swashplate critical regimes are shown in table 15. Several important statistics for each regime can be observed in this table. The second column shows the number of aircraft that have flown the regime at least one time. The GAG regime will always occur in 100% of aircraft in the fleet because it is based on counting takeoff/landing cycles. However, some regimes do not occur even once in some aircraft usage histories. For example, only 44% of aircraft in the fleet have performed a 45° left turn at V_{NE} airspeed (more specifically, at airspeed above 0.8 V_{NE}) in 2013. The CWC usage metric is shown along with aircraft usage statistics for 90th percentile, 50th percentile, mean, and max. Finally, a Pareto chart, which shows the shape of the fleet distribution from the maximum to minimum aircraft usage statistic, is presented in the last column. These statistics are only for the subpopulation of aircraft that have performed the maneuver at least one time.

Table 19. Critical regime fleet metrics—2013 results

Regime	# of A/C with Occurrences	% of A/C with Occurrences	Usage Metric Units	CWC	90 th Percentile	50 th Percentile	Mean	Max	Usage Pareto Distribution Shape
Left turn, 45° V _{NE}	55	44%	% time	0.15%	0.028%	0.002%	0.008%	0.049%	
Right turn, 45° V _{NE}	72	58%	% time	0.15%	0.032%	0.002%	0.008%	0.076%	
Entry/recovery left turn 30° & 45° V _{NE}	124	100%	Occurrences per 100 hours	95	160.9	54.0	69.7	372.3	
Entry/recovery right turn 30° & 45° V _{NE}	124	100%	Occurrences per 100 hours	95	194.8	56.3	78.0	299.0	
Moderate pullout, 0.8 V _{NE}	68	55%	Occurrences per 100 hours	90	0.7	0.2	0.5	6.0	
GAG	124	100%	Occurrences per 100 hours	450	209.0	128.9	153.8	520.3	

For both the left and right 45° V_{NE} turn, the 90th percentile usage rate is roughly 20% of the CWC usage spectrum assumption, which indicates a significant opportunity for HUMS usage credit. The 90th percentile usage statistic for both left and right E&R turn regimes were found to exceed the current CWC usage spectrum, while the 50th and mean are below the usage spectrum. This highlights the fact that while there are many areas in the usage spectrum that are perceived to be ultra-conservative, there are cases where the CWC usage spectrum may fall short for a specific regime, which is counterbalanced by conservatism in other regimes and the definition of the regime. In this specific case, the E&R regimes are grouped for 30° and 45° turns for simplicity in the fatigue analysis. However, as indicated in figure 51, 99% of the grouped occurrences are actually attributed to 30° turns, with 1% attributed to 45° turns. The difference in 30° and 45° turn occurrences is so large that this figure can only show the relative size in a log chart format. Because these two regimes are grouped together in the usage spectrum, the highest flight test fatigue load for the grouped maneuvers, which is derived from the higher AOB turn, is assigned to all those occurrences. This indicates that the usage spectrum is likely to be too conservative in grouping 30° and 45° turns together in a single line item even though a few aircraft exceed the CWC combined occurrence rate. This is another example of the opportunities that fleet data present in the optimal design of a fleet usage spectrum. A final note on turns is that right turns occur slightly more frequently than left turns in nearly every category; upon discussion with a test pilot, it was revealed that as a pilot typically sits in the right seat, turning right is preferred to turning left because of the increased visibility during the turn.

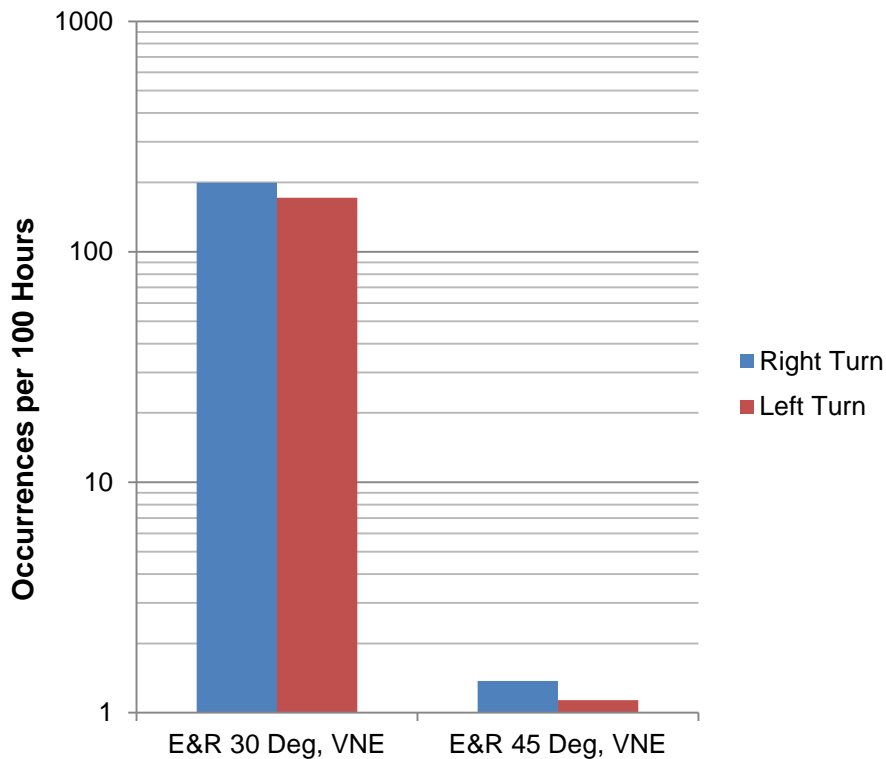


Figure 51. Comparison of 30° and 45° turn E&R occurrence rate

Moderate pullouts at $0.8 V_{NE}$ were found to occur significantly below the usage spectrum assumption of 90 occurrences per 100 hours. While this is the only pullout maneuver that is critical to the stationary swashplate fatigue analysis, the regime clustering capability gave insight into both moderate and severe pullouts. Severe pullouts are defined as a pullout exceeding 2 g of vertical acceleration. It was found that of the entire 2013 usage survey database, there were zero occurrences of a severe pullout.

The 90th percentile fleet GAG rate was observed to be roughly 50% of the usage spectrum. However, five aircraft exceeded the usage spectrum rate by 6–15%. While the majority of the fleet would benefit significantly from a usage spectrum adjustment, it would not be prudent to reduce the usage spectrum as it would be insufficient for the worst-case aircraft. In this case, the fleet data strongly support implementing an individual aircraft UBM paradigm, which is the focus of the current mock credit application.

The fleet results above indicate significant opportunity in adjusting the RT of the stationary swashplate both on a fleet-wide basis and for individual serial number components. In order to demonstrate the usage credit process for a single serial number component, a representative history of usage across the stationary swashplate's 14,000-hour RT is necessary. This project did not address the necessary logistical challenge of identifying a specific serial number component and tracking the installation history over its life in order to accumulate the associated usage data relevant to the specific serial number credit. Rather, for the demonstration of UBM technology and the mock UBM credit process, it is sufficiently representative to select an aircraft with 14,000 hours of usage history as a surrogate for the specific serial number swashplate usage history. Table 16 shows the relevant regime usage statistics for the five aircraft that have accumulated more than 14,000 flight hours over their lives. The highest time aircraft, identified as aircraft (A/C) #3, has accumulated 15,592 flight hours over its life. The usage statistics for this aircraft range from moderate to low relative to the five high-time aircraft. This aircraft was selected for a deeper dive usage analysis of 14,000 flight hours of fleet data and the specific mock credit documented herein. To build up a representative usage history, all usage data for A/C#3 were extracted from the HUMS database, filtered through the data quality assessment checks, and processed to extract the cumulative lifetime regime usage statistics relevant to the stationary swashplate credit. These results for A/C#3 are shown below in table 17. The lifetime results for A/C#3 are very similar to the 2013 results. The results in table 17, which show all usage data since the individual aircraft were new, are used in the next section to demonstrate how to calculate serial number credit from HUMS regime usage data.

Table 20. High-time aircraft usage statistics for 2013

A/C #	Total Flight Hours	2013 Flight Hours	GAG Rate (Occ /100 hr)	Left Turn, 45° V _{NE} (% Time)	Right Turn, 45° V _{NE} (% Time)	E&R Left Turn 30° & 45° V _{NE} (Occ / 100 hr)	E&R Right Turn 30° & 45° V _{NE} (Occ / 100 hr)	Moderate Pullout, 0.8 V _{NE} (Occ / 100 hr)
A/C #1	14,413	1,422	135.5	—	0.0015%	55.7	49.2	0.1
A/C #2	14,612	1,419	133.4	0.0022%	0.0016%	57.5	50.3	0.1
A/C #3	15,592	1,841	93.9	—	—	28.0	49.0	—
A/C #4	15,526	2,170	85.7	—	0.0020%	27.0	34.9	—
A/C #5	14,376	1,811	92.0	0.0008%	0.0004%	29.4	42.3	—

Table 21. A/C#3 usage statistics for all times

Regime	CWC Usage	Actual Usage	Units
Left turn 45° V _{NE}	0.1500%	0.0022%	% time
Right turn 45° V _{NE}	0.1500%	0.0032%	% time
Entry/recovery left turn 30° & 45° V _{NE}	95	38	Occurrence / 100 hr
Entry/recovery right turn 30° & 45° V _{NE}	95	58	Occurrence / 100 hr
Moderate pullout 0.8 V _{NE}	90	0.05	Occurrence / 100 hr
GAG	450	114	Occurrence / 100 hr
Total validated HUMS flight hours ¹ = 14,226			
Total operator logged flight hours ¹ = 15,592			

¹ = through September 2014

3.5.2.5 HUMS FATIGUE MODEL

The mock UBM credit intervention action is to adjust the cumulative flight hours of a specific serial number component based on the calculation of accumulated fatigue damage using the HUMS RR data in conjunction with the fatigue failure model of the component. When the desired output from the fatigue model is a percent life or cumulative fatigue damage rather than an RT, the fatigue model must be reformed to an equivalent HUMS compatible fatigue model that enables calculation of damage per unit of HUMS data, either occurrences or duration, as dictated by the type of regime. Additionally, as some amount of damage is still attributed to non-critical, non-monitored regimes, this damage must be added back in on a flight-hour basis. This requires a set of HUMS damage rates that are converted from the CWC damage rates. The result

of this conversion is shown in table 18. In this table, the CWC damage rates for the steady state turn regimes is translated into damage per second, while the CWC damage rate for the transient and GAG regimes are translated into damage per occurrence. The residual damage attributed to non-monitored regimes is translated from damage per 100 hours to damage per hour. Using these damage rate factors, the damage can then be computed directly from a HUMS flight using the equation shown below. Note that this equation does not bring in the reliability factors discussed in the next section.

Table 22. CWC damage rates compared with HUMS damage rates

Regime	CWC Usage / 100 hr	CWC Damage / 100 hr	HUMS Damage Accrual Basis	HUMS Damage per Unit
Left turn 45° V _{NE}	0.15%	0.0023	Damage per regime second	4.20E-06
Right turn 45° V _{NE}	0.15%	0.0023	Damage per regime second	4.20E-06
Entry/recovery left turn 30° & 45° V _{NE}	95	0.0007	Damage per regime occurrence	7.82E-06
Entry/recovery right turn 30° & 45° V _{NE}	95	0.0006	Damage per regime occurrence	6.65E-06
Symmetric Pullout, Moderate, 0.8 V _{NE}	90	0.0007	Damage per regime occurrence	7.36E-06
GAG	450	0.0006	Damage per regime occurrence	1.27E-06
Residual damage (Non-critical regimes)	N/A	0.0001	Damage per flight hour	1.48E-06

A = Left turn, 45° V_{NE} usage in seconds

B = Right turn, 45° V_{NE} usage in seconds

C = E&R left turn 30° & 45° V_{NE} usage in occurrences

D = E&R right turn 30° & 45° V_{NE} usage in occurrences

E = Symmetric pullout, moderate, 0.8 V_{NE} usage in occurrences

F = GAG usage in occurrences

G = Flight hours

$$\text{Damage} = A(4.2E-6) + B(4.2E-6) + C(7.82E-6) + D(6.65E-6) + E(7.36E-6) + F(1.27E-6) + G(1.48E-6)$$

In the equation above, the damage attributed to non-critical regimes is termed the residual damage rate and is accumulated on a flight-hour basis (i.e., G). An alternate approach to dealing with non-monitored regimes would be to subtract all the usage time incurred by the monitored regimes from the total flight hours before applying the CWC damage rate. The additional benefit to that approach in this application is negligible due to the extremely small amount of time incurred by the monitored regimes. However, it is possible that a high-occurrence non-damaging regime, such as LF, may be validated and monitored in a way to reduce the amount of time

allocated to any non-monitored damaging regimes. This concept can be understood by looking at figure 52. In this example, Regimes 1, 2, and 3 are monitored while Regimes 4 and 5 are not. Regime 4 is a damaging regime that normally would be assumed to occur using the CWC usage rate assumption. On the other hand, Regime 3 is a non-damaging monitored regime that is known to occur much more frequently than was assumed in the CWC usage spectrum. By accounting for the monitored time of non-damaging regimes, it is possible to reduce the amount of time that is allocated to the remaining unmonitored regimes to a damage rate less than what was assumed in the original CWC usage spectrum. Using this approach, it may be possible to achieve a UBM benefit for damaging regimes that are not explicitly monitored as long as benign regimes (e.g., LF and hover) can be shown to occur much more frequently than assumed in the CWC.

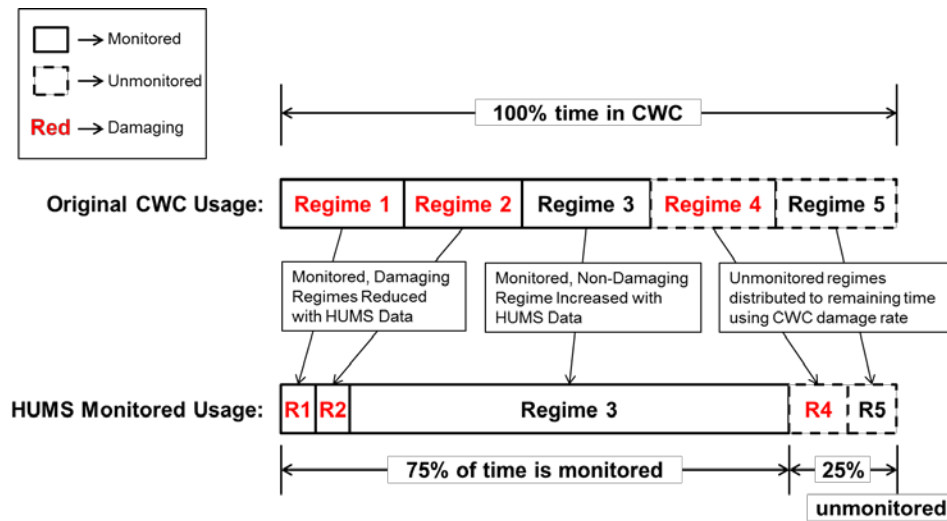


Figure 52. HUMS monitored and unmonitored usage accrual

3.5.2.6 Reliability Factors

As discussed in section 2.3, the calculation of component damage from HUMS recorded usage is not as simple as plugging in recorded usage rate data into a traditional fatigue life model. A methodology must be used to ensure six-9's reliability is maintained. A simple method was developed in a paper by Adams and Zhao [13] for applying what is called the UMRF to actual usage statistics when calculating usage credits from monitoring one regime. The UMRF is a method to increase the usage data by a factor that adds sufficient margin back into the life model when the life model is applied to an individual aircraft's measured usage data. This methodology was approved for the FAA-certified S-92 rotorcraft MR hub credit project, which was the first real application of HUMS usage data to adjust the RT of a rotorcraft component. The reliability approach established for the current mock credit application is twofold. First, the UMRF method will be expanded from the initial MR hub credit application, which was based on one damaging regime, to a more complex case of multiple damaging regimes. Using a different UMRF for each of the six stationary swashplate damaging regimes will allow rapid credit calculation and damage trending over the life of the component. Second, the probabilistic approach described in section 2.3 will be applied independent of the UMRF as a means to validate the expansion of the UMRF to multiple regimes. This will be documented in the subsequent validation methodology section.

The UMRF is defined as the ratio of the 90th to the 50th usage metric from the fleet for the specific regime under evaluation. These statistics were already presented in table 15 for the stationary swashplate critical regimes. The UMRF methodology essentially determines the median usage margin against a hypothetical 90th percentile CWC usage spectrum based on the fleet data. By determining the median usage margin that would exist in a CWC usage spectrum based on the fleet data, the same margin can then be applied with confidence to any individual aircraft's usage data. The primary benefit of this approach is that it is simple and provides sufficient conservatism to maintain comparable reliability to that sought in the original design and lifing calculation. There are several problems that may occur in the application of the UMRF methodology, which will be discussed throughout this section.

The first step in applying the UMRF is to calculate the factors themselves. This is easily done by dividing the 90th percent statistic by the 50th percent statistic using the fleet statistic results from table 15. The resulting UMRFs are presented below in table 19. The reliability factor of 1.6 for GAG is very similar to the value of 1.5 that was calculated for rotor cycle GAG in Adams and Zhao's paper [13]. Note that the GAG in this application refers to the takeoff/landing cycle. However, the reliability factors for the in-flight maneuvers are significantly higher. Left and right turn, 45° V_{NE} maneuver statistics resulted in a reliability factor of 13.7 and 16, respectively. To understand why the UMRF values are so exceedingly high for these maneuvers, the maneuver Pareto distribution is shown in figure 53. Because the UMRF is the ratio of the 90th to 50th percentile, the UMRF will increase as the 90th and 50th percentile values get further apart. This can be thought of as increased variation in the maneuver rate across the fleet. As variation increases, a 90th percentile-based usage spectrum will tend to provide greater margin against the fleet median usage. Because the goal of the UMRF methodology is to conserve this usage spectrum margin, the methodology results in higher factors with higher usage variation. This is somewhat of a paradox, as the objective of usage monitoring is to reduce or eliminate the effect of usage variation in the fatigue management process.

Table 23. Usage monitor reliability factors

Regime	Usage Metric Units	90 th Percentile	50 th Percentile	UMRF
Left turn, 45° V _{NE}	% time	0.028%	0.002%	13.7
Right turn, 45° V _{NE}	% time	0.032%	0.002%	16
Entry/recovery left turn 30° & 45° V _{NE}	Occurrences per 100 hours	160.9	54.0	2.98
Entry/recovery right turn 30° & 45° V _{NE}	Occurrences per 100 hours	194.8	56.3	3.46
Moderate pullout, 0.8 V _{NE}	Occurrences per 100 hours	0.7	0.2	4.48
GAG	Occurrences per 100 hours	209.0	128.9	1.62

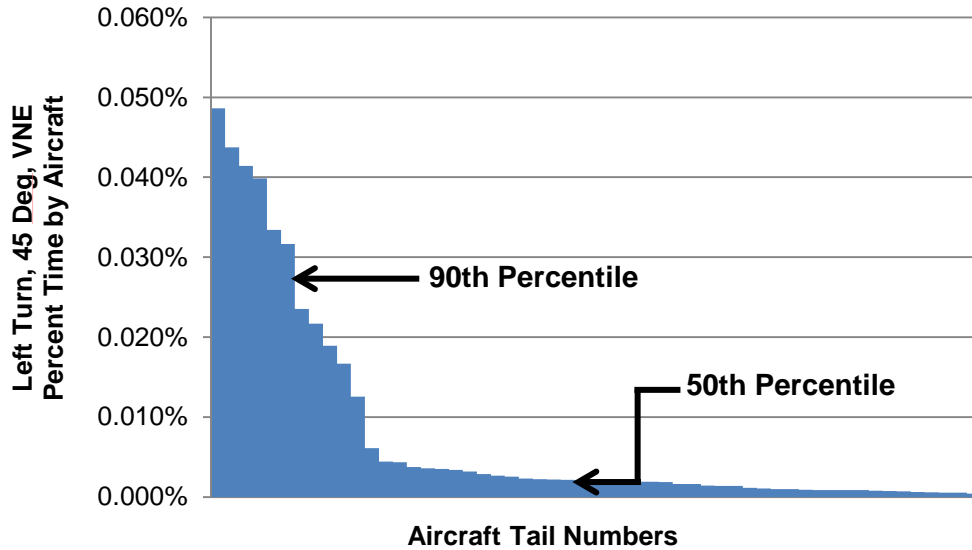


Figure 53. Left turn, 45° V_{NE} usage Pareto

Digging deeper into the statistics for the left turn, 45° V_{NE} maneuver, it was found that this maneuver had the fewest number of aircraft with usage data from the list in table 15. To calculate those statistics, aircraft with non-zero usage rate values were treated as a subpopulation from aircraft with usage rates of zero (because the maneuver was never flown in the 2013 data set) to avoid skewing statistics away from the critical population of aircraft that have performed maneuvers. The high-time A/C#3 from table 16 was an aircraft with no usage data for the left turn, 45° V_{NE} maneuver. However, when processing A/C#3 data since inception, some occurrences of the left turn, 45° V_{NE} maneuver were found, and the resulting usage rate was in line with the fleet's 50th percentile usage from the 2013 analysis. This indicates that for a maneuver that very rarely occurs, much more data are required to really understand the fleet usage statistics. It is very possible that the high UMRF values for the left and right turn, 45° V_{NE} maneuver are simply due to not having enough data when arbitrarily restricting the population to one calendar year, as was done herein for fleet analysis.

To alleviate this problem, an approach was taken to group together similar regimes into a single regime for the purposes of calculating the UMRF. This grouping allows more maneuver data to be considered in the UMRF calculation and generalizes the UMRF for similar regimes, such that the same factor can be applied to both. This grouping was performed for the left and right, 45° V_{NE} maneuver by combining the 30° and 45° turns and by combining the left and right turns. Further condensing was performed for the E&R turn regimes by grouping left and right turns together; for the moderate pullout regime, grouping the 0.8 V_{NE} and V_{NE} airspeed categories together was undertaken. The final UMRF factors, after consolidation of these regimes, are shown in table 20. These reliability factors can be applied directly to HUMS usage data prior to application of the damage equation developed in section 3.5.2.5.

Table 24. Final UMRF factors after regime consolidation

Regime	# of A/C with Occurrence	% of A/C with Occurrence	Usage Metric Units	90 th Percentile	50 th Percentile	UMRF
Left turn, 45° V _{NE}	124	100%	% time	1.446%	0.493%	2.93
Right turn, 45° V _{NE}						
Left turn, 30° V _{NE}						
Right turn, 30° V _{NE}						
Entry/recovery left turn 30° & 45° V _{NE}	124	100%	Occurrences per 100 hours	379.8	113.0	3.36
Entry/recovery right turn 30° & 45° V _{NE}						
Moderate pullout, 0.8 V _{NE}	101	81%	Occurrences per 100 hours	1.25	0.44	2.85
Moderate pullout, V _{NE}						
GAG	124	100%	Occurrences per 100 hours	209.0	128.9	1.62

3.5.2.7 HUMS Damage and UBM Credit Calculation

With an established regime monitoring approach, a HUMS-compatible damage model, and a set of reliability factors, it is now possible to take the usage data since inception for A/C#3 and turn these data into a damage accumulation trend. Using only the first 14,000 flight hours of usage data, the damage trend was calculated for the HUMS-based damage with and without the UMRF factors from table 20, along with the traditional CWC linear damage rate. The results were plotted in figure 54, and the damage metrics per regime are shown in table 21. From these data, A/C#3 has accumulated 41.5% damage when factoring in the UMRFs. By comparing the total regime damage from the raw HUMS data with that from the UMRF methodology (after removing the residual damage), the average effective reliability factor was 3.1. A future RT from the damage data indicates that the UMRF-based RT would be 33,700 hours, or 2.4 times the CRT. These data indicate that the stationary swashplate installed on this aircraft—assuming it was installed for the entire 14,000 flight hours—has significant opportunity for a usage-based RT credit.

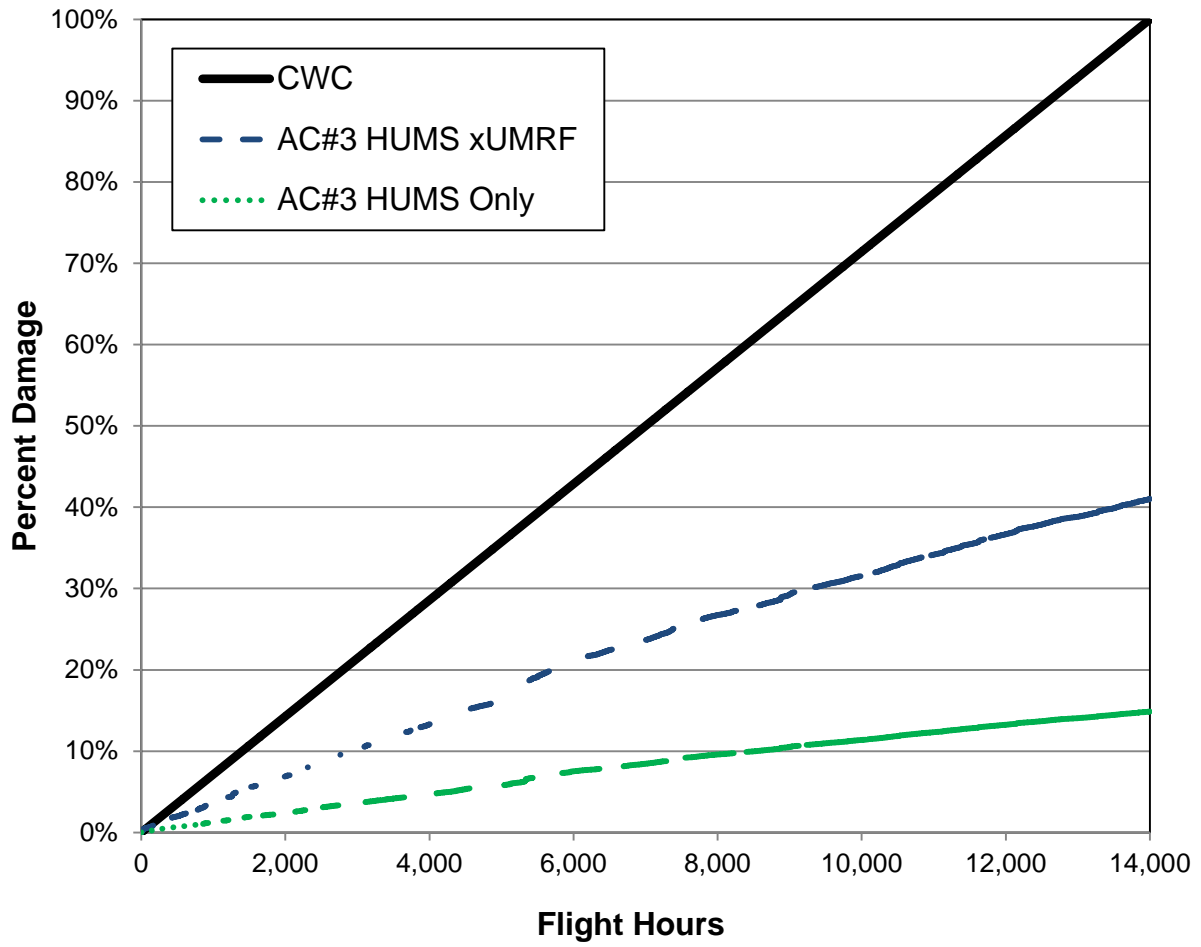


Figure 54. HUMS-based damage trend for A/C#3

Table 25. Damage summary for A/C#3 at 14,000 flight hours

	Damage Summary			Damage Summary (% of Total)		
	Raw HUMS	HUMS x UMRF	Assumed CWC	Raw HUMS	HUMS x UMRF	Assumed CWC
Left turn 45° V _{NE}	0.0046	0.0136	0.3111	3%	3%	31%
Right turn 45° V _{NE}	0.0068	0.0199	0.3111	5%	5%	31%
Entry/recovery left turn 30° & 45° V _{NE}	0.0420	0.1413	0.1017	28%	34%	10%
Entry/recovery right turn 30° & 45° V _{NE}	0.0551	0.1853	0.0865	37%	45%	9%
Symmetric Pullout, Moderate, 0.8 V _{NE}	0.0001	0.0002	0.0908	0%	0%	9%
GAG counts	0.0207	0.0335	0.0784	14%	8%	8%
Residual damage	0.0211	0.0211	0.0203	14%	5%	2%
Total	0.1505	0.4150	1.0000	100%	100%	100%
Expected retirement time (hrs)	93,000	33,700	14,000			

While figure 54 shows the damage trend for the first 14,000 flight hours, this was based only on the validated HUMS flight hours. In reality, the operator-logged flight hours achieved 14,000 flight hours sooner than this point after accounting for the removal of some HUMS data for validation filtering and a tendency for pilots to round-up or over-report flight hours. At the time the operator-logged 14,000 flight hours, the validated HUMS flight hours for A/C#3 totaled 12,577 hours, or roughly 90% of the operator-logged flight hours. It is likely that a majority of the 10% is a result of pilot over-reporting—essentially meaning the over-reported flight hours do not exist. While there are methods to determine how much of the 10% is due to invalid or missing data, as opposed to pilot over-reporting, the simple approach taken in this mock application is to assume that the entire 10% of flight hours are real and not captured or validated by the UBM credit process. The most conservative approach is to apply the baseline CWC damage rate to this 10% of flight hours. Other approaches may also be considered, such as adjusting the CWC damage rate based on fleet results. However, for the sake of simplicity, the 10% of flight hours are covered using the baseline CWC damage rate for this mock credit. At this point, the UBM credit can be calculated. The calculation steps are shown in figure 55. The final flight hour credit for A/C#3 is 6,765 hours, which is a credit of 48% of the original CRT.

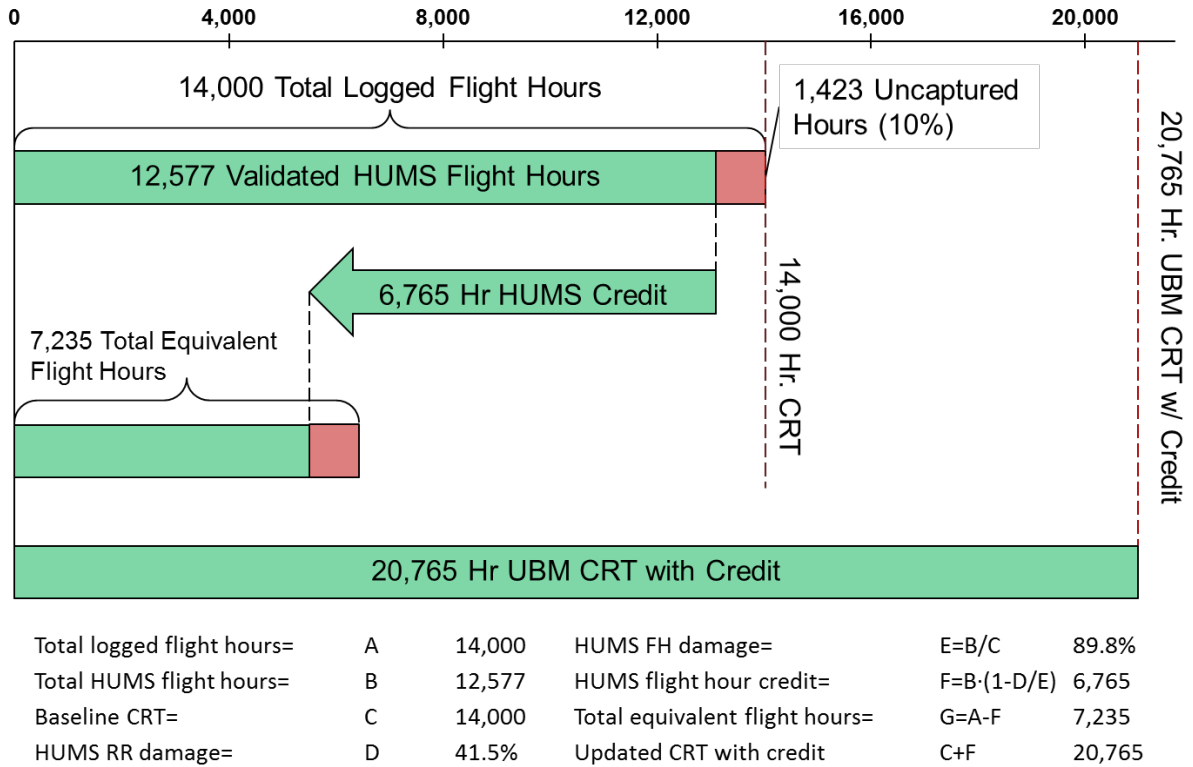


Figure 55. A/C#3 HUMS credit calculation

3.5.3 Validation Methodology

3.5.3.1 Regime Recognition Clustering

An approach to RR validation was developed under Beale and Davis' [2] effort and applied here in the validation of the S-92 RR clustering/prorating methodology. The approach requires the availability of flight load survey test data, which normally contain all of the relevant usage spectrum regimes. From the flight test data, a set of run logs are developed that identify precise start/stop times of each flight test maneuver, along with a maneuver code that is used to map directly to the S-92 aircraft usage spectrum.

In order for RR to track the steady state and transient maneuvers in a way that is consistent with the fatigue analysis, it must be validated to track duration and/or occurrences, depending on the type of regime. Transient regimes are quantified in terms of occurrences, and steady state regimes are quantified in terms of duration. Transient regimes are not typically measured in terms of duration, nor can the flight test run markers be used to validate the duration of a transient regime. This is illustrated in figure 56, which shows how a transient maneuver is typically captured by the flight test run logs. Here, a 45° left climbing turn maneuver is flown, but the capture window includes steady state climbing data at the beginning and end. This makes the transient maneuver duration statistics difficult to attain because the true start and stop time of the maneuver cannot be achieved without laboriously going through hundreds of maneuvers and assigning them manually. For the unique case of turns, however, RR must accurately track both duration and occurrences. This is because the fatigue usage spectrum separates out the turn E&R as distinct transient events while treating the rest of the turn as a steady state event. In these cases, the total duration of the turn event is based on the flight test run log time after removing the non-turn related HUMS-steady state regimes that immediately precede and follow the transient turn regime.

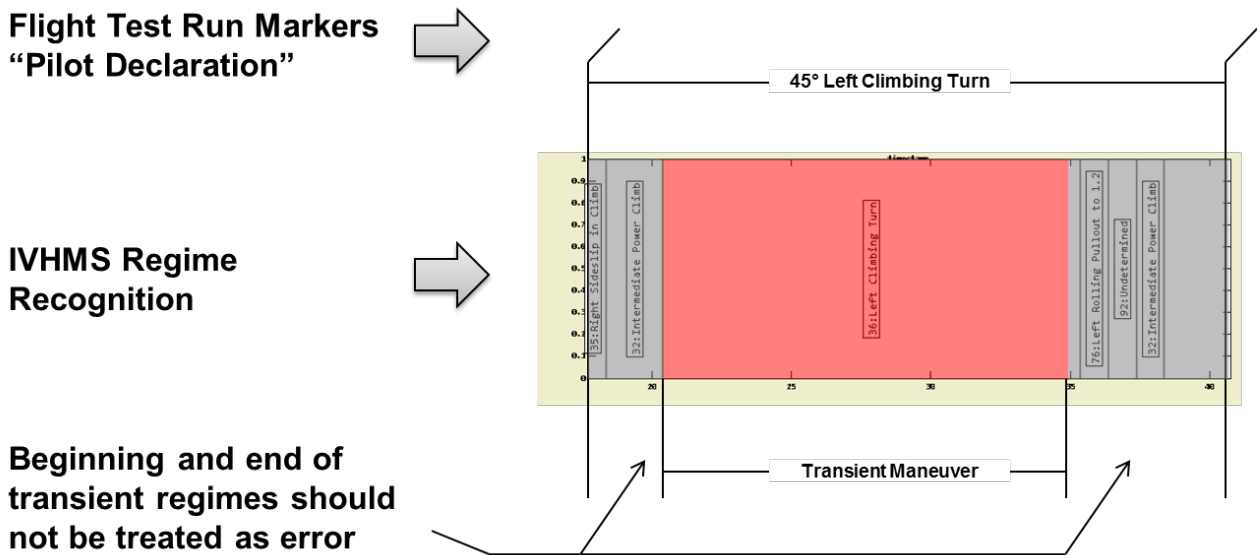


Figure 56. Example of run log markers for transient maneuver

The validation of the critical regimes used for the current mock UBM credit was performed with an existing set of S-92 aircraft flight test data, using 15 test flights conducted between January 2009 and September 2011 on two different test aircraft. For these flights, the Goodrich HUMS system was installed and configured with production representative software. These are the best known data sets SAC has to validate S-92 aircraft RR using flight test-declared truth regimes during a flight load survey. The regime validation metrics described above were applied to the entire flight test data set before clustering was applied and again after clustering was applied for the turn and pullout regimes.

The results of this validation effort are shown in table 22. The baseline RR algorithms are shown to have been consistently over-counting the occurrences for all turn regimes and not counting enough occurrences for the pullout and pushover regimes. For the generic 30° and 45° left and right turns, the baseline RR algorithms consistently undercounted duration, which is consistent with over-counting occurrences. On the other hand, the results of the clustering/prorating process were shown to dramatically improve both the counts and duration for all regimes. Accuracy of 96% or better was achieved on all metrics.

One exception is noted where low-g pullouts (less than 1.4 g) were not classified at all by RR and, therefore, could not be improved by clustering. This was initially a concern as the pullout regime is critical to the stationary swashplate, which was the focus of this mock credit. However, upon review of the fatigue loads generated for the low-g pullouts relative to the fatigue endurance limit for the stationary swashplate, it was found that the low-g pullouts are non-damaging events that are not critical to the HUMS usage-based fatigue analysis. Figure 57 shows how the maximum fatigue load generated from hundreds of pullout maneuvers compares to the peak g level recorded during the maneuver. Both the HUMS detection threshold and stationary swashplate fatigue damage threshold are shown for reference. These two thresholds create four quadrants in the plot. What is important to note here is that all of the damaging pullout events fall within the detectable range. The quadrant on the upper left is for conditions that were damaging but not detected by HUMS, which did not occur in the flight test. This indicates that the HUMS detection threshold of 1.4 g is adequate for the current mock credit application. Future analysis of this threshold may be required for future UBM applications of the pullout regime that involve different fatigue loads or components with a lower damaging threshold than was considered here.

Table 26. Regime recognition validation results

	Truth Data		Baseline RR Software				After Clustering/Prorating			
	Event Counts	Event Duration	Event Counts	Event Duration	% Event Counts	% Event Duration	Event Counts	Event Duration	% Event Counts	% Event Duration
Left turn 30	29	614.6	41	396.9	141%	65%	28	597.6	97%	97%
Right turn 30	29	626.2	35	365.3	121%	58%	28	614.2	97%	98%
Left turn 45	27	660.0	44	301.6	163%	46%	26	640.0	96%	97%
Right turn 45	27	649.5	39	237.0	144%	36%	27	671.2	100%	103%
Climb left turn 30	2	42.0	10	42.0	500%	100%	2	42.0	100%	100%
Climb right turn 30	2	61.8	7	61.8	350%	100%	2	61.8	100%	100%
PPD left turn 30	8	107.8	22	107.8	275%	100%	8	107.8	100%	100%
PPD right turn 30	8	110.9	20	110.9	250%	100%	8	110.9	100%	100%
Auto left turn 30	10	105.3	28	102.2	280%	97%	10	105.3	100%	100%
Auto right turn 30	8	77.8	20	75.5	250%	97%	8	77.5	100%	100%
Pullout > 1.4 g	85	N/A	46	N/A	54%	N/A	84	N/A	99%	N/A
Pullout < 1.4 g	15	N/A	0	N/A	0%	N/A	0	N/A	0%	N/A
Pushover	39	N/A	4	N/A	10%	N/A	39	N/A	100%	N/A

100

CWC name: Composite worst case regime name

Event counts: Total number of occurrences in flight test data or detected by RR

Event time: Total time spent in regime in flight test data or detected by RR

< 80%	80% – 95%	95% – 105%	> 120%
-------	-----------	------------	--------

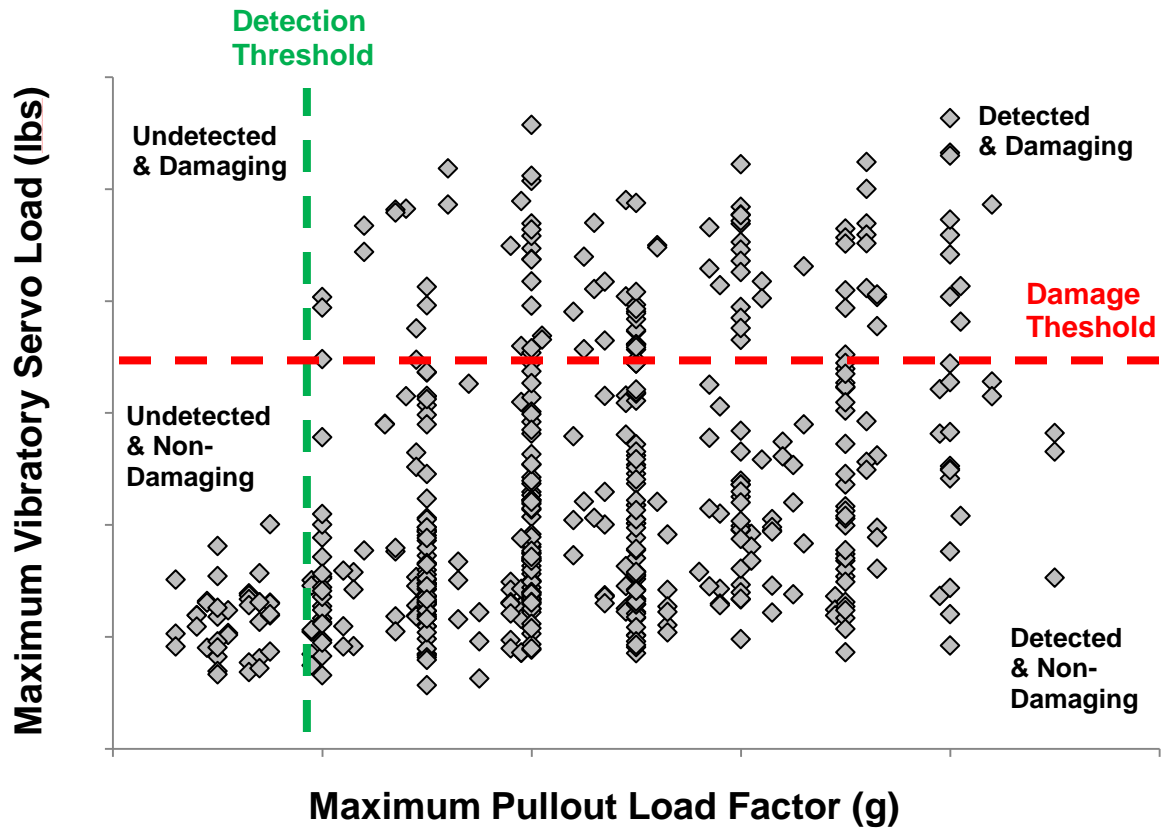


Figure 57. Detection and damage threshold for pullouts

3.5.3.2 HUMS Fatigue Model

The HUMS fatigue model can be validated simply by entering inputs that are derived from the CWC usage spectrum and then checking for a damage accumulation of 14,000 hours. The equation developed in 3.5.2.5 is repeated below for reference.

- A = Left turn, 45° V_{NE} usage in seconds
- B = Right turn, 45° V_{NE} usage in seconds
- C = E&R left turn 30° & 45° V_{NE} usage in occurrences
- D = E&R right turn 30° & 45° V_{NE} usage in occurrences
- E = Symmetric pullout, moderate, 0.8 V_{NE} usage in occurrences
- F = GAG usage in occurrences
- G = Flight hours

$$\text{Damage} = A(4.2E-60) + B(4.2E-6) + C(7.82E-6) + D(6.65E-6) + E(7.36E-6) + F(1.27E-6) + G(1.48E-6)$$

To validate this model with the CWC usage metrics, values A–F from the equation above, need to be derived from the usage spectrum rates for a 14,000-hour lifetime. With that given set of inputs, the expected damage result from the equation is 1.0.

To determine the values of A and B for the left and right turn, $45^\circ V_{NE}$ that are consistent with the CWC usage, the percentage time metrics from table 12 are multiplied by 14,000 hours and then by 3,600 seconds/hour. To determine the values of C, D, E, and F, the maneuvers per 100 hours metrics from table 12 are multiplied by 14,000 hours and then divided by 100. The test case input values for A–G are listed below in table 23. These test case inputs, when entered into the HUMS damage model, result in a cumulative damage value of 1.02. A damage value of 1 is achieved at 13,700 hours. This value is as expected because the 14,000-hour RT is actually rounded up to 14,000 hours from the true calculated lifetime of 13,700 hours in order to achieve a standard of only two significant digits.

Table 27. HUMS damage model test case inputs

HUMS Usage Parameter	CWC Test Value	Units
A	75,600	seconds
B	75,600	seconds
C	13,300	occurrences
D	13,300	occurrences
E	12,600	occurrences
F	63,000	occurrences
G	14,000	hours

3.5.3.3 Reliability Methodology

The reliability factors used in the example mock credit were developed using the UMRF methodology [13]. To validate the application of the UMRF for this multiple regime usage credit example, the reliability of the example stationary swashplate serial number is modeled using the probabilistic reliability framework described in section 2.3.

The fatigue reliability of the stationary swashplate was modeled from two perspectives. The first perspective is an a priori view of the fatigue problem where the strength, loads, and usage of the stationary swashplate are known in terms of fleet population statistics, but are unknown for a specific serial number component in service. This perspective, which is consistent with the traditional fatigue methodology, is termed the “fleet average reliability” because it only considers knowledge at the fleet level rather than at the individual aircraft level. The resulting reliability at a given RT is the expected reliability of any individual aircraft with unknown usage, loads, and strength. By modeling the fatigue reliability in this way, a baseline fleet reliability can be established by intersecting the current 14,000-hour RT against the resulting reliability curve. The result of this analysis is shown in figure 58. Using this reliability framework, the resulting fleet average reliability at the 14,000-hour stationary swashplate RT is 0.999998, or 5.8-9s. This result lines up well with the expected reliability of approximately six- 9s, which is the intent of the traditional fatigue life process. This serves to validate both the probabilistic fatigue model of the stationary swashplate and the traditional fatigue substantiation process. It is not expected that

every application will agree as well as shown here, as previous applications of this type of reliability analysis have shown that agreement within $\pm 1-9$ of reliability is a reasonable range of expected agreement, as noted in Thompson and Adams' paper [3]. This range of acceptability is shown in figure 58 by the green-shaded area. The goal of the mock UBM credit is to achieve a reliability that is comparable with the baseline reliability achieved without monitoring.

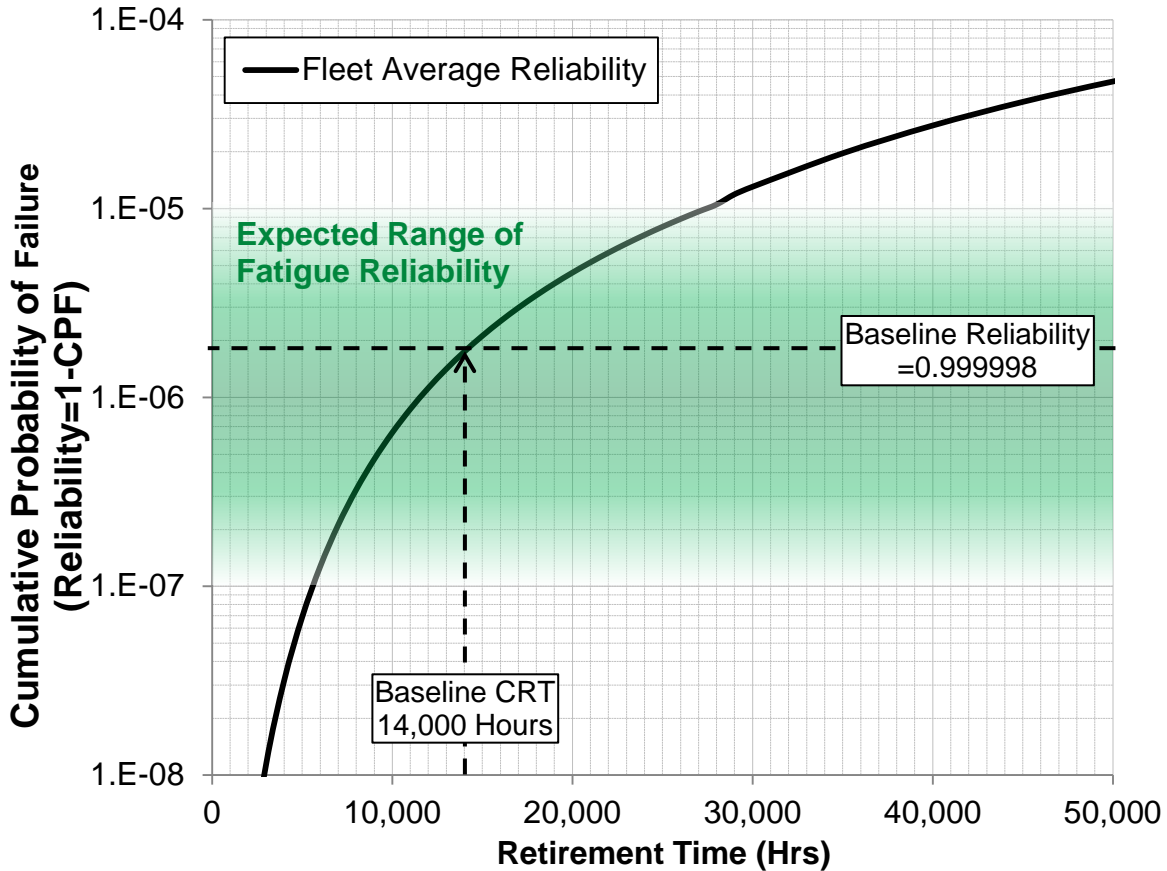


Figure 58. Fleet average reliability for stationary swashplate

The second perspective is an a posteriori view of the fatigue problem after considering the additional knowledge gained from a usage or load monitor. In this perspective, the strength and loads remain unknown as they did in the fleet average reliability model; however, the usage is now considered a known value. Termed herein as the serial number reliability, this perspective can be thought of as a Bayesian update to the original a priori view, as it considers the measured usage data for a specific component serial number rather than treating usage as unknown. This perspective adds additional information to the fatigue reliability problem, which reduces the uncertainty that existed in the a priori model. This perspective is consistent with the HUMS usage-based damage model, where the usage is no longer treated as an unknown. The serial number reliability analysis is performed by using the results from A/C#3 that are shown in table 17. The resulting serial number reliability curve, shown in figure 59, is presented relative to the original fleet average reliability curve. Two serial number reliability curves are shown in this figure. They indicate the expected RT based on the raw HUMS usage counts and HUMS usage counts with the UMRF reliability factors applied. These values are derived from table 21. By

comparing these values to the serial number reliability, it is possible to determine the reliability that was achieved with raw HUMS data and HUMS plus reliability factors.

Using the raw HUMS data projected, an RT of 93,000 flight hours was calculated, resulting in an estimated reliability of 0.99994, or 4.4-9s. This is consistent with the expectation that the use of raw usage data with no margin in fatigue damage analysis does not provide sufficient reliability. When using HUMS usage data with applied reliability factors, an RT of 34,000 hours is calculated, resulting in an estimated reliability of 0.999997, or 5.7-9s of reliability—which is well within the acceptable range of reliability and considered to be comparable with the baseline reliability of 5.8-9s. The UMRF methodology had the effect of adding back 1.3-9s of reliability. It is anticipated that future HUMS-based UBM serial number credits will have the requirement of demonstrating that the methodology results in reliability are comparable with baseline reliability but would not require a reliability assessment of each serial number. The analysis provided here serves to validate the methodology of applying reliability factors for recurring application of the mock credit to other serial numbers.

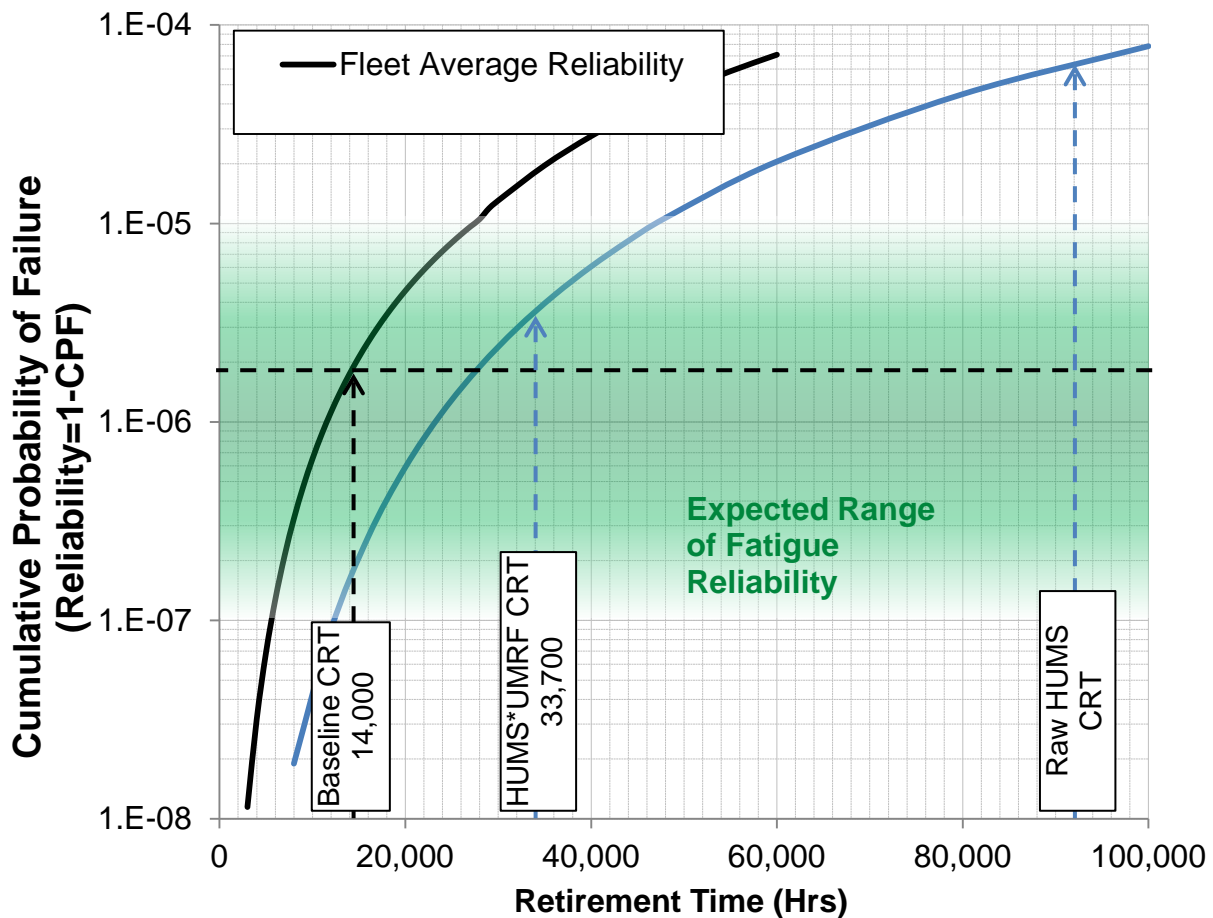


Figure 59. A/C#3 serial number reliability for stationary swashplate

This type of reliability analysis enables calculation of a HUMS reliability factor using an alternate methodology that does not rely on fleet data. As noted previously, the UMRF methodology provided an effective reliability factor of 3.1. Following the reliability analysis

presented here, it is possible to define a reliability factor that achieves the same goal of adjusting the raw HUMS CRT projection to provide the desired reliability. The serial number reliability curve in figure 59 intersects the baseline reliability target at 28,000 hours. Using this intersection point, the raw HUMS damage can be multiplied by a factor of $(93,000/28,000) = 3.3$. This methodology provides a reliability factor very similar in magnitude to the UMRF factors shown in table 20. It is interesting that the values are very similar because they rely on completely independent sources of data. The methodology provided here may be a more practical methodology, where monitoring the entire fleet in advance of a credit is not feasible or does not provide sufficient data to develop the UMRF factors.

4. GENERAL APPLICABILITY TO OTHER CREDIT TYPES

The HUMS-based UBM credit process presented in section 3 is demonstrated in the context of a specific serial number component credit, although the process can be applied to any rotorcraft component and may be easily extended to other UBM credit approaches. For example, a part number RT adjustment is a similar credit approach, where rather than adjusting the RT of an individual serial number component, the RT is adjusted one time for the entire fleet. In this case, the fleet monitoring technology would be applied to the entire fleet rather than one specific tail number rotorcraft. The part number credit approach is achieved through an update to the CWC rather than through UMRF-based adjustments for individual serial numbers, but the probabilistic method used to validate the resulting RT can still be applied for the part number approach.

With the application of more advanced usage monitoring approaches such as GW/CG or load estimation, fleet usage data can be further processed to provide more meaningful results that better indicate the severity of loads encountered during specific flight maneuvers. Leveraging these tools in the credit process requires a deeper understanding of the physics involved in the fatigue problem (e.g., maneuver load sensitivity to GW) such that the technology can be successfully applied in the context of a specific application, and requires more sophisticated validation analysis using independent flight test data.

It is envisioned that the details of any of the above UBM credits would have to be clearly documented in a similar manner, as laid out in section 3. A more generally applicable outline is presented below.

1. Description of application and associated credit
2. Physics of the application
 - a. Component failure modes
 - b. HUMS monitoring technique
 - c. Data quality assurance
 - d. Reliability methodology
 - e. Credit calculation
3. Validation methodology
 - a. HUMS monitoring technique
 - b. Reliability methodology

5. CONCLUSIONS AND RECOMMENDATIONS

This report documents the technical work conducted under Delivery Order (DO) 0002/0003 within indefinite delivery/indefinite quantity contract DTFACT-11-D-00004, which leveraged previous research and development (R&D) conducted by Sikorsky Aircraft Corporation (SAC) to develop and demonstrate the application of enabling usage and loads monitoring technologies (e.g., regime, gross weight [GW], center of gravity [CG], and loads) to fleet data to achieve benefits from usage-based fatigue life management or usage-based maintenance (UBM) processes. In particular, DO-0002/0003 continued to refine, validate, and apply regime clustering—reaching a maturity level that is considered sufficient to achieve certain important types of near-term HUMS-based UBM credits for components for which regimes such as turns, pushovers, and pullouts are critical drivers of RTs associated with life-limiting failure modes.

Data were also analyzed from a flight test conducted on a UH-60M aircraft, by the U.S. Army's Communications-Electronics Research, Development and Engineering Center, of fiber-optic landing gear load sensors that can be used to calculate GW/CG and measure landing loads. The prototype landing gear load sensors showed promise, with those installed in the TLG actually performing better than traditional foil-gage reference sensors used on the tail wheel strut as determined through comparison to truth data acquired from careful scale-measurements of aircraft weight and balance during aircraft flight tests.

On the other hand, prototype sensors integrated into the MLGs encountered significant measurement performance issues associated with the method of integration within the axle that will require a redesign of the integrated sensor package before it can be further matured, validated, and demonstrated to reach Technology Readiness Level 7 so that it can be prototyped in an operational environment. Through the use of a combination of traditional MLG strut sensors and the prototype fiber-optic TLG sensor, the viability of monitoring GW and CG was demonstrated. Flight test data were used to determine the effect on accuracy of taking landing gear measurements prior to takeoff during different ground operational conditions, including rotor stopped, rotor turning at idle, and rotor turning a 100% revolutions per minute and flat pitch. The insight gained will be valuable for defining viable data capture windows that maximize the data acquisition opportunities while minimizing errors in calculated GW and CG within the constraints of normal aircraft startup procedures.

Finally, an investigation of load monitoring requirements was conducted via simulation-based sensitivity studies to develop minimum requirements recommended for key load measurement attributes in support of future AC 29-2C MG-15 guidance on the integration of load monitoring technologies into HUMS.

The primary focus of DO-0002/0003, and therefore this report, was on the application of structural usage monitoring methods to achieve a “mock UBM credit.” Building on previous R&D efforts, selected usage monitoring methods and a viable end-to-end process for achieving UBM credits were applied to calculate flight-hour credits and, by extension, RT credits, for a representative life-limited component using individual aircraft regime statistics. A comprehensive assessment of the life-limited components contained in an S-92 rotorcraft was conducted to identify high-value candidate components for use in developing a mock credit. A total of 10 candidate components were identified that had various advantages and disadvantages

relative to the objectives of the FAA program. The main rotor stationary swashplate was selected based on this assessment because it was a moderately complex, but tractable, application that could be completed within the allocated budget and schedule of the FAA program. The stationary swashplate required accurate recognition of six critical regimes—including turns, push overs, and pullouts of different severity levels—in order to achieve a UBM credit.

The previously developed regime clustering method was applied in automated fashion to archived S-92 aircraft operational HUMS data, resulting in individual aircraft usage statistics across the fleet for critical regimes driving the RT for the stationary swashplate. Usage statistics for all S-92 aircraft were calculated for one year's worth of data and compared to the composite worst-case (CWC) usage spectrum, by individual tail number, in order to identify the best candidate serial numbers for UBM credits. The entire usage history of the selected serial number was analyzed to calculate a usage credit and new RT using regime-specific reliability factors to achieve approximately six-9's (0.999999) fatigue reliability, as validated within a probabilistic reliability framework.

The results were documented in a structure that paralleled AC 29-2C MG-15 guidelines for HUMS-based usage credits. The specific UBM credit was described, and the physics of failure of the target component were analyzed, to determine the critical regimes that required accurate monitoring versus those that could be managed through continued application of existing CWC fatigue damage rates. The end-to-end UBM credit process was described, starting with the acquisition of onboard sensor data and proceeding to the calculation of a usage-based flight-hour adjustment at SAC. In compliance with AC 29-2C MG-15, a hazard and criticality analysis of the failure modes of the end-to-end credit process was conducted to demonstrate that process risks were adequately addressed with mitigating actions commensurate with the use of existing S-92 aircraft HUMS software and existing SAC fatigue analysis and approval processes. The end-to-end process was applied to calculate the usage statistics from archived HUMS data for the selected serial number—demonstrating its ability to identify missing or invalid data, which totaled about 3% of the total data history, and address it through the use of CWC assumptions.

The existing fatigue life model for the S-92 aircraft was transformed to accept actual usage inputs in the form of number of occurrences for monitored transient regimes and flight time for monitored steady regimes, along with assumed CWC-based aircraft usage for unmonitored regimes. Trends in accumulated fatigue damage were plotted with and without reliability factors, which were employed to ensure baseline reliability was maintained. Flight-hour credits of approximately 60% and 85% were calculated with and without reliability factors, respectively. If historical usage patterns were maintained, it was projected that the RT of the specific serial number component could be safely increased by a factor of 2.4 when compared with a projected increase of more than 6.6 times the 14,000-hour published RT without the application of reliability factors.

The mock credit was confirmed by the validation of regime clustering and the resultant reliability of the projected RT increase. Existing flight test data were used to demonstrate that all of the critical monitored regimes could be identified to 96% or greater accuracy in terms of number of occurrences and/or time duration, as appropriate for transient and steady regimes.

Finally, the probabilistic reliability assessment framework was used to validate the use of regime reliability factors to achieve acceptable reliability while exploiting the benefits of monitored usage. The probabilistic framework was first validated by applying it to the original CWC usage and loads spectrum to calculate an RT of 14,000 flight hours and associated reliability of 5.8-9s. It was then applied to the mock usage credit to demonstrate that the use of regime reliability factors provided 5.7-9s of reliability, which was considered comparable with baseline reliability.

As a result of this R&D effort, SAC has concluded that the regime clustering and UBM methods described herein are sufficiently mature to facilitate going forward with formal UBM credit applications.

6. REFERENCES

1. FAA Report. (2012). *Structural usage monitoring and flight regime recognition—Compliance validation and demonstration using the health and usage monitoring system advisory circular 29-2C MG 15* (DOT/FAA/AR-12/4).
2. FAA Report. *Development and validation of structural usage and loads monitoring methods for use in determining rotorcraft usage credits* (DOT/FAA/TC-15-10).
3. Thompson, A.E., & Adams, D.O. (1990, May). *A computational method for the determination of structural reliability of helicopter dynamic components*. Paper presented at the 46th Annual Forum of the American Helicopter Society, Washington, D.C.
4. Bates, P.R., Davis, M., and Sadegh, P. (2010, May). *Rotorcraft dynamic component usage based maintenance process*. Paper presented at the American Helicopter Society 66th Annual Forum, Phoenix, AZ.
5. Isom, J.D., Davis, M.W., Cycon, J.P., Rozak, J.N., and Fletcher, J.W. (2013, May). *Flight test of technology for virtual monitoring of loads*. Paper presented at the American Helicopter Society 69th Annual Forum, Phoenix, AZ.
6. Beale, R.J. (2014, May). *Applications of virtual monitoring of loads to engineering decision making*. Paper presented at the American Helicopter Society 70th Annual Forum, Montréal, Canada.
7. Davis, M., Bouquillon, B., Smith, M., Allred, C., Sarjeant, R., Loverich, J., & Bordick, N. (2015, May). *Rotor load and health monitoring sensor technology*. Paper presented at the American Helicopter Society 71st Annual Forum, Virginia Beach, VA.
8. Zhao, J., & Adams, D.O. (2010, May). *Achieving six-nine's reliability using an advanced fatigue reliability assessment model*. Paper presented at the American Helicopter Society 66th Annual Forum, Phoenix, AZ.
9. Haldar, A., & Mahadevan, S. (2000). *Probability, reliability and statistical methods in engineering design*. New York: John Wiley & Sons.

10. Federal Aviation Administration. (2006, April). *Certification of transport category rotorcraft* (Advisory Circular 29-2C). Washington, DC.
11. SAE International (1996). *ARP-4761: Guidelines and methods for conducting the safety assessment process on civil airborne systems and equipment*.
12. RTCA. (1992). *RTCA/DO-178B: Software considerations in airborne systems and equipment certification*.
13. Adams, D.O., & Zhao, J. (2009, May). *Searching for the usage monitor reliability factor using an advanced fatigue reliability assessment model*. Paper presented at the American Helicopter Society 65th Annual Forum, Grapevine, TX.